OAK RIDGE
NATIONAL LABORATORY
MANAGED BY UT-BATTELLE
FOR THE DEPARTMENT OF ENERGY

ORNL/TM-2012/514

Fusion Materials Research at Oak Ridge National Laboratory

Progress during Fiscal Year 2012
October 1, 2011 through September 30, 2012

Compiled by:

F.W. Wiffen
L.L. Snead
A.A. Hulsey

October 2012

UT-BATTELLE
ORNL-27 (4-00)

U.S. DEPARTMENT OF ENERGY

OAK RIDGE National Laboratory

DOCUMENT AVAILABILITY

Reports produced after January 1, 1996, are generally available free via the U.S. Department of Energy (DOE) Information Bridge.

Web site http://www.osti.gov/bridge

Reports produced before January 1, 1996, may be purchased by members of the public from the following source.

National Technical Information Service
5285 Port Royal Road
Springfield, VA 22161
Telephone 703-605-6000 (1-800-553-6847)
TDD 703-487-4639
Fax 703-605-6900
E-mail info@ntis.gov
Web site http://www.ntis.gov/support/ordernowabout.htm

Reports are available to DOE employees, DOE contractors, Energy Technology Data Exchange (ETDE) representatives, and International Nuclear Information System (INIS) representatives from the following source.

Office of Scientific and Technical Information
P.O. Box 62
Oak Ridge, TN 37831
Telephone 865-576-8401
Fax 865-576-5728
E-mail reports@osti.gov
Web site http://www.osti.gov/contact.html

This report was prepared as an account of work sponsored by an agency of the United States Government. Neither the United States Government nor any agency thereof, nor any of their employees, makes any warranty, express or implied, or assumes any legal liability or responsibility for the accuracy, completeness, or usefulness of any information, apparatus, product, or process disclosed, or represents that its use would not infringe privately owned rights. Reference herein to any specific commercial product, process, or service by trade name, trademark, manufacturer, or otherwise, does not necessarily constitute or imply its endorsement, recommendation, or favoring by the United States Government or any agency thereof. The views and opinions of authors expressed herein do not necessarily state or reflect those of the United States Government or any agency thereof.

Materials Science and Technology Division

Fusion Materials Research at Oak Ridge National Laboratory
Progress during Fiscal Year 2012
October 1, 2011 through September 30, 2012

Compiled by:

F.W. Wiffen
L.L. Snead
A.A. Hulsey

October 2012

Prepared by
OAK RIDGE NATIONAL LABORATORY
Oak Ridge, Tennessee 37831-6283
managed by
UT-BATTELLE, LLC
for the
U.S. DEPARTMENT OF ENERGY
under contract DE-AC05-00OR22725

CONTENTS

LIST OF FIGURES

LIST OF TABLES

1.0 INTRODUCTION

Lance Snead (sneadll@ornl.gov)

The realization of fusion energy has proved a formidable challenge with its significant achievements coming through a close integration of the plasma physics and applied technology disciplines. Presently, the most significant technological challenge for the near-term experiments such as ITER, and next generation of fusion power systems, is the inability of current materials and systems to withstand the harsh fusion nuclear environment. The overarching goal of the ORNL fusion materials program is to provide the applied materials science support and understanding to underpin the ongoing DOE Office of Science fusion energy program while developing materials for fusion power systems. In doing so the program must be integrated both with the larger U.S. and international fusion materials communities, and with the international fusion design and technology communities. The overall program at ORNL on materials development will continue to actively develop low activation structural materials such as the Reduced Activation Ferritic/Martensitic Steels, the higher strength/higher creep resistance Nano Composted Ferritic steels, and Silicon Carbide Composites. A significant change this year was the increased emphasis on high heat flux testing and the development of refractory metals. This included the new use of an existing ORNL facility, adapted for the thermal testing of irradiated materials, the development and evaluation of new tungsten materials, and the study and understanding of the irradiation performance of tungsten through coupled modeling and experiment. In each case the materials will be developed in a design-informed fashion where properties improvements will be led by the latest fusion-relevant designs and directed at advancing the Technology Readiness Level of the materials systems. A limited effort within the ORNL program is directed towards diagnostic materials and high-temperature superconductors. In the area of diagnostics, ORNL continues to develop irradiation-hardened dielectric mirrors and to support basic irradiation materials science of ceramics for diagnostic systems. For high-temperature superconductors the ORNL program has undertaken a limited program to quantify the irradiation sensitivity of the most recently developed tape materials. Finally, this workscope integrates fundamental modeling into the development efforts as much as practicable.

This program makes heavy reliance on neutron irradiation in HFIR, the High Flux Isotope Reactor at ORNL. We expect this to be complemented by use of a newly commissioned ORNL-University of Tennessee ion irradiation facility when that facility is better suited to explore fundamental aspects of materials behavior under irradiation. In the longer term, we are looking forward to using a newly proposed facility that will allow irradiation in the neutron field on the ORNL Spallation Neutron Source. Both of these new opportunities are briefly described in this report.

This document provides a summary of FY-12 activities supporting the Office of Science, Office of Fusion Energy Sciences Materials Research for MFE (AT-60-20-10-0) carried out by the Oak Ridge National Laboratory. The four new projects selected in the Funding Opportunity Announcement solicitation of late 2011 are identified by “FOA” in the titles. Other relatively new work is found in Chapters 5 and 7, “High Heat Flux & Plasma Facing Materials” and “Special Purpose Materials.” The continuing DOE effort consists of a wide array of tasks and collaborations both within the US and with international partners. As discussed, major international collaborating partners include the Japan Atomic Energy Agency (the US-JAEA collaboration) and the Japanese National Institute for Fusion Sciences (the TITAN collaboration) on a range of fusion materials. This year a new collaborative initiative began with the Karlsruhe Institute of Technology in Germany focused on high heat flux materials and refractory metals.

2.0 FUSION MATERIAL IRRADIATION TEST FACILITY (FMITS) AT SNS

Phil Ferguson (fergusonpd@ornl.gov) and Mark Wendel

OBJECTIVE AND PROGRESS

An FY12 design study was directed at establishing the cost and feasibility of providing a fusion materials irradiation test station (FMITS) installed at the Spallation Neutron Source (SNS).

The completed design study produced:

1. Safety, environmental, and reliability bounding estimates for impact on the existing facility,
2. Confirmation by analysis that the instantaneous performance available to scientists using the SNS would not be diminished, and that the expected displacement rate and appm He to dpa ratio in FMITS were beneficial to the fusion program,
3. Physical concepts for the FMITS target hardware, cooling system, instrumentation, and gas-based temperature control,
4. An outline of operational procedures and required resources for initial installation, maintenance, operations, and installation and removal of each FMITS experiment to/from an SNS target.

The design and construction of an FMITS facility at SNS is expected to take about 30 months and cost \$10M total (at a 50% cost contingency). Previous experience with fusion material irradiation at HFIR was helpful in planning the effort and significantly reduces the technical uncertainty associated with implementation at SNS.

The findings were documented in an internal report (SNS-NFDD-ENG-TD-0003-R00) submitted to the Office of Fusion Energy, and one paper has been published on the study. A design review was performed on November 28, 2011, and the report confirms that there are no major showstoppers for proceeding with the FMITS.

The main mission of the SNS is neutron science, and it is important to show that this mission is not put at risk by the addition of FMITS. This risk can be managed by addressing the potential impacts to SNS on (1) safety and the environment, (2) reliability of the accelerator system, and (3) instantaneous neutronic performance. Based on the completed design study: (1) the safety and environment issues were bounded but require analysis and documentation to fully address the concerns, (2) the reliability has outstanding issues associated with delays for FMITS hardware replacement, and (3) there is insignificant risk to the instantaneous performance.

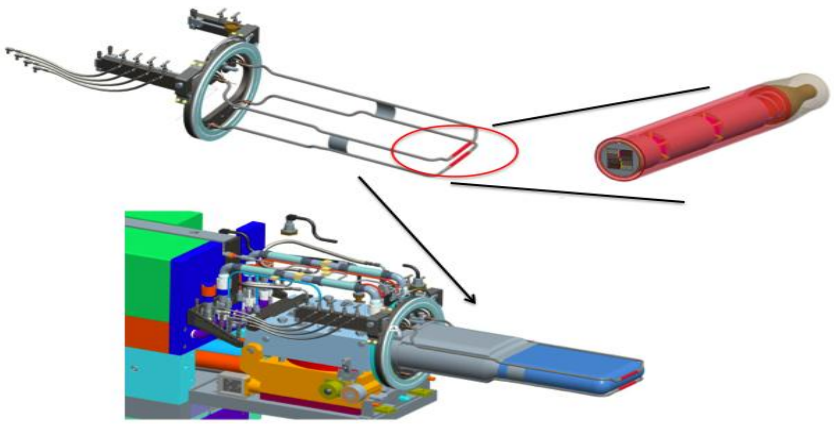

Figure 1. Diagram showing how materials samples are contained in a harness that is positioned over the existing SNS target assembly.

FUTURE PLANS

The 30-month/$10M project schedule and budget were rearranged and prioritized to fit a projected $1M funding level for FY2013, and it was found that such an investment should provide for the following FY-13 accomplishments:

1. SNS Reliability impact estimates will be improved. Advances will be made to the design of the hardware and the planned installation tooling beyond the concepts presented in the design study. The design study indicates that an additional four days are required due to FMITS for replacement of a target that reaches an unscheduled end-of-life. One of these improvements could be a reduction in the time required to remove and install the FMITS hardware from the target. Utilizing an FMITS cart in the process bay and selecting appropriate quick-disconnect fittings on the FMITS utility-jumpers could also reduce delays. Logistical planning for utilization of space in the process bay is also important. Design work that will lead to more robust FMITS hardware will reduce the risk of mishaps, associated with additional reliability impacts.

2. Safety and Environmental assessments will be advanced. The initial design study included a review of the SNS safety basis and showed that FMITS impact mostly provides marginal increases. It is necessary to show that a total flow blockage would not jeopardize the safety of the facility. This accident scenario will be mitigated by engineering design and analysis. The rough draft of a formal hazard analysis will also be accomplished. One outstanding environmental issue has to do with the activity of the FMITS exhaust gases. Additional analysis and design will be completed to decide if a gas hold-up tank is required, and if necessary, the hold-up tank will be designed.

3. Reduction in project time from 30 months to 24 months will be accomplished by advancing the FMITS hardware design. The hardware consists of: FMITS harness with connectors, target spine shield block replacement, and the two-component gas flow system. The reduction in project time assumes continuity between FY13 and the following 2 years. Any loss in momentum for the project could cause a delay, and any delay to the work results in a 6-month delay for installation since FMITS would be installed during one of the bi-annual maintenance outage. This improvement in the schedule is contingent upon the availability of time and resources during the corresponding outage.

4. Reduction in project cost contingency from 50% will be achieved by gathering specific quotes on FMITS equipment and designs, and by advancing the design where more is known about the time required to complete the project.

5. A Conceptual Design Review would be performed near the end of FY13, before ordering any FMITS operational equipment. Overall, the FMITS design work would be about 30% complete by the time of this review.

The total effort to accomplish these objectives is expected to be 3.3 FTEs and $30K of equipment. The manpower estimate includes 1.5 FTE for mechanical engineer and designer, 0.6 FTE for remote handling engineer, 0.4 FTE for gas-system/I&C engineer, and 0.4 FTE for safety officer and thermal-hydraulic engineer. The hardware costs are primarily for connector development.

3.0 STRUCTURAL METALS

3.1 FOA - STRUCTURAL MATERIALS WITH POTENTIALLY UNIQUE IRRADIATION RESISTANCE

S.J. Zinkle (zinklesj@ornl.gov), H. Bei, T.S. Byun, K.J. Leonard, A.G. Perez-Bergquist

OBJECTIVE

This project is exploring the basic radiation resistance of three unique classes of structural materials that may have the potential for very good resistance to neutron-induced property degradation.

SUMMARY

A new initiative is addressing the baseline properties, including the effects of neutron irradiation, of novel materials that may potentially possess exceptional radiation tolerance. The materials for this investigation include bulk metallic glasses, high configurational entropy crystalline alloys, and MAX phase ceramics including polycrystalline Ti_3SiC_2 and Ti_2AlC ceramics. Initial selection of material compositions has been completed, and fabrication of initial heats of material has either been completed (commercially available MAX phase material) or will be performed later in the fall of 2012. Characterization of the unirradiated materials will be performed over the next several months.

PROGRESS

The funding for this project selected through the FOA LAB 12-603 was received at ORNL in August, 2012. A postdoctoral research fellow for this project was recruited from LANL and joined ORNL in mid-September. Initial selection of material compositions for the bulk metallic glass, high entropy crystalline alloys, and MAX phase alloys has been completed, and fabrication of initial heats of material has either been completed (commercially available MAX phase material) or will be performed later in the fall of 2012. In all cases, the selected materials exhibit high mechanical strength and good toughness. For the bulk metallic alloys, we are concentrating on Cu-containing alloys and investigating several annealing temperatures that may produce different relaxed states (i.e., different degrees of short range order, while retaining long range structural disorder). The high entropy alloys are being fabricated in the fully single-phase regime, with a focus on face-centered cubic, fine-grained materials. We are examining potential compositions that do not contain Co due to radioactivity handling concerns following neutron irradiation. The MAX phase ceramics include commercially purchased polycrystalline Ti_3SiC_2 and Ti_2AlC. These MAX phase ceramics exhibit pseudo-ductile fracture behavior at elevated temperatures due to their inherent nano-laminar composited structure. This leads to an expectation that the nano-scale interfaces may provide exceptional radiation stability. However, any radiation stability will depend on the stability of the nano-structures and the possible anisotropic dimensional evolution typical of hexagonal crystal structures under irradiation.

FUTURE PLANS

Fabrication of initial heats of the bulk metallic glass and high entropy alloy materials will be performed during the fall of 2012, followed by physical and mechanical property and microstructural characterization of the unirradiated materials. It is anticipated that the elevated temperature (>400^{o}C) neutron irradiation of all of the materials to doses of 0.01-10 dpa will commence in the spring of 2013 (initial screening studies will be performed to doses of 0.01-0.1 dpa, and if the materials exhibit good radiation stability then higher dose irradiations to 1-10 dpa will be performed.

3.2 ADVANCED REDUCED ACTIVATION FERRITIC –MARTENSITIC (RAFM) STEELS: PRECIPITATE STABILITY

L. Tan (tanl@ornl.gov), Y. Katoh, L.L. Snead

OBJECTIVES AND BACKGROUND

A new class of Reduced Activation Steels, containing a high-density of finely dispersed precipitates, are under development. These materials are being developed as a more easily fabricated class of steels, compared to the ODS system, while maintaining the superior irradiation performance of ODS steels.

The stability of MX-type precipitates under isothermal aging, stress, and irradiation are being studied in this task. Chromium-rich $M_{23}C_6$, Laves phase (Fe_2W-type), and MX-type precipitates are conventional precipitates developed in reduced activation ferritic/martensitic (RAFM) steels. Stability of MX-type precipitates, usually formed on the nanometer scale, is essential for the strength and radiation resistance of these steels. Tantalum carbide (TaC), tantalum nitride (TaN), and vanadium nitride (VN) are conventional MX type precipitates developed in RAFM steels. Understanding the stability of MX precipitates will help in the development of advanced RAFM steels.

EXPERIMENTAL

Three model alloys, Fe-1WTaC, Fe-1WTaN, and Fe-1WVN, were designed using computational thermodynamics to favor the formation of TaC, TaN, and VN in the respective alloys. Each type of precipitates was controlled to have an equal molar fraction in the alloys.

Type SS-3 specimens were used in isothermal aging experiments and creep tests. During isothermal aging experiments, the specimens were sealed in helium filled quartz tubes and aged at 600 and 700°C. The 600°C creep tests were conducted at ~70% of the yield stress (σ_y). Specimens were also prepared for self-ion Fe^{2+} and neutron irradiation experiments.

Microstructural characterization, primarily using transmission electron microscopy (TEM), and mechanical tests including tensile and creep tests have been performed to evaluate the evolution of the MX-type precipitates under thermal, stress, and radiation.

RESULTS AND PROGRESS

The isothermal aging at 600 and 700°C h was completed for 100 and 1000 h, and aging for 5000 h is in progress. Room temperature tensile tests did not show any degradation in strength after 1000 h at 600°C but showed significant degradation after 100 h at 700°C. Alloy Fe-1WTaC had the smallest decrease in strength (up to ~11%), while alloy Fe-1WTaN exhibited the greatest decrease in strength (up to ~44%) after aging 1000 h at 700°C. Creep tests of the Fe-1WTaC, Fe-1WTaN, and Fe-1WVN alloy samples at 600°C and ~$0.7\sigma_y$ revealed creep lives of 371.0, 83.5, and 196.2 h, respectively.

Examples of the microstructural evolution of the precipitates under thermal (600°C) and stress conditions are shown in Figure 2. Both TaC and VN occurred as spherical particles with average diameters of 10 and 19 nm, respectively. In contrast, the dark-field images revealed needle-shaped TaN particles, approximately aligned with g(200), in alloy Fe-1WTaN. However, TEM images at different tilt angles confirmed that the TaN particles are in fact disk shaped. Unlike the gauge section subjected to high stresses during creep testing, the tab section of creep tested samples can be considered as isothermally aged without stresses. The size of TaC and TaN particles did not show noticeable changes after aging at 600°C. The stress (in the gauge section) also did not show significant effect on the size of TaC particles. In contrast, the TaN particles were fragmented into smaller pieces, whose orientation was changed to be approximately aligned with g(110). Additionally, a few Fe_2W-type Laves phase particles with size ~100 nm were observed at the gauge section of the crept Fe-1WTaC sample; this was not observed in the unstressed, aged samples even after 1000 h. The result suggests that the formation of the Laves phase was greatly accelerated by the stress during creep. Microstructural characterization of samples in the related conditions to fill in the blanks of Figure 2 is in progress.

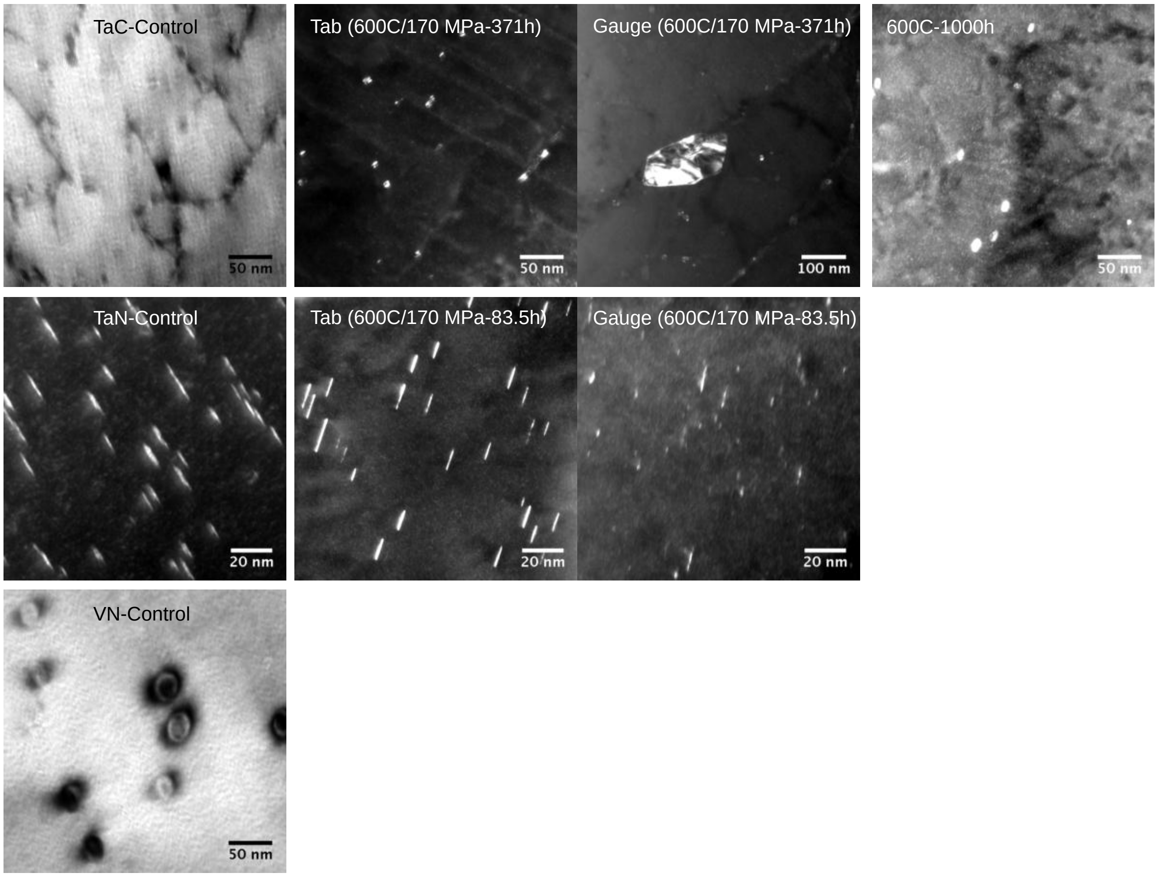

Figure 2. Bright-field (BF) and dark-field (DF) TEM images showing the evolution of nano-precipitates under thermal (600°C) and stress conditions.

The size and number density of the nano-precipitates have been statistically quantified. Figure 3 compares the experimental volume fractions of TaC, TaN, and VN particles to their calculated volume fractions. The data approximately follow the straight dashed line, indicating good agreement between the experiment and calculation, with the experimentally observed TaC particle volume slightly less than the calculated prediction. This may be attributable to the experimental difficulty in identifying the ultrafine TaC particles that are often located on dislocations. The three alloys were designed to have about the same mole fraction of precipitates, which led to the greater volume fraction of TaC followed by TaN and VN. The larger volume fraction of TaC benefited the higher strength and greater creep life of Fe-1WTaC compared to the TaN and VN bearing alloys. Despite the low alloy content of the experimental Fe-1WTaC, the creep life was close to that reported for F82H.

Self-ion Fe^{2+} irradiation of the alloys will be accomplished at University of Michigan through an accepted ATR-National Scientific User Facility proposal. The irradiations at 500°C to 20 and 200 dpa are scheduled in September and October 2012. The ion-irradiated samples will be shipped to ORNL for microstructural characterization. Additionally, a set of SS-J2 specimens has been included in a neutron irradiation campaign in HFIR, where they will be irradiated at 300, 500, and 650°C to damage levels ranging from ~0.1 dpa to ~20 dpa.

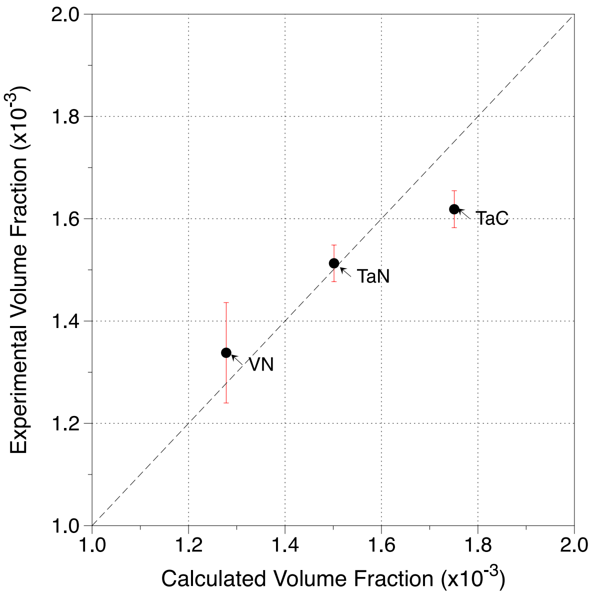

Figure 3. Calculated and experimental volume fraction of TaC, TaN, and VN precipitates in alloys Fe-1WTaC, Fe-1WTaN, and Fe-1WVN.

FUTURE PLANS

The HFIR irradiations will be completed by mid-2013, and samples will be tensile tested and microstructures characterized to track the evolution of the precipitates. Microstructural characterization and testing will continue to study the evolution of the precipitates. One or two new heats containing greater amounts of the MX precipitates will be developed to study the stability of the precipitates at higher densities and their effect on strength and radiation resistance.

3.3 RADIATION EFFECTS IN REDUCED ACTIVATION F-M STEELS

T.S. Byun (byunts@ornl.gov), D. Hamaguchi (JAEA), T. Nozawa (JAEA), Y. Katoh,

OBJECTIVE

This experiment is evaluating the post-irradiation mechanical properties of the reduced activation ferritic-martensitic steel F82H, focusing on the effects of irradiation on fracture resistance, as a collaborative ORNL/JAEA program. The specific goals are to provide the basic understanding and produce a database for the F82H steel to advance its technology readiness level.

SUMMARY

HFIR capsule RB15J irradiated a number of ferritic-martensitic (FM) steel specimens for ten reactor cycles and most of the post-irradiation evaluation has been carried out. The majority of specimens were the subsize precracked Chevron-V notch (PCCVN) and disk-compact tension fracture (DCT) specimens of the Japanese FM steel F82H and tungsten inert gas (TIG) weld variants on this steel. So far, fracture testing of the PCCVN specimens has been completed: all of the PCCVN were tested at room temperature or below to build temperature-transition curves. Fractography of the tested specimens is underway using the SEM unit in the 3025E facility. The DCTs are to be tested when the grip assemblies are prepared. Also, a servohydraulic machine is to be installed in the hotcell facility for low cycle fatigue tests of dog-bone type specimens from the same experiment.

PROGRESS AND FUTURE PLANS

Irradiation The RB15J capsule was irradiated in a reflector beryllium position nearest the outer boundary of the outer HFIR fuel element. Nominal irradiation temperatures were 300 and 400°C, actual temperatures were recoded from thermocouples in the experiment, and maximum fluence on the experiment midplane produced 6 dpa in steels.

Static Tests The test materials include the 9Cr-based reduced activation FM steel (F82H IEA or base metal), TIG weld metal (F82H IEA TIG WM), heat-affected zone materials (F82H IEA TIG FGHAZ and F82H IEA TIG OTHAZ). Two types of PCCVN specimens, M5PCCVN (1/2-size precracked Charpy) and hf-1/3CCVN (1/3 size precracked Charpy), include all of the four base and weld variants, while the 0.14 and 0.18 inch thick DCT specimens include base metal and weld metal only. Static fracture toughness tests (J-R tests) were performed for 83 PCCVN specimens (74 and 9 each of 1/2-size and 1/3-size PCCVN, respectively) at or below room temperature in the MTS servohydraulic testing machine in the 3025E hotcell facility. Table 1 lists the specimen groups (each group includes 1 to 15 specimens tested over small temperature ranges), the irradiation and test conditions and the J_c values. The fracture toughness data are the average of the 1 to 15 values for the groups. K-curve analysis will be performed for these datasets to build the temperature transition curves and the reference temperature (T_0). Scanning electron microscope (SEM) fractography is underway, with an example shown in Figure 4.

DCT Testing Fracture toughness testing of the irradiated DCT specimens is in preparation. Specimens to be tested are shown in Table 2. Prior to fracture testing, the hardness of selected samples has been measured in order to confirm irradiation temperatures. The hardness data are also listed in Table 2. Test setup including design and machining of DCT fixture for more efficient testing is underway.

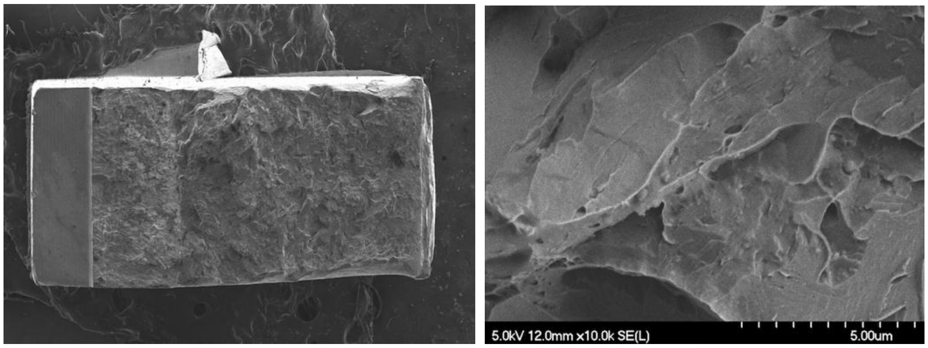

Figure 4. Example fractographs: low and high magnification SEM images for an F82H TIG WM specimen irradiated to 4 dpa at 308°C.

Table 1. Irradiation conditions and fracture toughness data for F82H base, weld, and HAZ specimens. Each group includes 1 to 15 PCCVN specimens.

Material	Irradiation Temp. [°C]	Dose [dpa]	Hv	Test Temp. [°C]	Average J_C [kJ/m^2]
F82H IEA	304	4	300	-80 to -60	90.4
F82H IEA	308	4	309	-70 to -50	105.9
F82H IEA	391	5.8	236	-150 to -130	39.7
F82H IEA	391	5.8	231	-130 to -100	84.2
F82H TIG FGHAZ	308	3.9	325	-20	87.4
F82H TIG FGHAZ	304	4	347	-20 to +23	99.6
F82H TIG FGHAZ	391	5.8	277	-90	33.9
F82H TIG OTHAZ	387, 391	5.8	223	-130 to -100	40.4
F82H TIG OTHAZ	291	5.8	216	-40	99.5
F82H TIG WM	308	4	337	-20 to +23	23.3
F82H TIG WM	391	5.8	277	-120 to -80	14.3
F82H TIG WM	391	5.8	263	-130 to -90	19.7

Table 2. DCT specimens irradiated in RB15J capsule

ID	Material	Specimen type	Irr. temp. [^{o}C]	Dose [dpa]	Hv	# of Specimens
0WEa	F82H IEA	0.18" DCT	384	5.6	236	4
0WEe	F82H IEA	0.18" DCT	396	5.7	235	4
0VXA	F82H IEA	0.14" DCT	316	4.5	307	7
1VXA	F82H TIG WM	0.14" DCT	315	3.2	336	7

Post-Irradiation Fatigue Testing Plan

A servohydraulic testing machine for low cycle fatigue tests of irradiated RB15J fatigue specimens (dog-bone bar type) has been purchased and modified for hotcell operation. Installation is expected to be done in a few months. Also, a new grip assembly has been designed and is being fabricated.

3.4 FOA - DEVELOPMENT OF ODS FeCrAl FOR FUSION APPLICATIONS

D.T. Hoelzer (hoelzerd@ornl.gov) and B.A. Pint

PROJECT OVERVIEW

The dual coolant (He and Pb-Li) system is the leading U.S. blanket concept for DEMO. Oxide dispersion strengthened (ODS) ferritic alloys are candidate structural materials due to their superior high-temperature mechanical properties and radiation tolerance. However, conventional ODS Fe-Cr alloys have not shown good corrosion resistance in Pb-Li. The objective of this project is to develop an ODS Fe-Cr-Al alloy with improved compatibility with Pb-Li above 550°C, while retaining the inherently attractive properties of ODS alloys.

PROGRESS

This research will develop an ODS FeCrAl alloy that will form a protective Al-rich oxide to inhibit dissolution in Pb-Li and have a stable dispersion of nano-size oxide particles. Previous capsule testing at ORNL has shown minimal mass loss of commercial ODS FeCrAl with 20%Cr and 5%Al after 1,000h in Pb-Li at 800°C. One objective is to reduce the Cr and Al contents as much as possible. For Cr, this will minimize embrittlement issues caused by formation of the α' Cr-rich phase during exposure to neutron irradiation. For Al, lower Al contents will make the alloy easier to form and weld.

For the oxide dispersion, since Al forms a strong bond with O it generally reduces the high-temperature stability of oxide particles, which also degrades several inherently attractive properties of ODS alloys, such as high-temperature creep properties and resistance to irradiation damage and swelling. The Al addition presents a challenge since many oxide phases are les thermodynamically stable than α-Al_2O_3. However, Y_2O_3 is more stable and other elements will be examined, such as Zr and Ti, to determine if a Y-rich complex multi-component (CMC) oxide phase will promote a decrease in size and increase in number density of the CMC phase.

The research planned for the first year focuses on the following tasks:

1. Determining the optimum Cr and Al contents in model FeCrAl alloys that (a) promote Pb-Li compatibility via the formation of an Al_2O_3 surface scale and (b) reduces the propensity for embrittlement by formation of α' Cr-rich phase during exposure to neutron irradiation.
2. Investigating the relative stability of several CMC oxide phases relative to the Al_2O_3 phase.

3. Producing an initial heat of ODS FeCrAl by mechanical alloying with a composition based on the first two tasks.

Microstructural characterization will play an indispensable role in each of the three tasks on development of the high-Cr ODS ferritic alloy.

Work has been initiated on two tasks involving the optimization of the Cr and Al contents in model FeCrAl alloys and investigation of the stability of several CMC oxide phases relative to the Al_2O_3 phase. Six model FeCrAl alloys with systematic variations in Cr and Al contents have been obtained with 3-5%Al and 10-20%Cr. Specimens, capsules and Pb-Li ingots have been prepared and 1000h capsule experiments at 700°C will begin early in FY13. The literature review on oxide phase stabilities in the Al_2O_3-Y_2O_3-MO_2 (M=Ti, Zr or Hf) systems was completed. The database of thermodynamic parameters for the Al_2O_3-Y_2O_3-ZrO_2 system was completed and will be used for computational modeling of phase diagrams to predict the equilibrium oxide phases as a function of temperature and composition. Similar databases will be obtained for the Al_2O_3-Y_2O_3-TiO_2 and Al_2O_3-Y_2O_3-HfO_2 systems. The sample design for conducting the experimental investigation of the oxide stability was completed and samples are currently being fabricated. The two-component oxide phases that will be investigated are TiO_2, ZrO_2,

HfO_2 and Y_2O_3. Specimens of the TiO_2, ZrO_2 and HfO_2 oxides will each be in contact with an Y_2O_3 specimen and the combination of each set of two oxides will be in contact with Al_2O_3. Samples made by slurry processing will be annealed at different temperatures and the reaction products analyzed. The goal of the computation and experimental work is to identify a CMC with greater stability than the current Y-Al oxides in ODS FeCrAl alloys.

FUTURE PLANS

The results of these first two tasks will be combined to purchase the first alloy powder compositions in early 2013. The powder will be ball-milled to make the first batches of ODS alloys for characterization and evaluation in creep and compatibility experiments.

3.5 CHARACTERIZATION OF THE ADVANCED ODS ALLOY 14YWT-SM12

D.T. Hoelzer (hoelzerd@ornl.gov), K.A. Unocic, E.T. Manneschmidt and M.A. Sokolov

PROJECT OVERVIEW

The advanced oxide dispersion strengthened (ODS) 14YWT ferritic alloy was developed for extreme neutron irradiation environments such as those encountered in plasma facing component structures of fusion reactors. To provide further evidence of the radiation tolerance of 14YWT, a variety of test specimens were fabricated from the ODS 14YWT (SM12 heats) ferritic alloy and included in the specimen matrix of the HFIR JP30/31 experiment that is irradiating specimens in 3 sub-capsules at temperatures of 300, 400 and 650ºC to a neutron dose of ~20 to 25 dpa. The reference characterization of unirradiated specimens was to correlate different processing conditions for producing three 14YWT-SM12 heats with their microstructures and mechanical properties and for future comparison with irradiated material. The three 14YWT-SM12 heats were prepared by extruding ball milled powder into bars at 850, 1000 or 1150ºC followed by rolling parallel to the extrusion direction at 1000ºC to 50% reduction in thickness into plates. This comparison will help guide future development of the ODS alloys for fusion reactor applications.

PROGRESS

The microstructural analysis of the 14YWT-SM12 heats showed very similar microstructures despite being produced with three different extrusion temperatures. The back scattered electron (SEM-BSE) and bright field (BF) transmission electron microscopy (TEM) analyses showed grain structures that were similar in size (<1 μm), size distribution and morphology (slightly elongated parallel to extrusion direction) in the three heats. The grains were mostly featureless with a low number density of non-uniformly distributed oxide particles larger than ~10 nm. A significant result obtained from energy-filtered TEM (EFTEM) analysis of 14YWT-SM12a (1150ºC extrusion) was that a high number density of small particles appearing with dark contrast were observed in Fe-M jump ratio maps as shown in Figure 5. These particles were not observed in the BF contrast image (Figure 5a.) The dark contrast results from local displacement of Fe atoms by the particle that lowers the inelastic scattering intensity in that region. The size of the particles determined from line intensity histograms at full-width half-maximum (Figure 5c) showed that many of the particles were less than ~5 nm in diameter. Titanium (Ti) L-composition maps showed that the small particles contained Ti and were consistent with the Ti-, Y- and O-enriched nanoclusters, which are characteristic of the ODS 14YWT ferritic alloy.

(a) (b) (c)

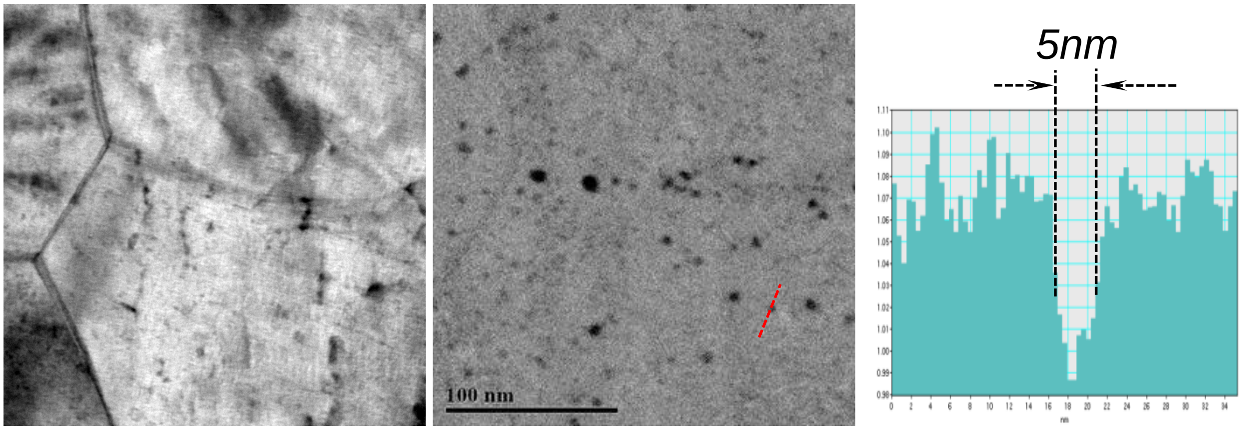

Figure 5. EFTEM analysis of 14YWT-SM12a near the thin foil edge showing (a) BF contrast image, (b) Fe M-jump ratio map and (c) line intensity histogram of a dark imaging particle.

The tensile properties of the 14YWT-SM12 heats were measured from room temperature (25ºC) to 800ºC at a strain rate of 1 x 10^{-3} s^{-1}. The results are shown in Figure 6. These indicate that the yield and ultimate tensile stresses and uniform and total elongations of the three heats were very similar over the temperature range. Compared to tensile properties of previous 14YWT heats, the 14YWT-SM12 heats showed generally lower strength and higher ductility. The yield stresses and ultimate tensile strengths of the SM12 heats were all near ~1050 MPa and ~1200 MPa, respectively, at room temperature and decreased with temperature to ~260 MPa and ~300 MPa, respectively at 800ºC. The uniform and total elongations of the SM12 heats were ~9-10% and ~21-24%, respectively, at room temperature, which is significantly better than the 1 to 2% uniform elongation typically observed in previous 14YWT heats. The changes in uniform and total elongation with increasing temperature showed similar trends for the SM12a and SM12c heats compared to the SM12d heat. For the SM12a and SM12c heats, the uniform elongation decreased slightly with temperatures while the total elongation remained nearly constant up to 400-500ºC and then increased to a peak value near 700ºC. The changes in uniform and total elongations with increasing temperatures were much less for the SM12d heat.

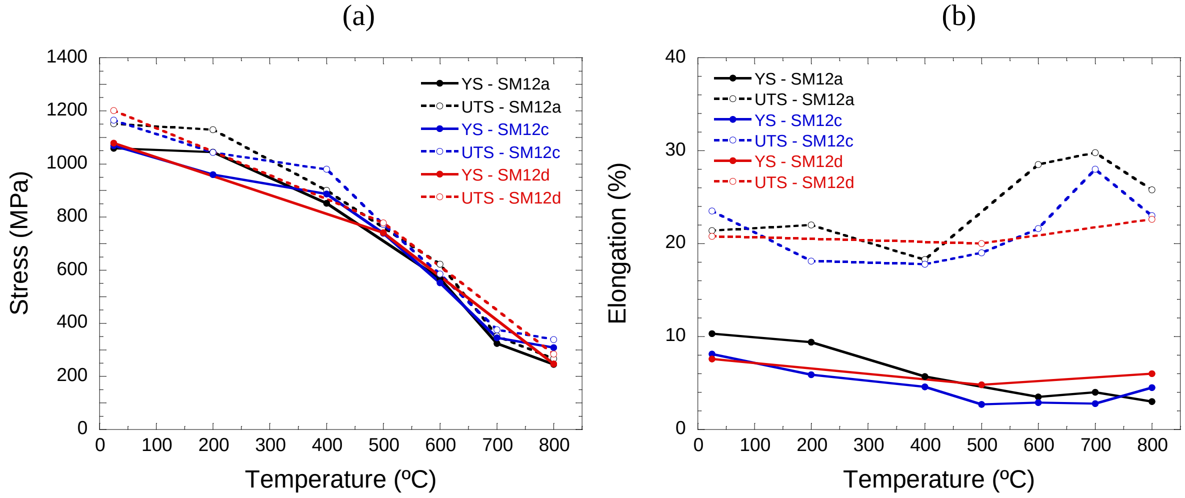

Figure 6. Tensile properties of the three 14YWT-SM12 heats over the temperature range from 25ºC to 800ºC. (a) Yield and ultimate tensile stresses and (b) uniform and total elongations.

The lack of significant differences in the microstructures and tensile properties of the three 14YWT-SM12 heats was attributed to the heat treatment of 1 h at 850ºC before the extrusions at 1150ºC (SM12a), 1000ºC (SM12c) and 850ºC (SM12d.)

PLANNED WORK

Future effort will focus on detailed microstructural characterization using advanced TEM microscopes and on fracture toughness testing to determine the fracture toughness transition temperature and ductile tearing resistance as a function of temperature.

3.6 ATOMIC-SCALE STRENGTHENING IN ODS AND IRRADIATED STEELS.

Yury Osetskiy (osetskiyyn@ornl.gov) and Roger Stoller.

OBJECTIVE

This extensive simulation program is designed to investigate the basic mechanisms of strengthening in advanced steels. In particular, mechanisms which lead to strengthening in ODS materials (nano-precipitates) and in irradiated steel (helium bubbles) are studied in detail.

APPROACH

This study includes strengthening due to nanometer-scale particles in ODS-like materials and the effects of irradiation produced He on plastic deformation. The main method applied is atomic-scale modeling using molecular statics (MS) and molecular dynamics (MD) methods together with the best available potentials to calculate interatomic interactions.

PROGRESS

Research is being carried out along two separate directions: 1) Modeling the strengthening in ODS steels and 2) Helium in metals. Work in FY12 was related to strengthening effects in both systems and the comparative study revealed interesting similarities and differences in plastic deformation mechanisms.

Comparison of critical resolved shear stress (CRSS), which is a measure of obstacle strength, for seveal main “inclusion-like” obstacles, e.g. having no dislocation character, is presented in

Figure *7*. The data were obtained by MD modeling at 300K with an applied strain rate $10^5 s^{-1}$. All these particles were simulated in an Fe matrix crystal containing about (2-6) $x10^6$ mobile atoms and a ½<111> edge dislocation moving under applied stress. The methods used to model voids, bubbles and secondary phase precipitates were described earlier. A new method is used in this work to consider the rigid particle. The particle is simulated as non-compressible and non-shareable and is considered as a superparticle with the corresponding mass in Newtonian motion equations for all the atoms in the system. This particle can move under forces from matrix atoms, however atoms inside it cannot move relative to each other. Modeling conditions were kept the same for all the obstacles to ensure a direct comparison of the results.

Rigid particles are expected to be the strongest; however this was found to be particle size dependent. This results because for rigid particles the interaction mechanisms depend on size. If particle is large enough, >2nm, the Orowan mechanism provides the maximum possible strength among all obstacles. This mechanism is characterized by a long dipole of screw dislocations formed at the critical stress and formation of an “Orowan loop” when the dipole closes. If the rigid particle is small, <2nm, an edge dislocation can bypass by formation of a superjog. A vacancy cluster of corresponding size is left near the particle. Such a particle is weaker than a void or equilibrium He-bubble of the same size.

The effect of interaction geometry on CRSS was also studied and the results demonstrate that rigid particles do not follow the mechanism observed for other “inclusion-like” obstacles. Thus if an edge dislocation cuts voids at different levels relatively to its centre, i.e. above or below, the CRSS is always lower than the maximum value related to the equator level and is a function of the void effective area at the cross-section of the dislocation slip plane. It is important that the dislocation-void interaction mechanism does not depend on the level at which the dislocation slip plane cuts the void provided they intersect. Similar results were obtained for shareable precipitates (Cu in Fe) and, in preliminary studies, for He-bubbles. However, in the case of rigid particles the situation is qualitatively different and size dependent as can be seen in Figure 8 where results for 2 and 4 nm voids and rigid particles are presented. Thus, if a dislocation intersects a 2nm rigid particle below its center (X=-R/2) it is a stronger barrier than that through the center (X=0), while if the slip plane is above the particle centre (X=R/2) it is significantly weaker. In the above center case it is even weaker than the corresponding void. The explanation of this results and the result for 4nm rigid obstacles is in the details of atomic scale mechanisms and we are trying to formalize this in current research. However, we can note that simple statistical models used to estimate the net strengthening when the properties of the particular obstacles are taken as a parameter, for example the dispersed barrier hardening model, cannot be applied because the rigid particle strength and effective size affect the total hardening in a more complicated way than e.g. voids. More details on this will be clarified by future research.

Other directions of this research include effects of He-to-vacancy ratio (He/Vac) on bubble strengthening and effect of ambient temperature on both ODS and bubble strengthening. Some results are presented in Figure 9 and Figure 10. Thus, the dependence of strength of a 2nm bubble versus He content was tested at 300K and is presented in Figure 9. This shows that increasing He/Vac from 0 to 0.5 increases CRSS from <140MPa to >150MPa. Note that the ratio He//Vac=0.5 is close to equilibrium. Further increase of He-content over-pressurizes the bubble and decreases the critical stress to a very low value at He/Vac=2. This drop is because the interaction mechanism changes for strongly over-pressurized bubble and at He/Vac=2 a bubble does not act as an inclusion-like obstacle. Instead, it releases a small cluster of self-interstitial atoms towards an approaching dislocation and the dislocation absorbs this cluster, creating a superjog in such a way that the dislocation line does not intersect the bubble. A comparison of temperature effects on CRSS for a 2nm rigid particle and a bubble with constant value of He/Vac=0.5 is presented in Figure 10. One can see that both curves are approximately parallel in their temperature dependence. However, simulating the exact behavior at experimental conditions should take into account two temperature effects: 1) the irradiation temperature at which the bubble should be at equilibrium and 2) possible change in equilibrium He//Vac ration at the test temperature. This should induce some correction in Figure 10when the results are obtained.

FUTURE DIRECTION

This work will continue to evaluate the strengthening processes in materials of interest for fusion applications, and converge on a set of confirmatory experiments to validate underlying modeling.

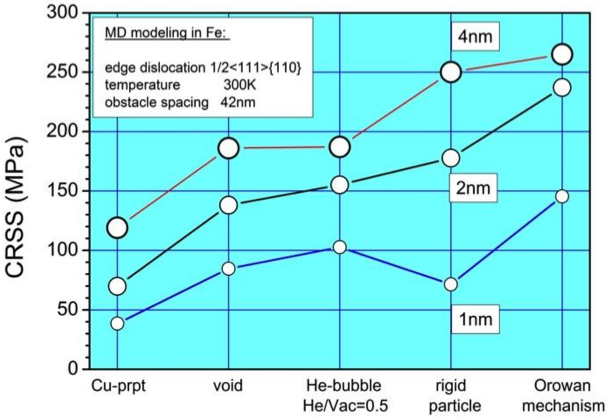

Figure 7. Critical Resolved Shear Stress (CRSS) for different obstacles of sizes from 1 to 4 nm diameter obtained by MD at strain rate $10^5 s^{-1}$ at 300K.

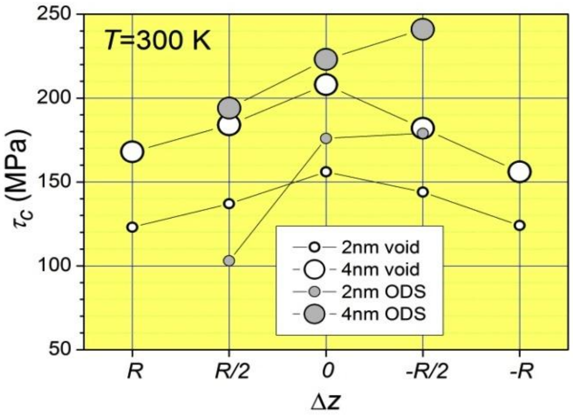

Figure 8. Comparison of CRSS for voids and rigid particles at different interaction geometries. "0" means the dislocation slip plane intersects an obstacle though the equator, R/2 – slip plane is a half obstacle radius above its centre, etc.

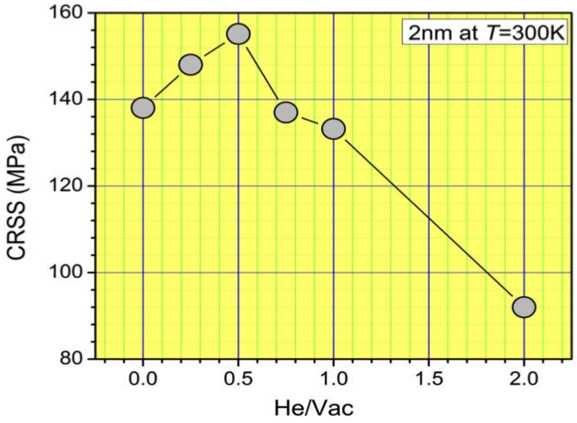

Figure 9. Dependence of CRSS for 2nm buble versus He/Vac content. He//Vac<0.5 corresponds to an under-pressurized bubble and vice versa.

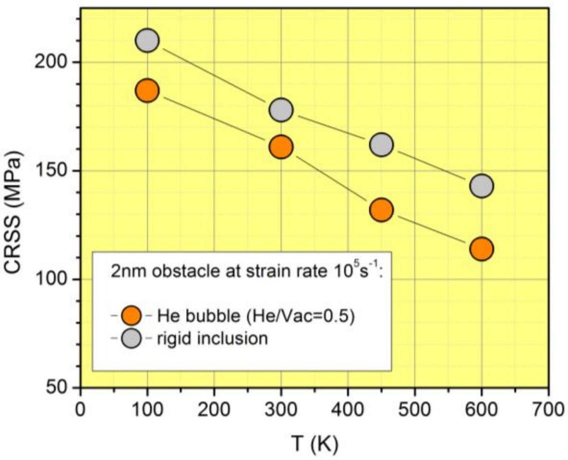

Figure 10. Comparison of the temperature dependence of CRSS for a 2nm rigid particle and He-bubble. The He-bubble was simulated with constant He/Vac=0.5.

3.7 DEVELOPMENT OF A NEW EQUATION OF STATE FOR HELIUM IN IRON

R. E. Stoller (stollerre@ornl.gov) and Y. N. Osetskiy

OBJECTIVE

A new Fe-He equation of state is needed to describe the behavior of helium atoms in bubbles during damage structure calculations. This better equation of state will improve the predictive capability for the Fe-based materials that are candidates for fusion structural applications

PROGRESS

Because of the high helium levels generated by nuclear transmutation reactions, predictions of structural material performance under DT fusion conditions must account for how the helium influences microstructural evolution during neutron irradiation and the related mechanical properties. One of the primary issues that must be addressed is the behavior of He-vacancy clusters which evolve into finite-sized bubbles with the potential for growing into voids. In this case, a 'bubble' is defined as a cavity which is stabilized by the helium pressure it contains. If helium is removed a bubble will shrink. In contrast, a 'void' is a cavity which has grown large enough that growth can be maintained by the absorption of a net vacancy flux. The gas pressure plays essentially no role in void stability. The properties of small He-vacancy clusters, such as the helium and vacancy binding energy, are critical to predicting bubble stability. These processes can only be accurately described by atomistic simulations such as molecular dynamics (MD) which requires an interatomic potential to describe the behavior of both the metal and helium atoms. In order to improve our predictive capability for the Fe-based materials of most interest to fusion structural applications, a new Fe-He interatomic potential was developed based on *ab initio* calculations of the interactions between He and point defects in Fe. Additional work using this potential has characterized the properties of small He-vacancy clusters and parameters such as the He-to-vacancy ratio as a function if cluster/bubble size and temperature. The observations of that work are being extended to develop an atomistic equation of state for helium in iron which can then be applied in a broad range of mesoscale to predict microstructural evolution.

In order to provide a basis for fitting the pressure-temperature relationship required for the equation of state (EOS), a series of MD simulations has been initiated. The primary conditions are described in Table 3. The temperature range was chosen to cover a range which includes much lower and higher temperatures than the expected applications of the EOS. The bubble sizes encompass those of interest to fusion reactor materials, and an accurate extrapolation to larger sizes will be verified. If needed, larger sizes may be included, although the expectation is that the pressure will be sufficiently low at large sizes that a more simple equation of state will be appropriate. For each of the bubble sizes, the pressure will be obtained for a broad range of He/vacancy ratios, from highly over-pressurized to a void-like under-pressurized state. The pressure at mechanical equilibrium will also be determined.

The primary issue in fitting the EOS is to choose an appropriate function to describe the compressibility of the gas. We will first adopt the hard-sphere model of Brearley and MacInnes for testing and evaluation. One difference between the atomistic results and the assumptions typically applied in developing an EOS is illustrated in Figure 11. The general thought is that the gas atoms occupy the complete bubble volume. However, MD simulations using the ORNL Fe-He potential in concert with the Fe potential of Ackland, et al. indicate that the Fe-He interaction leads to a small exclusion volume near the bubble surface. This is demonstrated in Figure 11(right) in which the time-averaged positions of the iron surface atoms (green) and helium atoms (gold) are shown. Figure 11(left) shows graphically the corresponding radial distribution of He atoms. The result of this standoff distance is that the effective volume of the bubble used to compute the pressure is smaller and the pressure is higher.

All of the simulations in Table 3 have been completed and the statistical fitting of the data is underway.

FUTURE EFFORT

The first presentation of these results is planned for October 2012 at the NuMat International Nuclear Materials conference in Osaka, Japan. Definition and refinement of the He-Fe equation of state will continue, building on the work completed thus far.

Table 3. Conditions for MD simulations

Temperature (K)	Bubble radius (nm)
200	0.25, 0.5, 1.0, 2.0, 5.0
300	same as above
400	same as above
500	same as above
600	same as above
700	same as above
800	same as above
900	same as above
1000	same as above
1100	same as above

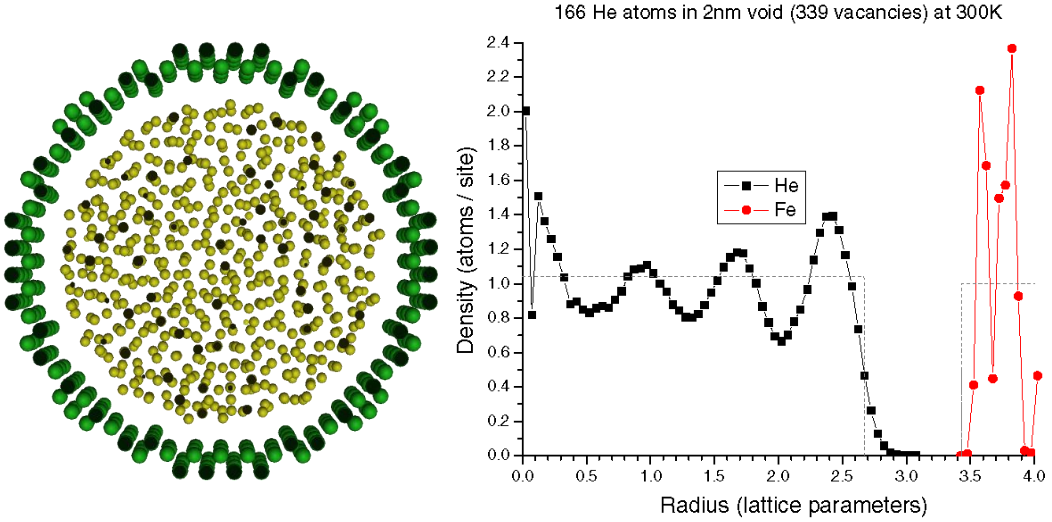

Figure 11 Illustration of how Fe-He interaction leads to the formation of a gas-free region near the bubble surface for a 2 nm diameter bubble

3.8 STEEL AND SiC COMPATIBILITY WITH Pb-Li AT 600-700°C

B. A. Pint (pintba@ornl.gov)and K. A. Unocic

OBJECTIVE

One proposed U.S. test blanket module for ITER uses ferritic-martensitic alloys with both eutectic Pb-Li and He coolants at ~475°C. In order for this blanket to operate at relevant power plant temperatures (up to 700°C in a DEMO-type reactor), several Pb-Li compatibility issues must be addressed. Some of the issues currently being investigated are the behavior of oxide dispersion strengthened (ODS) Fe-Cr alloys compared to conventional wrought material, the performance of Al-rich coatings to inhibit corrosion, and dissimilar material interaction between SiC and ferritic steel.

SUMMARY

The current work focuses on isothermal exposures in Pb-Li to provide an initial indication of compatibility. Long-term (1-5 kh) exposures in Pb-Li showed that ODS (including 14YWT) and wrought alloys had similar rates of mass loss. Similar exposures showed that thin Al-rich coatings on both types of alloys significantly reduced mass loss due to the formation of a thin, protective $LiAlO_2$ surface oxide layer. However, Al depletion from the coating was significant after 5,000h suggesting that either thicker coatings or Al-containing alloys will be needed for long-term performance at 700°C. Similar experiments at 600°C are in progress. Finally, to rule out dissimilar material interactions between SiC and steel, a series of capsule experiments were conducted at 500-700°C in Pb-Li. Only minor changes were observed; however, exposures in flowing Pb-Li are needed to confirm these observations.

PROGRESS

Several series of capsule experiments were completed to understand the long-term compatibility of candidate materials in Pb-Li at temperatures up to 700°C. Figure 12a shows the typical mass loss observed for ODS and wrought Fe-Cr alloys in Pb-Li at 700°C. Because Fe and Cr dissolve at similar rates, there is no effect of increasing the Cr content from ~8%Cr in Grade 92 ferritic-martensitic steel to 14% in ODS 14YWT. Figure 12a also shows that a thin Al-rich coating prevents mass loss for up to 5,000h at 700°C. The shaded area in Figure 12b shows a typical starting Al profile in the coating made by vapor deposition, used as a surrogate for a commercial coating process such as slurry aluminizing. After 5,000h, the Al content has been significantly depleted, suggesting a limited lifetime.

In any liquid metal system there is a possibility of dissimilar material interactions such as the transport of C between materials or the deposition of dissolved elements. Since SiC is less thermodynamically stable than many carbides, dissimilar material interactions were investigated between Fe and SiC by placing SiC specimens in SiC and mild steel capsules and doing the same for unalloyed Fe specimens. The mass change data was confounded by minor chipping of the SiC specimens, Figure 13. Nevertheless, the mass changes were relatively small and post-exposure characterization revealed only minor changes between the two types of capsule experiments.

FUTURE PLANS

Experiments are in progress to repeat the 5,000h coating experiments at 600°C and with a thicker starting coating at 700°C. There is limited additional benefit in continuing capsule testing and future work will focus on the construction of a flowing Pb-Li thermal convection loop.

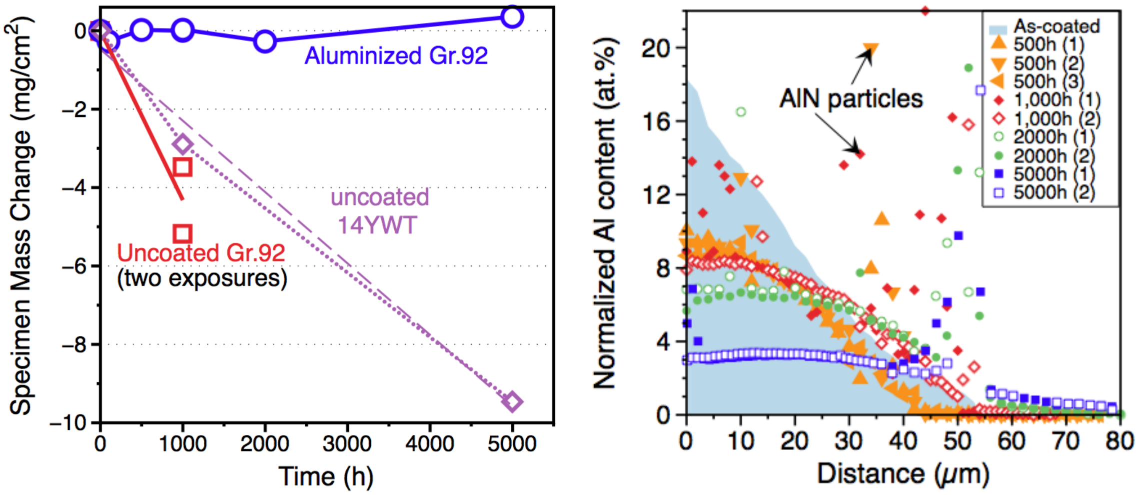

Figure 12. (a) Specimen mass change as a function of exposure time in Pb-Li at 700°C (b) Normalized Al content by electron probe micro analysis as a function of depth for coated Gr.92 specimens after exposure for 500h and 1,000h at 700°C in Pb-Li. Typical as-coated Al profile is shown in the shaded area.

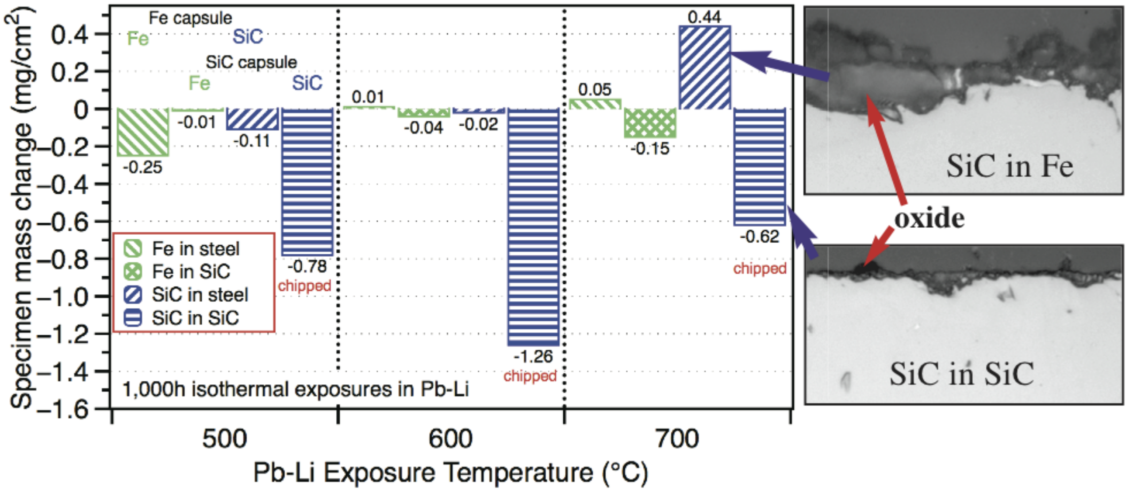

Figure 13. Specimen mass change from a series of capsule experiments with carbon steel or CVD SiC capsules and Fe and CVD SiC specimens exposed to Pb-Li for 1,000h at each temperature.

3.9 VANADIUM ALLOY MECHANICAL PROPERTIES AFTER EXPOSURE TO FLOWING LITHIUM

K. A. Unocic <unocicka@ornl.gov> and B. A. Pint

OBJECTIVE

A flowing Li monometallic thermal convection loop was operated with V-4Cr-4Ti tensile test specimens to confirm the alloy compatibility with Li. After exposure, the mechanical properties were evaluated and the microstructure characterized. The results were compared with other studies.

SUMMARY

The characterization of V-4Cr-4Ti tensile specimens exposed to flowing Li in a loop at temperatures 400-700°C was completed and comparisons were made to isothermal Li exposures and to thermal anneals at similar times and temperatures. The yield stress tended to increase with decreasing exposure temperature and the amplitude of the dynamic strain aging (DSA) serrations decreased in a similar trend. Because similar results can be obtained with thermal annealing, it appears the Li exposure had minimal effect on the mechanical properties and most of the observations can be explained by the thermal exposure. The microstructure changes due to the Li exposure, such as changes in the TiCON precipitates, were limited to the near surface region of the specimens where changes in the hardness were observed.

PROGRESS

The monometallic (tubing and specimens were all V-4Cr-4Ti) thermal convection loop was run for 2,355h in 2007 with a peak temperature of 700°C and the coldest location at ~400°C such that each specimen was exposed at a different temperature based on its location. This study was performed to complete the characterization of the loop-exposed SS-3 type tensile specimens that were tested at room temperature and 500°C in vacuum with base pressure of 10^{-6}Pa (10^{-8} Torr) at a strain rate of $10^{-3}s^{-1}$. Specimens of the same material were thermally annealed in quartz ampoules for 2,355h at 400, 550 and 700°C to determine the effect of time at temperature on the mechanical properties.

At 500°C, V-4Cr-4Ti typically shows DSA with serrations in the stress-strain curve. Figure 14 shows that the amplitude of the DSA serrations was a function of yield stress, which increased with decreasing exposure temperature. A similar relationship was observed with the ultimate tensile strength. For the higher temperature exposures (both with and without Li exposure), there was minimal effect on the DSA behavior. Of note is that the specimen annealed at 550°C had similar DSA behavior as the 459°C specimen from the bottom of the hot leg in the loop. A previous explanation was that the lower temperature exposures showed a lower amplitude because O was depleted in the presence of Li but little C and N update occurred. However, with a similar amplitude observed for the 550°C anneal, this explanation does not seem to be applicable. It appears more likely that the Li exposure had little effect on the properties and instead the thermal aging dominated the observed changes.

Microstructure changes after Li exposure appeared to be concentrated near the specimen surface. For example, the specimen exposed at 627°C in the loop is shown in Figure 15. The TEM images from the center of the specimen showed randomly distributed spherical Ti-rich particles and a relatively low hardness, <2.5GPa. In the outer ~40µm the hardness peaked at ~4.5GPa and a combination of precipitate free zones and much larger Ti-rich precipitates were observed in the outer ~100µm. EELS point analysis, Figure 15c, showed these precipitates contained C, O and N, as has been previously observed.

FUTURE PLANS

No further Li exposures are planned. This work is largely complete and one further anneal is in progress at 400°C to compare with the prior result.

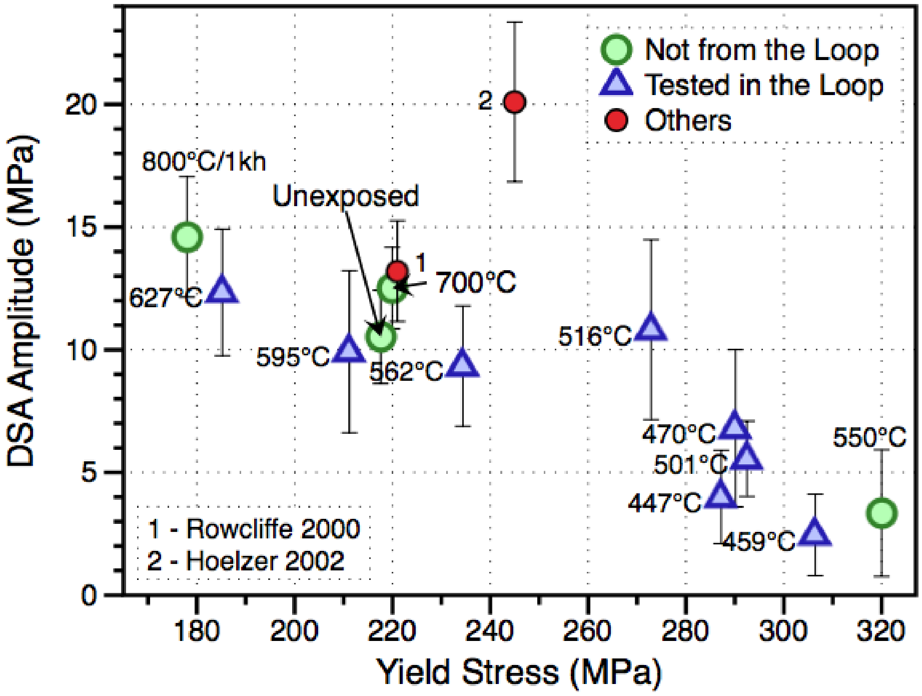

Figure 14. Amplitude of dynamic strain aging observed at 500°C as a function of 500°C yield stress for V-4Cr-4Ti specimens exposed in the Li loop, other exposures and other data from the literature. The bars note the standard deviation of the measurements.

[Figure 15 is on next page.]

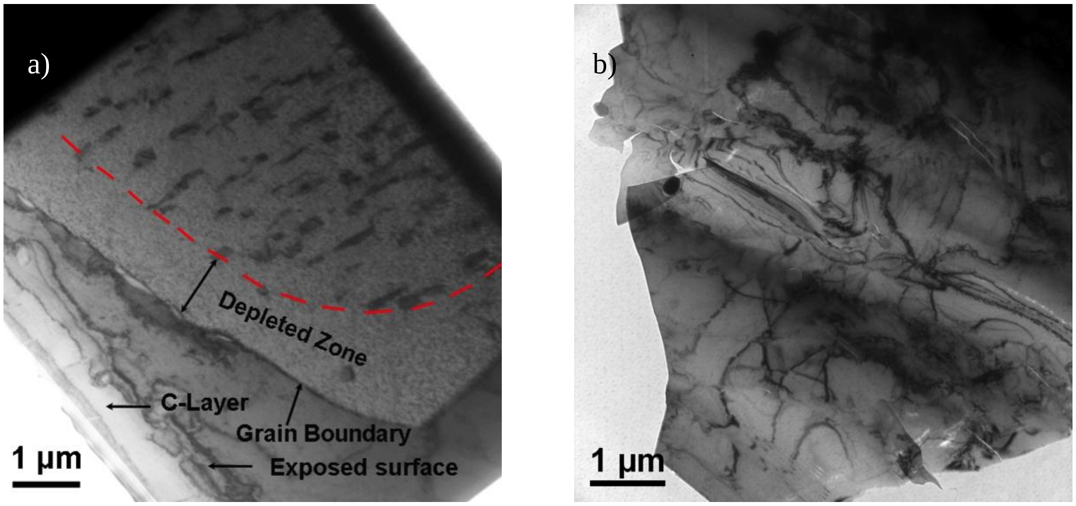

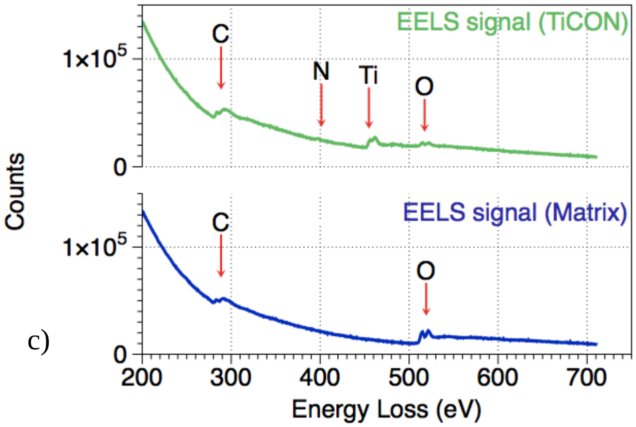

Figure 15. TEM image of the 627℃ loop specimen prepared from the near edge (a) and from the center (b) of the SS3 specimen (grip section). c) EELS spectra generated from the matrix and TiCON precipitate formed in the Li affected area.

3.10 MICROSTRUCTURAL CHARACTERIZATION OF FRICTION STIR WELDED ODS-14YWT FERRITIC ALLOY AND F82H TEMPERED MARTENSITIC STEEL

D.T. Hoelzer (hoelzerd@ornl.gov), K.A. Unocic and Z. Feng

PROJECT OVERVIEW

Friction stir welding (FSW) is an innovative solid-state joining technique that was invented in 1991. The basic concept of FSW involves plunging a specially designed tool that rotates at high speeds into the seam between work pieces and joining them by solid-state mixing involving high temperatures and extreme levels of plastic deformation. Since the FSW technique is based on the solid state joining concept, it has recently been applied to joining high performance oxide dispersion strengthened (ODS) alloys that have complex microstructures. In this study, specimens of the advanced ODS 14YWT ferritic alloy (Fe-14Cr-3W-0.4Ti-0.3Y_2O_3) were joined to itself and to an F82H steel plate by FSW. The 14YWT ferritic alloy contains a highly tailored microstructure that consists of a high concentration of 2-4 nm dia. Ti-, Y-, and O-enriched oxide particles, or nanoclusters (NC), and nano-size (<500 nm) grains. The primary goal of this study was to investigate the feasibility of successfully joining 14YWT by FSW without degrading the desired microstructural features and properties.

PROGRESS

The trial FSW run was performed with a polycrystalline boron nitride tool that resulted in overall good bonding between two 14YWT specimens and between 14YWT and F82H specimens as shown in Figure 16. No apparent interface was observed between the joined 14YWT specimens and the joined interface between the 14YWT and F82H specimens was sharply delineated. However, several large pores associated with a higher number density of smaller pores were present on the advancing side of the weld in the thermo-mechanically affected zone (TMAZ) of 14YWT. Further refinements in the FSW parameters should significantly reduce the porosity.

Grain size variations and the interfaces between joined specimens caused by FSW were clearly revealed using backscattered electron (BSE) imaging as shown in Figure 17. The grain size did not change appreciably between the unaffected zone (UAZ) and TMAZ of 14YWT on the retreating side (Figure 17a). However, a thin line of porosity was present along the interface that indicated consolidation of material by FSW was not optimized. On the advancing side, extensive material flow occurred toward the surface in the TMAZ of 14YWT (Figure 17b) Grains in this region increased in size by 2 to 3 times. The Vickers Hardness measurements decreased from 499 to 376 VHN (~20%) across the UAZ and TMAZ interface of 14YWT, but the decrease was attributed to the Hall-Petch effect.

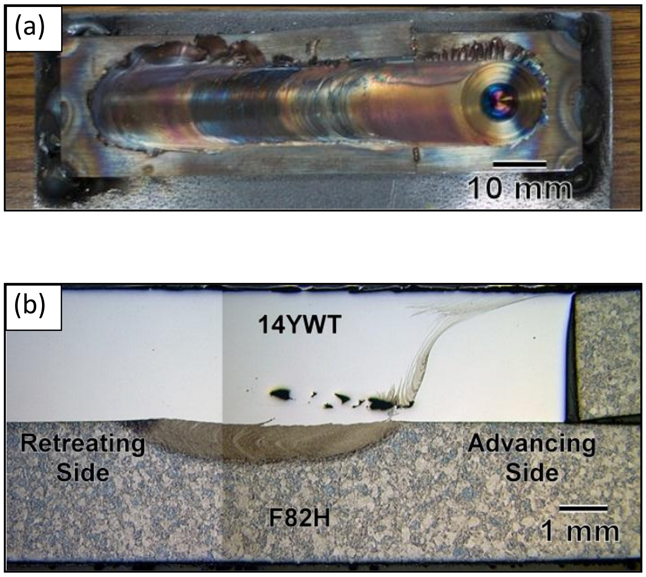

Figure 16. (a) Macro image of the FSW sample and (b) light micrograph showing the cross sectional view of the FSW 14YWT/F82H sample.

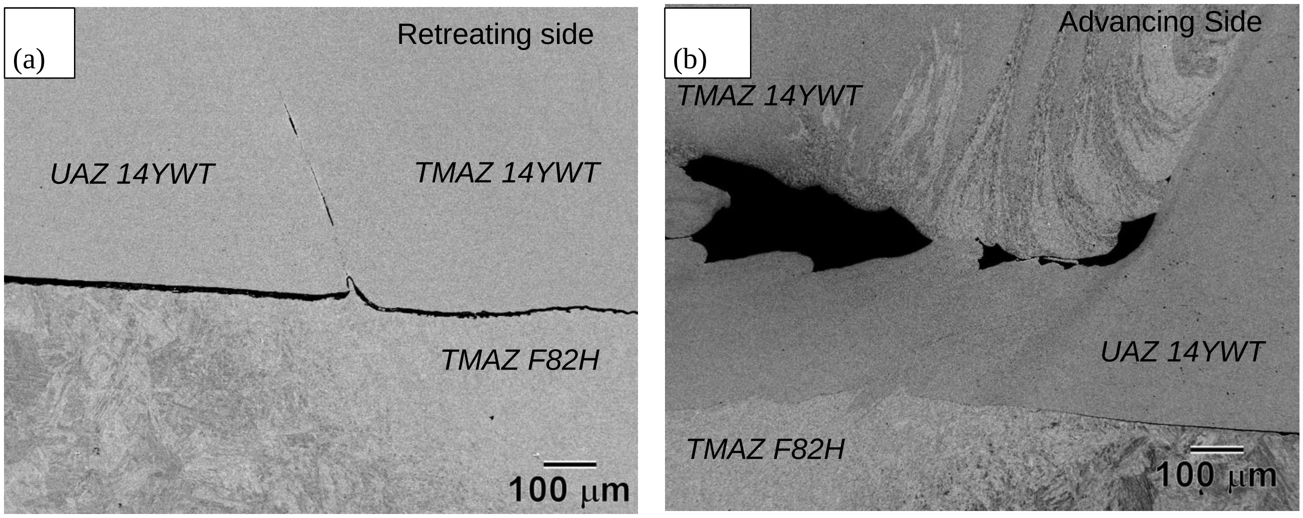

Figure 17. BSE micrographs showing the interfaces between HAZ and TMAZ of 14YWT and F82H specimens on the (a) retreating side and (b) advancing side of the friction stir weld zone.

A specimen was prepared by the lift-out and focused ion beam (FIB) method from the region consisting of the joined interface between the 14YWT specimens and analyzed by TEM and high-resolution STEM (scanning transmission electron microscopy) to determine the effect of FSW on the stability of the Ti-, Y-O-enriched nanoclusters. A significant result was that the Ti-, Y- O-enriched nanoclusters may have survived the high temperatures and severe deformation imposed during FSW as shown in Figure 18. The nanoclusters (and a few larger oxide particles) appear with dark contrast compared to the Fe-rich matrix. Nanoclusters as small as 2 nm are clearly resolved in the FSW zone of 14YWT.

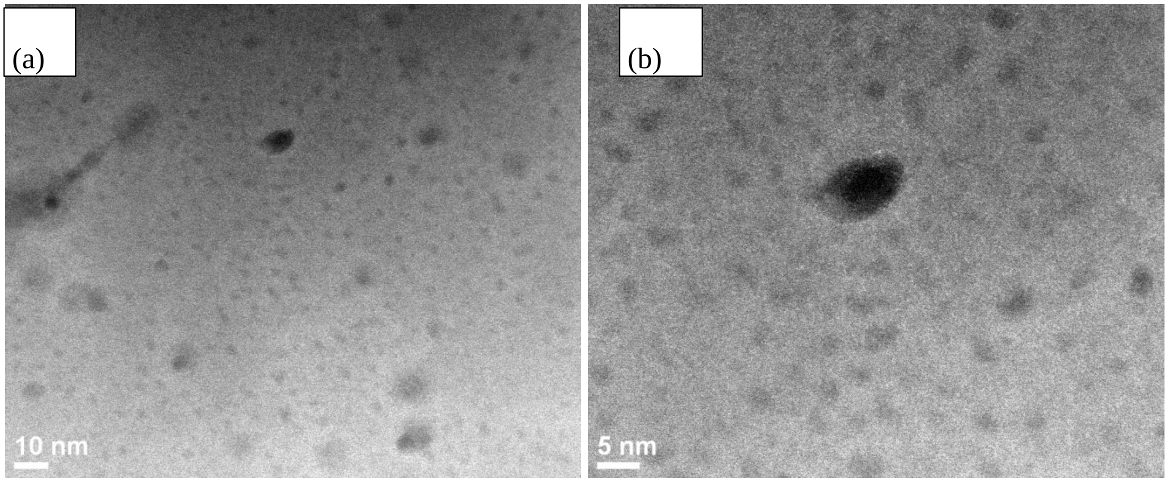

Figure 18. High number density of Ti-, Y- and O-enriched nanoclusters revealed by HAADF STEM near the joined interface between 14YWT specimens at (a) lower and (b) higher magnifications.

FUTURE PLANS

This effort will be combined with the new FOA project on friction stir welding to include additional research focused on optimization of FSW parameters to reduce the formation of porosity, enhance the consolidation of material, and improve FSW techniques for advanced ODS and reduced activation ferritic/martensitic steels. It will include detailed microstructural characterization studies of FSW weldments and weld-affected material.

3.11 FOA FRICTION STIR WELDING OF ODS ALLOYS

Zhili Feng (feng@ornl.gov), Zhenzhen Yu, D.T. Hoelzer, M.A. Sokolov, Lizhen Tan, Wei Zhang

OBJECTIVE

This project addresses the critical technology gap of joining oxide dispersion strengthened (ODS) steels, nanostructured ferritic alloys (NFAs), reduced-activation ferritic/martensitic (RAFM) steels, and dissimilar metal joining between ODS/NFAs and RAFM steels through friction stir welding technology. The research focuses on understanding the stability of the strengthening phases in the weld region, and the bonding mechanisms between dissimilar structural steels as a function of FSW process conditions.

PROGRESS

The funding for this project, selected through the FOA LAB 12-603, was recently received at ORNL. Work on this project started late in FY12. Effort was limited to discussion and locating materials. Initial planning has been completed, and the availability of ODS alloy has been established. Contact with the Helmholtz-Zentrum Geesthacht Centre for Materials and Coastal Research (GKSS) in Germany is exploring possible collaboration on in-situ small/wide angle neutron/synchrotron study of friction stir welding of ODS alloys. The tools for FSW experiments have been fabricated for welding trials planned in the first quarter of FY2013. The planned welding experiment will build on the experience gained in joining ODS alloys and our initial attempts on using FSW to join ODS/NFA and RAFM, reported in section 3.10, above.

PLANNED RESEARCH

Approach

We will take a science-based approach focused on the understanding and quantification of the fundamental variables of the processes that govern the bonding of materials, formation of weld defects,

and the microstructural evolution in FSW – the temperature (T), stress (σ), strain (ε), strain rate ($\dot{\varepsilon}$), and material flow. Through the use of advanced computational models and the unique and powerful in-situ neutron experiment, we seek to develop the predictive capability to quantitatively correlate these fundamental variables to the process parameters that an operator can control and adjust. It is also possible to quantify the microstructural changes in FSW – the stability of nanoclusters and oxides in ODS/NFAs and the phase transformation in RAFM steels – in terms of the phase transformation thermodynamics and kinetics theories that describe the phase changes as function of temperature and other energetic and kinetic variables. This new approach will also make it possible to proactively tailor the microstructures and properties through process condition changes based on the principles and theories of materials science and engineering. Figure 19 illustrates the overall scheme of the proposed approach.

Experimental Matrix

The R&D activities are organized into the following inter-related major tasks, structured for three years:

- Task 1 – FSW process development for similar and dissimilar weld
- Task 2 – Fundamental understanding of FSW process and microstructure/property relationship of ODS/NFAs and RAFM steels
- Task 3 – Microstructure and property characterization
- Task 4 – Producing and testing representative weld joints and welded components

The relationship among these tasks is illustrated in Figure 20.

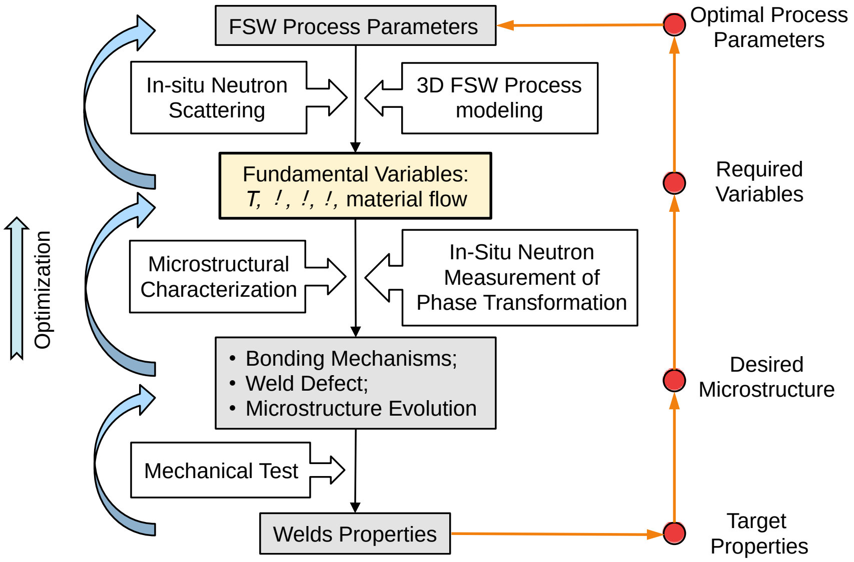

Figure 19.The proposed research approach based on fundamentals of FSW process.

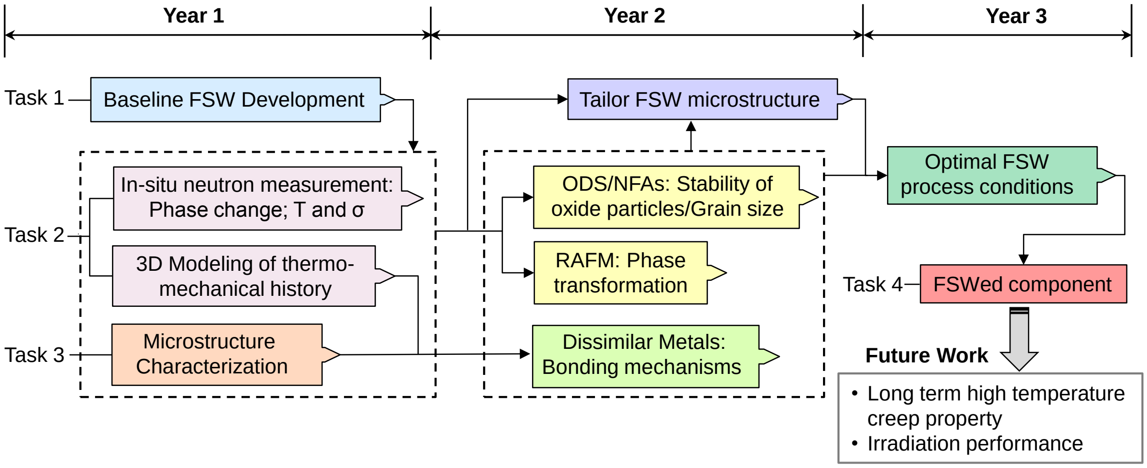

Figure 20. Relationship among the tasks and future testing plans.

4.0 COMPOSITE MATERIALS

4.1 IRRADIATION EFFECTS IN SiC AND SiC/SiC COMPOSITES

Y. Katoh (katohy@ornl.gov), L.L. Snead, K.J. Leonard, C. Shih, and P. Dou (ORNL), T. Hinoki and T. Koyanagi (Kyoto University), A. Hasegawa (Tohoku University), and T. Nozawa (JAEA)

OBJECTIVE

The overarching goal of this work is to advance fundamental understanding of the effects of neutron irradiation on silicon carbide (SiC) ceramics and SiC-based ceramic composites. FY-2012 emphasis was on irradiation creep of SiC and the effects of high-fluence and/or high temperature irradiation on SiC fiber – SiC matrix (SiC/SiC) composites.

SUMMARY

1) Phase I irradiation creep experiment on primary transient creep behavior of SiC and SiC/SiC completed with important fundamental findings related to the irradiation creep phenomena and the underlying mechanisms. Phase II experiment is currently in HFIR. Phase III experiment was developed.

2) Properties and microstructures of the reference SiC/SiC composite irradiated to >70 dpa at elevated temperatures were extensively examined. Important findings include lack of degradation of CVI SiC matrix and strength decrease for early generation near-stoichiometric SiC fiber Hi-Nicalon™ Type-S.

3) Properties of SiC/SiC composites with various SiC fibers and SiC matrices were examined following HFIR irradiation to ~6 dpa at 800 to 1,300ºC. Understanding of the effects of medium-fluence neutron irradiation at these temperatures was obtained for the advanced radiation-resistant SiC/SiC composites.

PROGRESS AND STATUS

Irradiation Creep of SiC

Experimental studies of irradiation creep of SiC ceramics and composites are part of the US-Japan TITAN collaboration. The program consists of three experimental phases: Phase I - primary transient creep using the bend stress relaxation (BSR) technique, Phase II - BSR creep of SiC ceramics and fibers beyond the primary transient, and Phase III - in-pile creep with gas-pressurization tensile loading.

Irradiation of the Phase I experiment was completed in 2011 with PIE and analysis of the results. This experiment measured the stress relaxation of elastically strained monolithic and composite SiC during irradiation up to ~2 dpa at intermediate (390 to 540°C) to high (790 to 1180°C) temperatures. The fractional stress relaxation appeared to be independent of initial stress, indicating a stress exponent of unity. The creep strain increased with the increasing fluence while the strain rate significantly decreased. A linear relationship between the creep strain and the transient swelling occurs due to irradiation defect accumulation, Figure 21. The apparent irradiation creep compliances for silicon carbide are substantially smaller than those associated with metals and alloys. Moreover, this observation and supporting analysis implied a small steady-state creep compliance at higher fluence levels for intermediate temperatures. Microstructural examination suggested that incoherent grain boundaries play a major role in determining the primary transient irradiation creep of these materials at high temperatures with a potential additional contribution from basal slip at very high temperatures. The unidirectional composite specimens exhibited slightly smaller creep strains than the matrix material does, indicating a contribution from more creep resistant fibers.

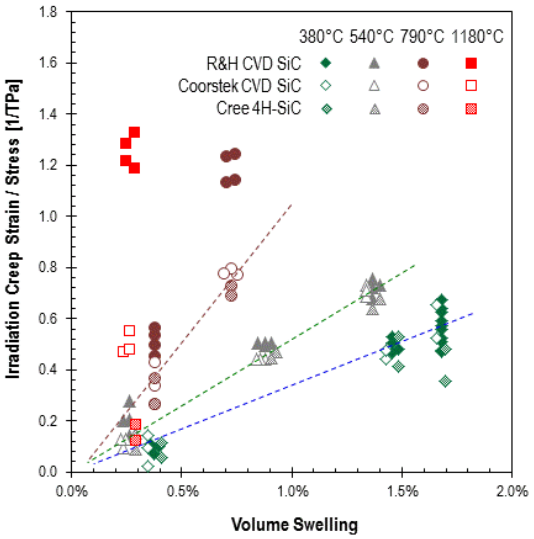

Figure 21: Stress-normalized irradiation creep strain vs. volume swelling indicating linear swelling - irradiation creep coupling at 380 and 540°C. Some data points are horizontally offset for visibility.

The Phase II experiments irradiate specimens of monolithic SiC and commercial and developmental near-stoichiometric SiC fibers in BSR fixture assemblies in HFIR at 300 to 1,200ºC. The fluence levels are 10 to 20 dpa for the monolithic specimens and 1 to 20 dpa for fiber specimens. During FY-2012, six rabbit capsules for irradiation to 1 or 10 dpa completed irradiation and five capsules for irradiation to 10 or 20 dpa remain in reactor to achieve the planned fluence levels in early FY-2013.

An in-pile creep experiment that utilizes the force from a gas-pressurized metallic bellows to apply tensile loading to the test specimen was developed as a part of the Phase II experiment. A major technical challenge of accommodating the complex mechanism to apply tensile stress of an adequate magnitude from an internally pressurized metallic bellows in a small rabbit capsule while maintaining the appropriate temperatures for the specimen and the bellows was overcome through an innovative design employing a molybdenum alloy load transfer frame and an internal shell structure that surrounds the test specimen and controls the heat generation and transfer.

High Fluence (>70 dpa) Irradiation Effects on SiC/SiC

The effects of high fluence neutron irradiation were determined for the reference radiation-resistant grade SiC/SiC composite, Hi-Nicalon™ Type-S, pyrocarbon (PyC)/SiC multilayered-interphase, chemically vapor-infiltrated (CVI) SiC-matrix composite. The flexural strength, fracture mode, elastic modulus, swelling, and thermal conductivity of this material after neutron irradiation to >70 dpa at 300 to 800ºC in HFIR were determined. The fluence levels are considered to correspond or exceed the life time fluence for the blanket structures and internals of fusion power reactors except the near plasma-facing surfaces including the first wall.

Most notably, the effects of irradiation to these high fluence levels on swelling, thermal conductivity, and elastic modulus of this composite indicated no further changes beyond those that occur at a few dpa, proving the true saturation in these properties. The composite material retained the pre-irradiation proportional limit stress (PLS), and the non-linear fracture mode after irradiation at 800°C. The lack of degradation in PLS implies the strength retention for the CVI SiC matrix, which essentially is high purity polycrystalline SiC. However, the ultimate flexural strength is reduced after irradiation to ~70 dpa at all temperatures with increased degradation with decreasing irradiation temperature (Figure 22). This indicates the degradation of the reinforcing fibers, because the ultimate failure stress for the continuous fiber-reinforced ceramic composites is determined solely by the statistical strength properties of the fibers. Moreover, the fracture mode showed an obvious transition from pseudo-ductile composite failure to brittle failure during irradiation at 300°C. These results presented an imminent need of further study to identify the cause and the mechanism for this irradiation-induced transition in failure mode at relatively low irradiation temperatures and the degradation of fiber strength.

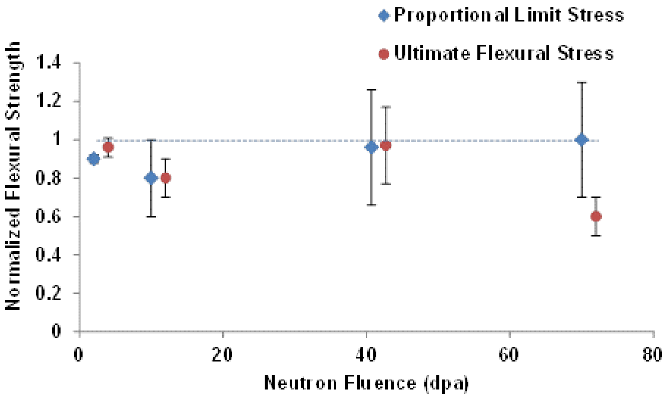

Figure 22. Fluence dependence of ultimate flexural strength of Hi-Nicalon™ Type-S, CVI SiC matrix composites irradiated at 800°C.

High Temperature Irradiation Effects

The PIE of various SiC ceramics and composite specimens irradiated in the US-Japan collaborative RB-18J experiment continued. Previous evaluation of baseline properties was supplemented by extended TEM examination, thermal conductivity determination at elevated temperatures, and thermal expansivity determination.

The 18J experiment irradiated various SiC/SiC composites consisting of near-stoichiometric SiC fibers, stoichiometric and fully crystalline SiC matrices, with PyC or multilayered PyC/SiC interphase to a fluence of ~6 dpa at 800 to 1,300ºC. The results generally indicated the lack of detrimental irradiation effects on the advanced SiC/SiC composites, except for the thermal conductivity decrease that saturates during early irradiation. The results are included in a draft paper that summarizes the properties of these composites in unirradiated and irradiated conditions.

As a part of the 18J experiment, monolithic 3C-SiC specimens were neutron irradiated with the simultaneous helium injection using the in-situ helium injection technique. The initial transmission electron microscopy examination revealed extensive cavity production, presumably subcritical helium bubbles, in the in-situ helium-injected specimen irradiated at 1,300ºC.

FUTURE PLANS

Complete the Phase II creep experiment and PIE and the Phase III gas-pressure-driven tensile creep experiment, to define the steady-state irradiation creep behavior of SiC ceramics and composites. The effects of high fluence neutron irradiation continue to be the priority research topic for SiC ceramics and composites. PIE of the Hi-Nicalon™ Type-S CVI composites irradiated to >70 dpa will continue to identify the causes of observed mechanical property degradation. Composite systems with alternative SiC fibers will be examined. A new irradiation experiment to evaluate the irradiation effects on two-dimensional woven fabric composite specimens and the unidirectional model composite specimens with the Hi-Nicalon™ Type-S and the Tyranno™-SA3 fibers will initiate irradiation. Finally, detailed microstructural examination will be carried out on the in-situ helium-injected specimens.

4.2 MOLECULAR DYNAMICS MODELING OF 10 AND 50 keV CASCADES IN 3C-SiC

G. D. Samolyuk (samolyukgd@ornl.gov), Y. N. Osetskiy and R. E. Stoller

OBJECTIVE

The objective of this research is to investigate the damage in 3C-SiC induced at fusion irradiation condition and describes microscopic origin of these experimentally observed phenomena.

PROGRESS

In fusion service irradiation will change the microstructure and hence the properties of 3C-SiC. Understanding the details of this process is necessary for predicting changes, estimating component lifetimes, and developing improved materials. Experimental studies have demonstrated that depending on the structural material composition and particular conditions such phenomena as amortization, swelling, changes in physical and mechanical properties were observed.

We used the LAMMPS (Large-scale Atomic/Molecular Massively Parallel Simulator, see http://lammps.sandia.gov) code for atomistic molecular dynamics simulations. The interactions between atoms were described by a hybrid Tersoff/ZBL potential. Simulation cells containing from 80x80x80 unit cells (409,600 atoms) were used for 10 keV primary knock-on atom (PKA) kinetic energy cascades and 120x120x120 unit cells (13,824,000 atoms) for 50 keV PKA cascades. The initial system was equilibrated for 2 picoseconds with time steps of 0.1 femtosecond. Each cascade was initiated by giving a Si atom the kinetic energy of 10 or 50 keV while holding zero total momentum. The cascades evolved for 20 ps and the time step is modified such that the distance traveled by the fastest particle in the system is less than 0.014 Å. Constant volume is held through the iteration and the lattice parameter is chosen for zero system pressure in equilibrium at a particular temperature. The Wigner-Seitz cell analysis method was used to determine defects in the modeling system.

A code was developed for post processing the Molecular Dynamic (MD) results. We simulated cascades produced by 10 keV kinetic energy at temperatures of 300, 600, 900, 1200 and 1500 K (8 cascades at each temperature) and 50 keV PKA kinetic energy at temperatures of 600 and 1500 K (2 cascades at each temperature). Similar to previous results, it was observed that main defects in 3C-SiC corresponds to carbon interstitials (C(I)) and carbon vacancies (C(V)) distributed as shown in Figure 23. The temperature dependence of the number of defects is weak. 30 % of defects accumulated in clusters of size ~20 defects which is usually interpreted as an amorphous domain. 20% of all defects stay in pair clusters. Most pair clusters corresponds to C(I)-C(V) pairs with averaged distance between vacancy and interstitial less than one lattice parameter. Surprisingly, these defects do not annihilate with annealing. In order to investigate the origin of this stability we calculated the barrier to C atom migration from its initial position [1/4, 1/4, 1/4] to a metastable position [3/4, 3/4, 3/4] along [111] direction. The resulting configuration corresponds to a C(I)-C(V) distance between defects of $\sqrt{3}/2\ a_o$. The barrier strength obtained has a non-physically large value (~ 10 eV, Figure 23) for both Tersoff (shown green in Figure 24) and MEAM (red) potentials, whereas first principles calculations give a value equal to 0.2 eV (shown in purple). This large barrier suppresses any migration in the modeling system. In 2002 Gao and Weber (GW) proposed a potential which reasonable describes interstitial diffusion in SiC, however the migration barrier calculated with this potential is too small (blue in Figure 24) and is still far from the first principles result.

FUTURE WORK

Development of new interatomic potentials is needed for further investigation of radiation damage in SiC.

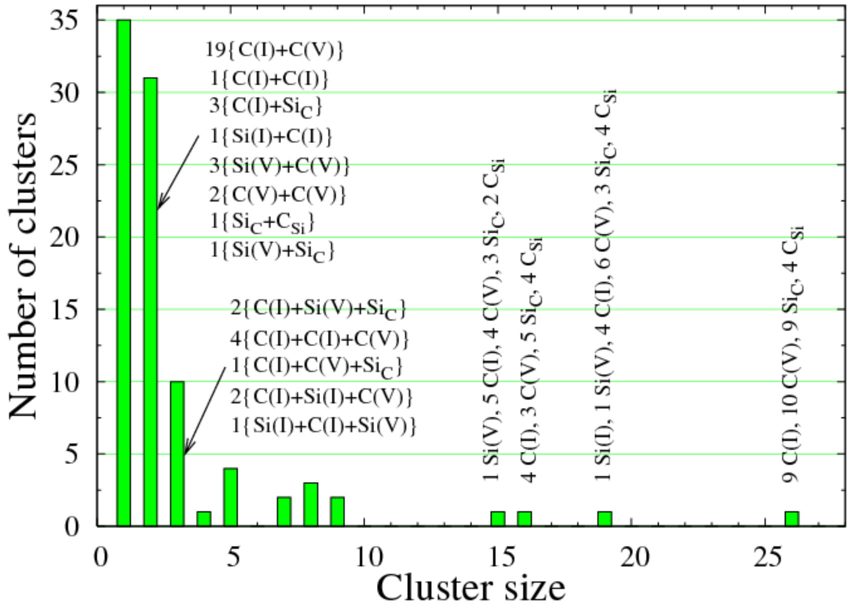

Figure 23. Defect clusters distribution in 10 keV cascade after 20 ps at 300 K.

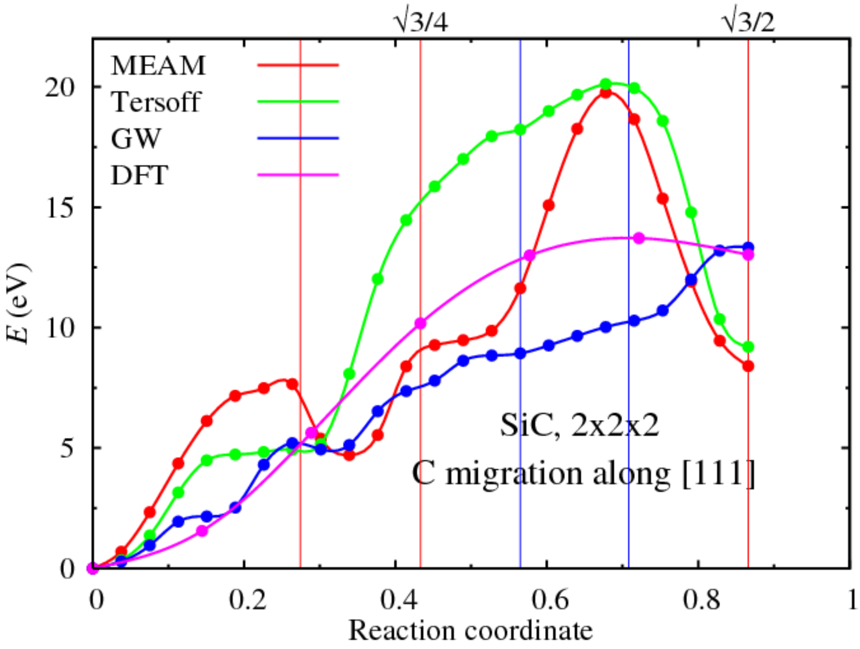

Figure 24. The potential associated with C atom migration from position [1/4, 1/4, 1/4] to metastable position [3/4, 3/4, 3/4] along [111] direction, calculated with three interatomic potential and from first principles.

4.3 JOINING OF SILICON CARBIDE

Y. Katoh (katohy@ornl.gov) and L.L. Snead, T. Hinoki (Kyoto University) T. Koyanagi (Kyoto), M. Ferraris (Politecnico di Torino), and C.H. Henager, Jr. (PNNL)

OBJECTIVE

The objective of this work is to develop a fundamental understanding of the issues related to SiC-SiC joining and identify potentially viable joining methods. An initial assessment of low fluence neutron irradiation effects on joint integrity was attempted. Development of the test methods appropriate for use with small specimens is part of this task.

SUMMARY

Development and evaluation of low-activation joining technologies for silicon carbide ceramics and composites for use in fusion and fission reactors were carried out as a collaborative project of the U.S. Fusion Materials Program, Politecnico di Torino, and Kyoto University. Specifically, following the successful development of a torsional shear test method adequate for use with irradiated miniature specimens, shear test specimens of silicon carbide ceramics or composites joined by titanium diffusion bonding, transient eutectic-phase silicon carbide joining, calcia-alumina glass-ceramic joining, or titanium silicon carbide MAX phase joining were prepared, the unirradiated properties and microstructures characterized, and then evaluated following neutron irradiation to 3 to 4 dpa at 500ºC in HFIR. Encouraging results were obtained from the initial irradiation experiment, showing a complete lack of detrimental irradiation effects on the joint strength.

PROGRESS AND STATUS

Joining Methods

A critical need and lack of methodologies to join silicon carbide composite for fusion applications of SiC ceramics has been identified. While a number of conventional and advanced techniques are available to join SiC, or SiC/SiC to itself or other materials, it is their performance in a fusion environment that is unknown. Available joining methods include diffusion bonding using various active fillers, transient eutectic phase routes such as nano-infiltration and transient eutectic-phase (NITE) process, glass-ceramic joining, brazing, SiC reaction bonding, MAX-phase joining, preceramic polymer routes, transient liquid metal joining, and selected area chemical vapor deposition (CVD). Primary considerations specific to the fusion energy application include the resistance to neutron irradiation, adequate strength and reliability, compatibility of the processing condition with design requirement, chemical compatibility with the specific operating environment, and the ability to satisfy the hermeticity requirement. In the current work, diffusion bonding using titanium filler, NITE joining using slurry or tape approach, calcia-alumina glass-ceramic joining, and Ti3SiC2 MAX phase reaction bonding were evaluated. The joint specimens for evaluation were produced using either CVD SiC, NITE-SiC, or Tyranno™-SA3 / NITE SiC-matrix composite as the base material to be bonded. Joint samples of adequate quality were produced, with an example shown in Figure 25.

Methods for Strength Determination

One of the challenges faced in the development of ceramic composite joints is the lack of adequate standard test methods for reliable and reproducible mechanical properties. This is particularly the case when limitations are imposed by specimen preparation, test article geometry or dimensions. Practically, simple methods such as cantilever shear, double-notched shear, and asymmetric four point flexure are frequently adopted for shear strength determination. However, none of those test methods is capable of producing reasonably pure shear stress state within the joint and the interfacing volumes. Torsion loading of solid specimens was identified as one of the appropriate test methods that are capable of providing true shear strength in miniature specimens of ceramic joints.

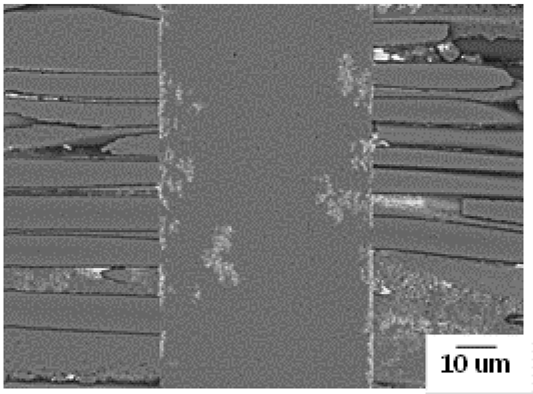

Figure 25. Cross-sectional backscattered electron image of transient eutectic phase-joined SiC/SiC composite showing solid bonding between the joint layer and both SiC matrix and SiC fibers.

A torsional shear test method using solid cross-section specimens was developed. The objective was to develop a small specimen test technology (SSTT) so that reproducible and reliable shear strength values are obtained in a true shear stress state with specimen sizes compatible with the internal dimensions of the small HFIR "rabbit" irradiation capsules .

Among a variety of specimen geometries and sizes considered, test specimens specifically with the 6 mm x 6 mm x 3 mm envelope dimensions, 1 mm curvature diameter for the fillet section, and square grip sections were chosen based on extensive finite element analysis and experimental validation. Test instruments were designed adopting compliant socket fillers and flexibly-coupled self-alignment mechanism and built at Politecnico di Torino, ORNL and Kyoto University to enable inter-laboratory comparative tests.

Test specimens of monolithic and composite SiC joined by various techniques were prepared. It was demonstrated that high quality specimens could be produced either by machining of joined plates or through joining of machined one-half specimens. The initial inter-laboratory comparative study proved excellent reproducibility for the strength of epoxy-joined CVD SiC samples and 3003 aluminum alloy calibration specimens. Based on these encouraging results, development of a full-consensus test standard for the torsional shear strength of ceramic joints has been initiated in the ASTM Committee C28 on Advanced Ceramics.

The SiC joint specimens were tested for torsional shear strength, with testing primarily at ORNL. All the unirradiated specimens exhibited adequate strength, of order ~100 MPa for the titanium diffusion bonded, MAX-phase bonded, and CA glass-ceramic bonded specimens, ~150 MPa for the green sheet-based NITE joints, and over 200 MPa for the slurry-based NITE joints. Note that these values do not necessarily represent the strength of joints themselves but are apparent shear failure stresses for the joined test article, as the failure did not necessarily occur within the joint layer.

Irradiation Effects

A series of irradiation experiments was carried out in the target zone of HFIR using rabbit irradiation capsules. A capsule design developed specifically for the miniature solid hourglass torsion specimens accommodated 16 specimens, typically 4 replicate specimens each for 4 material variations, in a single capsule. Each capsule contained SiC temperature monitors for post-irradiation determination of irradiation temperature. Irradiation was to 3 to 4 x 10^{25} n/m^2 (E>0.1 MeV) at 500 and 800°C. Results have been obtained for the 500°C irradiation, with post-irradiation examination in the ORNL LAMDA laboratory. The most striking result was the complete lack of significant degradation in shear strength upon irradiation for all the joint test articles that have been tested so far, namely the titanium diffusion bonded, CA glass-ceramic bonded, and NITE-bonded (slurry or tape) CVD SiC, NTIE-SiC, or NITE-SiC/SiC, as shown in Figure 26. This work has shown that selected methods of joining whereby the active joint material promotes an essentially stoichiometric joint appears to produce a joined structure of SiC ceramics and composites of adequate strength that is maintained during irradiation at 500ºC to at least a few dpa.

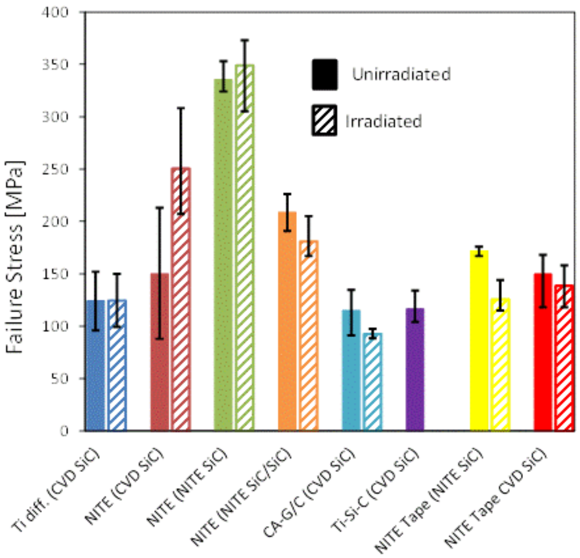

Figure 26. Shear strength of non-irradiated and 500°C, 3 to 4 dpa-irradiated SiC joint specimens prepared in this study, as determined by torsional shear test developed in this study.

FUTURE PLANS

The remaining 800ºC capsule have completed irradiation in HFIR and transferred for disassembly. The specimens will be tested for shear strength in LAMDA. Detailed microstructural examination will be performed for neutron-irradiated specimens to evaluate the structural integrity and chemical stability.

4.4 FOA - SILICON CARBIDE JOINING TECHNOLOGY FOR FUSION ENERGY APPLICATIONS

Y. Katoh (katohy@ornl.gov), J.O. Kiggans, T. Cheng, L.L. Snead, C.H. Henager, Jr. (PNNL), M. Ferraris (Politecnico di Torino), T. Hinoki (Kyoto University)

OBJECTIVE

The objective of this new project is to develop technologies for joining silicon carbide (SiC) composites for fusion energy applications.

SUMMARY

A technical program for the development of SiC joining technology for fusion energy applications was initiated as a new project supported by the U.S. Fusion Materials Program. In the base program on composites the issues and challenges related to irradiated SiC joints were defined and promising joint candidates identified. The project will develop technologies for joining SiC composites, primarily for fusion blanket integration, advancing the TRL level of the SiC composite system. The work scope consists of three task elements: 1) development of technology for SiC to SiC joining, 2) development of standardized test methods, and 3) irradiation effects study of the down-selected joining technology.

PROGRESS AND STATUS

Proposal and Technical Plan Overview

With the fabrication technology and the baseline irradiation performance established, joining technology development is among the remaining critical requirements for SiC composites. Various design concepts for helium- or lead lithium-cooled ceramic structure blankets assume extensive joining of SiC composite components. Assembling SiC-based flow channel inserts for the dual-cooled lead-lithium blanket will also depend on developing a joining technology. However, no joining methods for SiC ceramics or composites have proven adequate for use in the fusion blanket environment. Moreover, no appropriate ASTM or other accepted test methods are available for evaluating ceramic joints, making any international development effort in this area difficult. This project will develop the needed technologies, with a work scope consisting of three task elements.

Task 1 – Joining Technology: Adequate technologies for joining silicon carbide composites will be developed. In the previous effort in the U.S program collaborating with international partners, five joining techniques (4 pressurized and 1 pressureless) were selected for study from more than ten candidates, based primarily on predicted irradiation stability and currently available process and performance information. The new project will re-evaluate the potential joining techniques based on a) the latest information on emerging technologies, b) result from an initial low dose irradiation study, and c) input from the blanket design community on performance requirements. A limited number of promising techniques and unexplored yet promising concepts will be selected for further developed.

Task 2 – Test Method Development: Development of a consensus test standard for the evaluation of shear strength of ceramic composite joints will be pursued. Based on our finding that the commonly used single lap shear test provides unacceptably erroneous joint strength, development of a solid hourglass torsion technique was initiated by the fusion ceramic community. This task will validate at least one test method, likely the hourglass torsion test, for true shear strength evaluation of ceramic composite joints. This will be developed into a standard procedure in collaboration with ASTM Committee C28 on Advanced Ceramics complete with round-robin international testing. Modification of the current hourglass design is anticipated based on current unirradiated test results.

Task 3 – Irradiation Effects Study for Down-selected Technologies: Effects of neutron irradiation on selected joints will be determined. Joining techniques with positive low dose irradiation performance in the current TITAN campaign will be irradiated to extended doses in a range of temperatures. Joining techniques which are newly selected based on non-irradiation performance will be subjected to limited low dose irradiations in HFIR, , and the irradiated joint specimens will be evaluated for mechanical properties, phase stability, and microstructures.

Development of Joining Methods

The most promising joining methods were selected and processing of the highest priority joints was initiated at ORNL. The initial effort will establish the methods and procedures of processing for improved repeatability and scalability by titanium diffusion bonding, molybdenum diffusion bonding, and slurry-based NITE joining. Examples of the microstructures obtained in the early processing effort are shown in Figure 27. The titanium diffusion bonding produced a joint layer of TiC containing finely scattered MAX phase with the apparent double-notched shear strength of 98 (±9) MPa, achieving reasonable strength for this system. The molybdenum diffusion bonding resulted in the silicide-carbide tri-layered joint with substantial porosity in the midplane. The shear strength appeared to be 55 (±15) MPa, indicating the need for optimizing the processing condition.

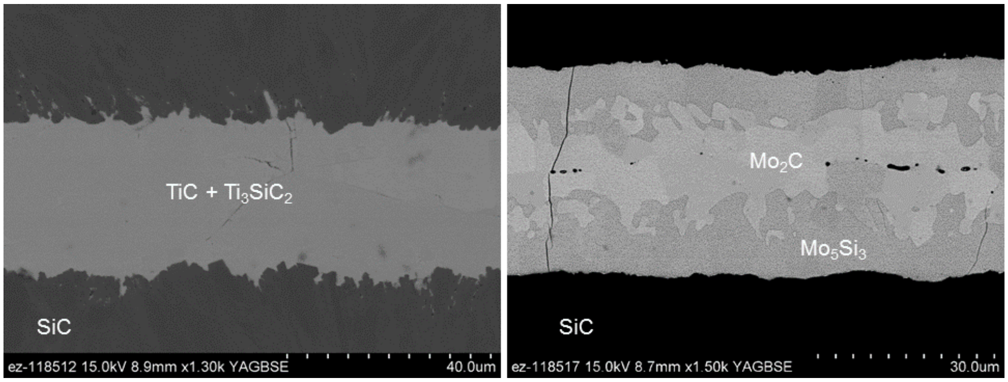

Figure 27. Backscattered electron images of diffusion bonded SiC with active metal inserts: titanium (left) and molybdenum (right).

Test Standards

Discussion on development of standard test methods for strength of the ceramic joints was initiated in ASTM Committee C28 on Advanced Ceramics. The working group on ceramic composites for nuclear applications is coordinating this task, and a task group on joint strength test methods is currently being populated.

Irradiation Effects Study

Plans for an irradiation study in HFIR have been drafted. The irradiation experiment will evaluate the effects of neutron irradiation to higher fluence levels than in the previous experiment up to a temperature of 1,000ºC, relevant to advanced SiC-based blanket concept designs. The miniature solid hourglass torsion test specimens developed in the previous fusion work will be adopted.

FUTURE PLANS

Joint materials for evaluation will be fabricated and test specimens prepared and characterized. This will include continuation of process development and optimization by ORNL and the collaborators. The irradiation effect study will continue. The ASTM Committee C28 task group on ceramic joint strength test methods will define the priorities for standard development and draft the first test standard. The ORNL researchers and the collaborators will participate by performing the supporting research and experiment.

4.5 SiC COMPATIBILITY WITH Pb-Li

B. A. Pint (pintba@ornl.gov)

The limited work on this topic is covered in Section 3.9

5.0 HIGH HEAT FLUX AND PLASMA FACING MATERIALS

5.1 IRRADIATION EFFECTS IN TUNGSTEN MATERIALS

T.S. Byun (byunts@ornl.gov), M.A. Fechter, Y. Katoh, M. Rieth (KIT)

OBJECTIVE

While tungsten has been studied for nuclear application for decades, the irradiation effects fundamentals are poorly understood, in large part due to the extreme sensitivity of properties to material processing. The objective of this study is to understand the behavior of pure tungsten (W) and tungsten materials before and after irradiation and to provide feedbacks for developing plasma facing materials/components with improved toughness and ductility.

SUMMARY

This radiation effects study on tungsten (W) and tungsten materials was initiated in FY2012, in collaboration with KIT. Irradiation of miniature bar and tensile specimens in HFIR is currently underway. Post-irradiation evaluation (PIE) has been planned and preparations made.

PROGRESS

Irradiation Experiment

Table 4lists the five tungsten materials chosen for the irradiation experiment: single crystal W with [100] orientation, single crystal W with [110] orientation, 0.1 mm thick W foil with texture (as-rolled), rolled and 1800°C-annealed W foil, and 0.5 mm thick W/Cu laminate material. The specimen types selected were 0.1 × 4 × 16 mm coupons and SS-J2 tensile specimens, which also have 4 × 16 mm outer profile but 0.5 mm in thickness. Figure 28 displays these types of specimens (the corner cut in the second coupon was to separate rolled and annealed specimens). Note that this SS-J2 tensile specimen design does not have pin holes in the grip section and will be tested using a shoulder loading grip, Figure 29. This collaboration is between ORNL and Karlsruhe Institute of Technology (KIT), Germany. KIT provided their foil tungsten and W/Cu laminate materials, i.e., the tungsten materials 3 – 5 in Table 4. These tungsten materials are included in 22 HFIR capsules. Table 5 summarizes the HFIR irradiation campaign, planned to achieve neutron fluence 0.02 to 20 × 10^{25} n/m^2 (E>0.1 MeV) four irradiation temperatures.

FUTURE PLANS

Mechanical Property

After irradiation these specimens will be used for uniaxial tensile and small punch tests to obtain mechanical property data including strength, ductility, and ductile-brittle transition temperature (DBTT), after which microscopy will be performed. Tensile tests will be carried out using the shoulder loading grip set in the Instron testing machine equipped with vacuum furnace in 3025E hotcell facility. After the tensile tests have provided key mechanical properties, the tested specimens will be used for microstructural investigations. The irradiated coupon specimens will be used for small punch (or ball indentation) testing in the same tensile machine using a jig designed for clamping flat specimens. This will provide load-displacement curves, and multiple (2 – 3) measurements can be made on each coupon specimen. The strain energy to failure is calculated to construct a strain energy versus temperature curve for each irradiation condition and material. At least eight tests will be carried out to obtain a full energy transition curve and to determine DBTT.

Microstructural Examination

Using either tested or untested specimens, as available, extended TEM studies will be performed for characterizing defect and deformation microstructures in irradiated materials. The ultimate goal of this study is to explore embrittlement mechanisms and then to propose improvement in W material design and processing. Small pieces will be cut from the tested tensile specimens and transmission electron microscopy (TEM) samples will be fabricated in a Focused Ion Beam (FIB) machine in the low activation

(LAMDA) lab. This fundamental study of radiation induced embrittlement and ductilization will be closely cooperating with computational simulation activities in the program.

Table 4. Tungsten materials and specimens being irradiated in HFIR

Material	Description	Specimen Type	No. of Specimens
1. Single Crystal W [100]	Crystal orientation [100]	Tensile SS-J3	33
2. Single Crystal W [110]	Crystal orientation [110]	Tensile SS-J3	33
3. Foil W	As-rolled	Coupon	170
4. Foil W	Rolled and annealed	Coupon	170
5. Laminate W	Rolled W/Cu lamellar composite	Tensile SS-J3	34

Table 5. Irradiation conditions for the tungsten specimens being irradiated in HFIR

Irradiation Temp. [°C]	Fast Fluence ($\times 10^{25}$ n/m^2) (E>0.1 MeV)	No. of Tensile Specimens per Capsule	No. of Coupons per Capsule	Capsule I.Ds
80 – 100	0.02 – 20	8	10	PC-1 to 5
300	0.02 – 12	6	20	TB-300-1 to 4; T9G-11 & 13
500	0.1 – 12	6	10	TB-500-1 to 3; T9C-14 & 15
650	0.1 – 20	6	20	TB-650-1 to 4; T9C-4 & 24

Figure 28. Specimen types of tungsten materials being irradiated in HFIR. Note that the SS-J2 specimen has 16 mm length (5 mm gage section length) × 0.5 mm thickness × 4 mm head width (1.2 mm gage section width). RD stands for rolling direction in rolled specimens.

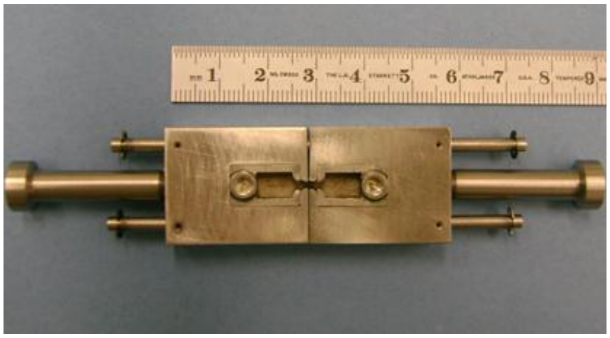

Figure 29. A cradle type grip for SS-J tensile specimens. This grip set was developed for shoulder loading as well as for easy loading of thin miniature specimens in hotcell.

5.2 HIGH FRACTURE TOUGHNESS IN A TUNGSTEN ALLOY

Mikhail Sokolov, sokolovm@ornl.gov

OBJECTIVE

Certain tungsten alloys have been expected to have high fracture toughness, in contrast to the typical poor toughness of commercial wrought tungsten materials. The goal of this experiment was to measure fracture toughness of a W-25 Re alloy, known to have improved tensile ductility.

ACCOMPLISHMENTS

Every discussion of the use of tungsten in fusion applications cites its desirable attributes, including a very high melting point, good thermal conductivity, low sputtering yield and low activation resulting in simplified long-term waste disposal. Desired applications are plasma facing components and structural material in plasma facing components. However, tungsten has not been considered for use as an engineering material for many reasons, the most serious being its brittle nature over a wide range of application temperatures. The addition of rhenium is known to improve the ductility of tungsten alloys but the data related to the effect on the important fracture properties are quite limited. As part of recent work fracture toughness and ductility of a plate of W-25%Re alloy were measured at ORNL over a wide range of temperature. Precracked 3-point bend tests were used to generate fracture toughness values and tensile properties were measured on small sheet specimens.

This W-25%Re alloy exhibited very good strength and ductility over a wide temperature range as shown in Figure 30. (Over a substantial part of this temperature range unalloyed tungsten would show almost no ductility.) The good ductility suggested that this alloy may also exhibit good fracture toughness. However, the measured fracture toughness, shown in Figure 31 well exceeds expectations. The W-25Re alloy exhibited not only fully ductile fracture at room temperature and above, but the measured values of fracture toughness were comparable to some structural steels. Although these data demonstrate that this W alloy with high Re content is ductile, the search for ductile, structurally-sound W alloys for fusion application is not over. It is apparent that high Re content reduces thermal conductivity of W alloys to levels typical of structural steels. Moreover, a high Re content in W can result in phase instability under irradiation. This work shows that, through appropriate alloying, it is possible to produce forms of the material with “engineering useful” ductility. Based on these results, more fusion-relevant tungsten alloys should be actively investigated.

FUTURE PLANS

The planned effort on this task is complete. There is no additional work currently underway.

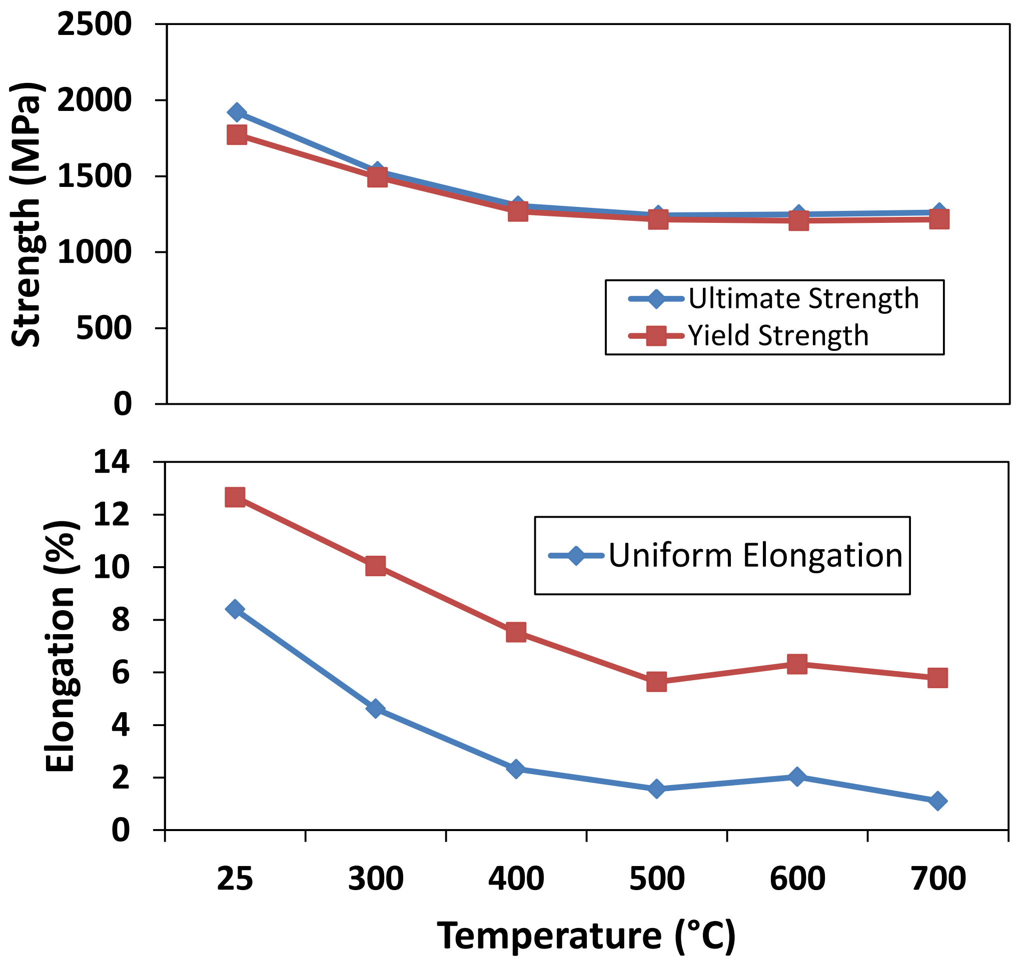

Figure 30. Tensile properties of W-25%Re alloy.

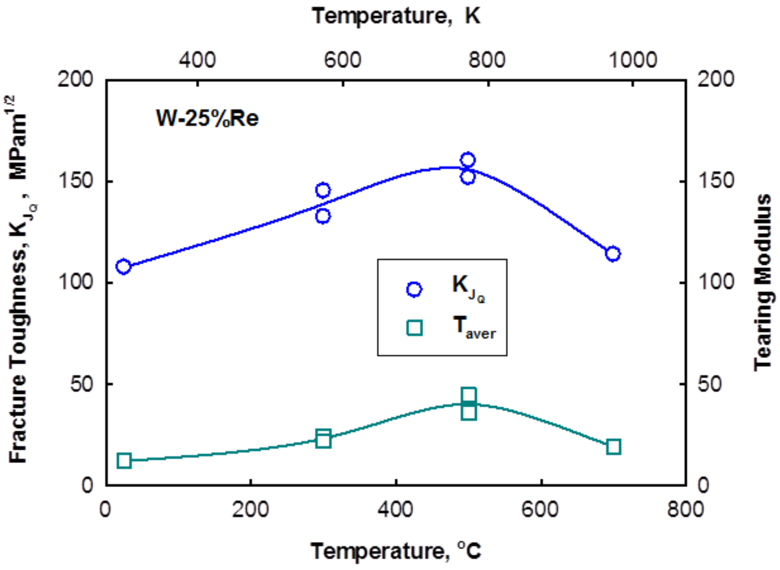

Figure 31. Fracture toughness and tearing modulus of W-25%Re alloy.

5.3 ELECTRON-BEAM ADDITIVE MANUFACTURING OF TUNGSTEN MATERIALS FOR FUSION

Evan Ohriner (ohrinerek@ornl.gov), Ryan Dehoff, Adrian Sabau

OBJECTIVES

Fabrication of tungsten is extremely difficult and expensive. Moreover, given that irradiation embrittlement may require graded or “composited” forms of tungsten, advanced manufacturing techniques adaptable to first wall and/or diverter component fabrication are sought. The goal of this task is to produce graded tungsten-iron layers on a steel substrate using the ARCAM electron beam melting additive manufacturing system now under development at ORNL.

PROGRESS

A structure that has graded composition from a tungsten rich surface to an iron rich interface with a steel substrate is anticipated to have improved resistance to thermal cycling due to reduced thermal stresses in the layers. The higher power density of electron beam as compared to laser processing offers the potential for achieving this high tungsten content layer. The ultimate goal is surface composition of nearly pure tungsten with total layer thickness of about 1mm. This structure could be put in service as produced, or bonded to a substrate of steel or other material selected to provide the properties required in service.

Additive manufacturing is a process of making three-dimensional solid objects from particulate material. The ARCAM EBM process uses a high-power electron beam to site-specifically melt metal powder. This process enables the fabrication of complex geometries that would be impossible to fabricate through other methods. Computer software is utilized to slice the component into specific layers typically between 50 and 200 µm. A substrate material is placed in the center of the powder bed and preheated by scanning a defocused electron beam. Once the determined preheat temperature is reached, a layer of powder is distributed over the substrate material. The powder layer is preheated and partially sintered together using the defocused electron beam. After the preheat cycle, the focused electron beam is utilized to melt the powder contained within the bounds of the computer slice file. Once the entire layer is fused the component is lowered and powder is again distributed, preheated, and melted in a continuous process until the entire component is fabricated. This process offers several advantages over other additive manufacturing technologies. As the process is conducted at locally elevated temperatures, significantly less residual stress develops and typically brittle materials can be fabricated. This has been demonstrated using the ORNL system on extremely brittle materials such as titanium aluminide. The entire process is conducted in a vacuum, therefore eliminating the possibility of impurity pickup of molten metal during processing.

ARCAM equipment that is being used in this work has until now been limited to processing power materials with melting temperatures up to that of titanium. The use of tungsten with a substantially higher melting temperature is requiring modification of the rake mechanism as shown in the view of the interior of the additive manufacturing equipment in Figure 32. The high density of tungsten also imposes higher stresses on the rake mechanism, which contributes to the need for redesign of the rake.

A total of 70 kg of tungsten powder has been purchased. This powder is from standard production and is non-spherical with somewhat limited flow characteristics. A prototype of the inside of the electron beam melting (EBM) system has been built to quantify the powder flow-ability and the ability of the rake to perform adequately. Spherical tungsten powder is available but at substantially higher costs.

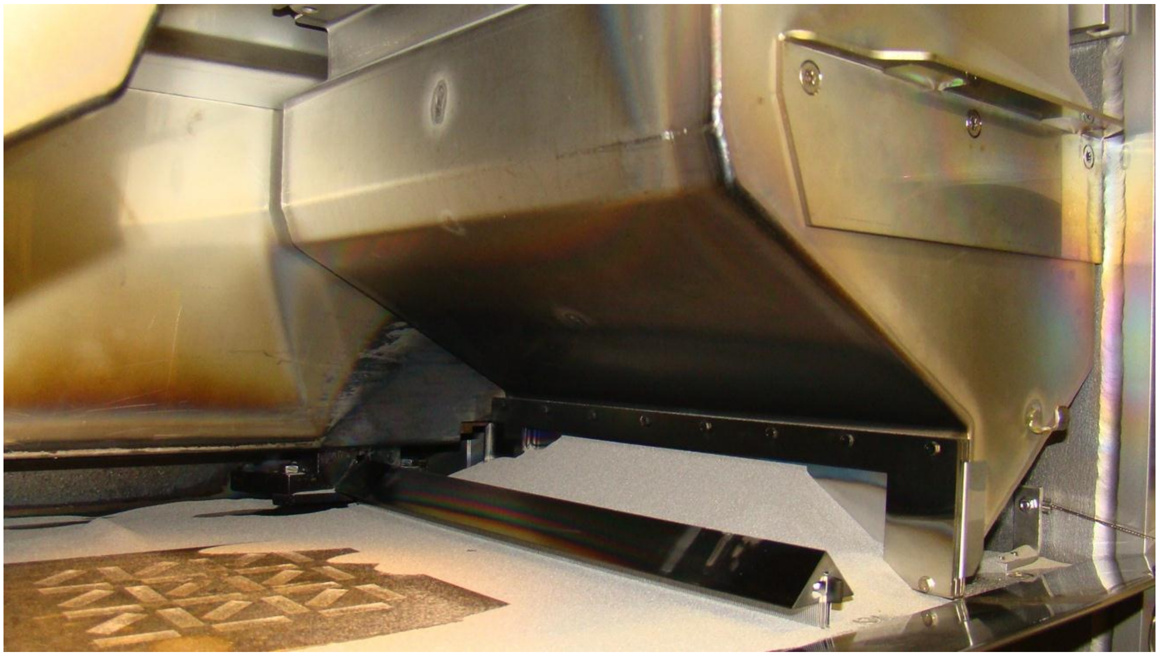

Figure 32. Powder hopper and raking mechanism of the ARCAM system. The rake mechanism impinges on the powder pile, causing powder to spill over the rake. The powder that falls over the rake is evenly distributed over the powder table/start plate.

A new ARCAM machine has been received and is currently fabricating a Co-Cr material that has a significantly higher processing temperature than materials previously fabricated. A number of issues related to processing of high temperature materials are being addressed that will be directly relevant when we begin processing W powders.

ORNL has received level 3 training from ARCAM related to the development and processing of new materials in the electron beam melting technology. This training is required before putting new materials into the ARCAM EBM machine to ensure safe operating procedures. ARCAM has provided insight and advice on the development process for new materials including modification to the raking mechanism to allow the utilization of small quantities of non-spherical powder. A double rake mechanism developed at ARCAM will be used to distribute powder over the start plate. This allows powder that does not flow freely from the hopper to be utilized. If the melting of tungsten is successfully demonstrated using the available powder, then spherical tungsten may be utilized for the development of more complex three-dimensional structures.

FUTURE PLANS

Preliminary trials with the current powder will be used to make some test samples to verify that the material can be fused using the EBM process. With successful completion of the trials, test section production will commence.

5.4 HIGH-HEAT FLUX TESTING OF IRRADIATED MATERIALS USING PLASMA ARC LAMPS

A.S. Sabau (sabaua@ornl.gov), E. Ohriner, J. Kiggans, Y. Katoh, T.S. Byun and L. Snead

OBJECTIVE

The objective of this work is high-heat flux testing of irradiated materials for plasma facing components and of mock-up divertor components using Plasma Arc Lamps (PAL). This will provide basic materials property information and constitutive equations for materials behavior in the harsh fusion environment.

SUMMARY

The ORNL high-heat flux testing facility using Plasma Arc Lamps was demonstrated using non-irradiated W specimens. The components of the test chamber were designed by taking into account radiation safety and materials compatibility requirements posed by high-temperature exposure of low levels irradiated tungsten articles, insuring the readiness of the new facility for irradiated samples.

PROGRESS AND STATUS

Facility Design

Components of the test chamber were designed taking into account radiation safety and materials compatibility requirements in order to allow the testing of low levels irradiated tungsten articles (Figure 33a). Special considerations were devoted to the air evacuation from the test chamber and back-filling with Ar, which is necessary to avoid oxidation of W at high temperatures. The chamber has been designed to accommodate the larger samples required for the high heat flux prototype component testing anticipated in the PHENIX program. Irradiated specimens are to be placed in a shallow recess in the molybdenum holder that is attached to a water-cooled copper alloy rod (Figure 33b).

Several molybdenum specimen holders were machined to allow variation of the sample temperature. The Mo test section contained thermocouples to provide data on sample temperature. In addition to the quartz plate on the top of the chamber, the molybdenum sample holder on the top of the copper cooling rod assembly is enveloped by an end-capped cylindrical quartz tube (right photo) to confine any possible radioactive material released from irradiated specimens.

A second generation of Al enclosure is in fabrication with improvements that will include new HEPA filter attachments for the testing of irradiated specimens. Also, a second generation of Mo specimen holders was designed. These Mo specimen holders are in fabrication. The use of infrared pyrometers to measure the tungsten specimen surface temperature was evaluated based on the specific features of this application (field of view, spot sizes, distance from specimen, emissivity-independent temperature measurement, and temperature ranges). A single color pyrometer was ordered, to operate at 1.6 micron wavelength with a 2 mm spot at 390 mm distance, for measuring temperatures from 350 to 1,700 C.

Experimental, Computational Procedures, and Results

Proof-of-principle experiments were conducted using an existing Al enclosure, with a test chamber assembled within the Al enclosure. The PAL facility was demonstrated during a visit of the Japanese delegation of a PHENIX planning workshop. The 750kW PAL, which provides a uniform incident heat flux, was used in these experiments. The coolant needs of the PAL system, especially for long duration pulses, were evaluated. The PAL coolant temperatures were also recorded during high heat flux testing. The sample was placed at an offset distance of 3.2 cm. At the power setting used, the heat flux was measured to be 2.35 MW/m^2 at 2 cm offset distance. It was estimated that the incident heat flux on the sample was approximately 1 MW/m^2. The temperature data was acquired at two locations in the Mo holder and at two locations in the Cu rod during the 30 s test. The locations where thermocouples were placed are shown in Figure 34a. A typical temperature evolution during the demonstration tests is shown in Figure 34b. This result illustrates that appropriate temperature ranges can be attained with PAL and the test assembly developed for this application.

FUTURE EFFORTS

Efforts are now focused on *enhancing*: (1) safety during testing of irradiated specimens, (2) evaluation and control of the specimen temperature, and (3) extending the duration of high-heat flux test runs. The second generation test chamber will be assembled within the new Al enclosure, including new HEPA filter attachments that are to be used at various stages in the testing of irradiated specimens. For thin samples, the surface temperature cannot be directly measured. Thus, the sample temperature will be evaluated based on a combined experimental/computational procedure involving the measured thermocouple temperature within the sample holder during testing and pyrometer sample surface temperature during the cooling segment of a calibration run. The second generation of Mo specimen holders will be used in testing. The temperatures of the specimen will be evaluated for each Mo holder, with individual holders designed and evaluated to reach and maintain appropriate temperature ranges. The current system pulse duration is limited by the cooling available to the PAL to 30-40 s. A 500 gal chiller, which is adjacent to the PAL system, will be connected directly to the PAL to extend sustainable PAL pulses to 450 s.

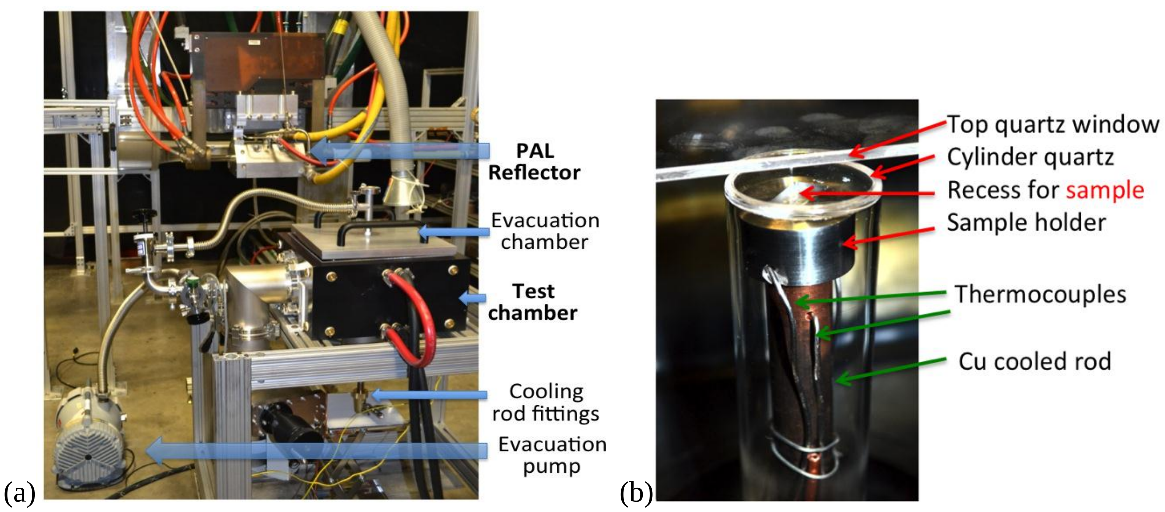

Figure 33. High-heat flux testing facility: (a) PAL and test chamber stands as prepared for the evacuation procedure, (b) test stand composed of quartz cylinder for containment of volatile RAD gases, water cooled rod, Mo sample holder, and thermocouples.

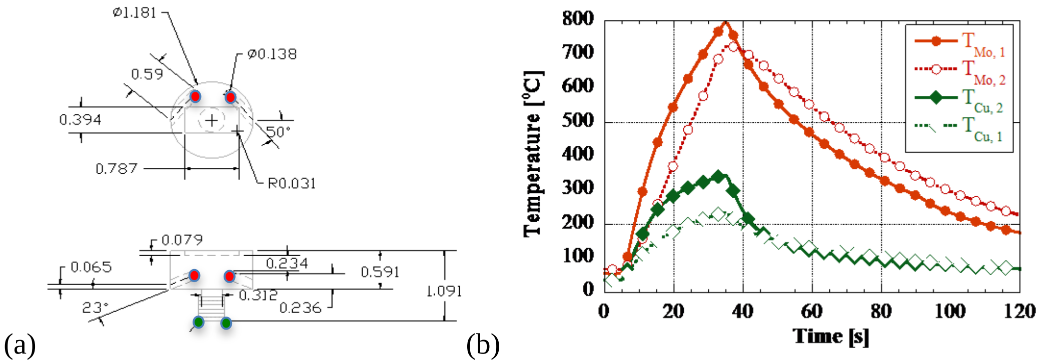

Figure 34. Temperature evolution during a demonstration test: (a) location of thermocouples in the sample holder (red dots) and cooled rod (green dots) and (b) temperature evolution (red – Mo sample holder, green - Cu water-cooled rod (dimensions are given in inches).

5.5 MODELING OF THERMAL TRANSPORT - PHENIX PLANNING

A.S. Sabau (sabaua@ornl.gov), Y. Katoh, and L. Snead

OBJECTIVE

This task will construct a database on thermal management options, issues, and capabilities of the plasma-facing components (PFCs) under divertor conditions of fusion reactors. This database will be used to evaluate the cooling efficiency of the components in design of DEMO divertors.

SUMMARY

As part of the planned collaboration with Japanese partners in the PHENIX project, Task 1 thermal modeling initiative was discussed at a workshop held at ORNL on Aug 2, 2012. Nygren of SNL and Sabau of ORNL will collaboration on this effort. The proposed effort envisions the evaluation of advanced cooling concepts for tungsten armor components using He gas and/or liquid metal cooling systems (LiPb). In addition to the energy transport phenomena, the thermo-mechanical response of tungsten layered materials and advanced tungsten materials under complex steady-state and pulse heat loads will be investigated.

PROGRESS AND STATUS

This project is in planning status and ORNL is in direct contact with the Japanese partners in the PHENIX project. It was agreed that the following phenomena must be considered in modeling the energy transport: (1) thermal contact resistance at material interfaces, (2) spatially dependent heat transfer coefficients at coolant-wall interfaces, (3) component deformation during pulse heat loading, (4) degradation of thermal conductivity with reactor operation time, and (5) degradation of mechanical properties with operation time. To the best of our knowledge, the thermo-mechanical behavior of subcomponents under the thermal gradients of the full divertor has not been considered.

FUTURE EFFORTS

Future efforts will investigate the behavior of several candidate plasma facing materials (monolithic and layered materials, and other advanced materials) and components under the complex heat loads, pulses and steady-state operating conditions of a DEMO reactor. Several cooling configurations of the divertor armor components will be designed and evaluated based on several criteria, including cooling efficiency, thermal induced stresses, and integrity of cooling system.

Further discussion and planning of this effort is scheduled at the next meeting of the PHENIX partners at a targeted workshop at the NuMAT conference in Osaka (October 22-26, 2012.)

6.0 COMPUTATIONAL MATERIALS SCIENCE

6.1 SIMULATION OF BALLISTIC RESOLUTIONING OF HELIUM FROM BUBBLES IN IRON BY MOLECULAR DYNAMICS

Roger E. Stoller (stollerre@ornl.gov)

OBJECTIVE

This research models the behavior of transmutation generated helium in metals, focused on the resolution of bubbles due to the ballistic ejection of helium atoms from neutron impact.

PROGRESS

Helium generation and accumulation plays a dominant role in microstructural evolution under DT fusion irradiation conditions. Therefore, it is important to develop an understanding of the mechanisms that can influence the formation and growth of bubbles in fusion structural materials. The process known as ballistic resolutioning could limit bubble growth by ejecting gas atoms back into the metal matrix when (if) a high energy recoil atom passes through the bubble. Classical, constant pressure molecular dynamics was used to study this process. A recently-developed Fe-He interatomic potential was employed with periodic boundary conditions in cubic simulation cells containing up to 1024k atoms. The primary variables examined were: irradiation temperature (100 and 600K), iron knock-on atom energy (5 and 20 keV), bubble radius (~0.5 and 1.0 nm), and He-to-vacancy ratio in the bubble (0.25, 0.5 and 1.0). Helium ejection by high energy iron recoils was clearly observed on a time scale consistent with a ballistic mechanism.

The results are summarized in Figure 35 and Figure 36. The curves in Figure 35 show the total number of He atoms displaced from the bubble surface by at least 1 lattice parameter, more than 10 lattice parameters, and between 5 and 10 lattice parameters. The rapid evolution of helium resolutioning is quite clear with the maximum number of He atoms ejected being reached by <40 fs. This time is quite short on the time scale of displacement cascade evolution in which the peak number of displaced atoms is not reached until >0.5 ps. This is shown by the black curve in Figure 35 which plots the number of Frenkel defects created. This number is still increasing rapidly well after the number of He ejected has saturated.

The dependence of He resolutioning on the irradiation conditions are shown in Figure 36 for a 1 nm bubble size (339 vacancies). The data points indicate the mean value and the error bars are the standard error of the mean. The trends are quite clear. At both 100 and 600K there is less resolutioning from 20 keV cascades than from 5 keV cascades. This seems somewhat counter-intuitive, but is a result of the reduced elastic scattering cross section as the particle energy increases. At either cascade energy, resolutioning is reduced at the higher temperature. This is consistent with the greater thermal motion of the He atoms making it more difficult for collisions to transfer large amounts of energy in elastic collisions. Lastly, it is clear that bubble pressure, represented by the He/vacancy ratio, has a strong influence of the number of He atoms ejected.

FUTURE WORK

These results illustrate the potential for He resolutioning to limit bubble growth. Further analysis will provide guidance for developing ballistic resolutioning parameters that can be employed in reaction rate theory models of He-vacancy cluster dynamics. The use of atomistic-based resolutioning parameters will improve the fidelity at the higher length and time scale models used to predict microstructural evolution and the swelling and hardening produced by cavities in irradiated materials.

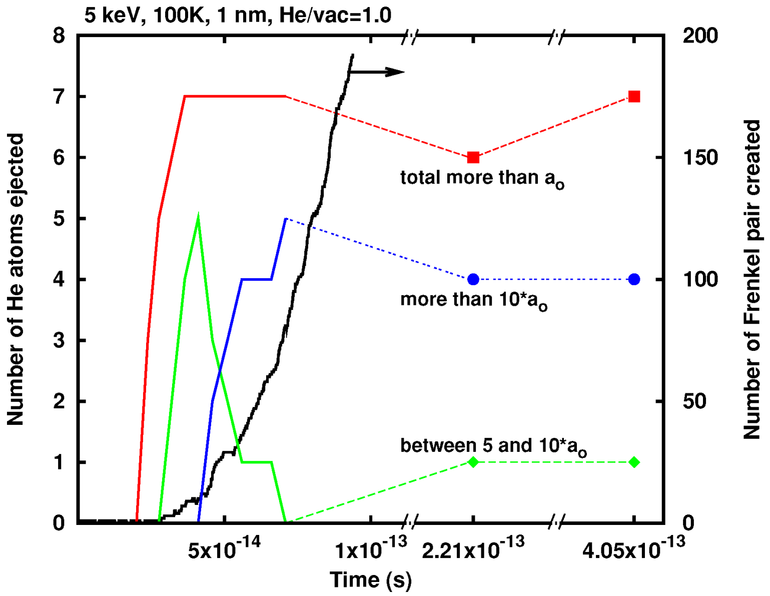

Figure 35. Time dependence of He ejection from a 1 nm bubble and point defect formation in a 5 keV cascade at 100K. He/vacancy ratio is 1.0.

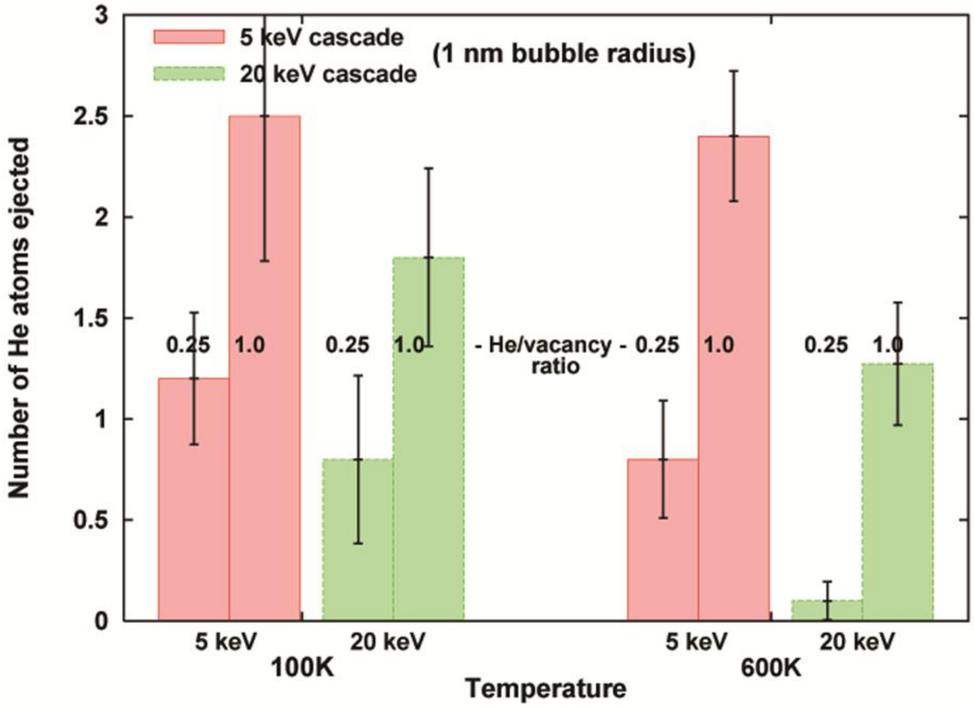

Figure 36. Summary of ballistic He resolutioning from 1 nm He bubbles in iron as a function of temperature, cascade energy, and He/vacancy ratio.

6.2 THE INFLUENCE OF TRANSITION METAL SOLUTES ON DISLOCATION CORE STRUCTURE AND VALUES OF PEIERLS STRESS AND BARRIER IN TUNGSTEN

G.D. Samolyuk (samolyukgd@ornl.gov), Y.N. Osetsky and R.E. Stoller

OBJECTIVE

The objective of the present investigation is to study possible substitutes for rhenium in tungsten alloys that will result in a similar ductilizing effect as Re has in W.

PROGRESS

Tungsten is the prime candidate for use in the divertor of future fusion reactors because of its high melting temperature and resistance to sputtering However, its lack of ductility is an impediment to its use. The ductility of these metals can be improved by alloying with rhenium. However, Re is a very rare and expensive element. We use first principles technique to find alternate elements which may provide a similar increase in ductility at lower cost. The previous first principles density functional calculations demonstrated that alloying with Re in a $W_{1-x}Re_x$ alloy leads to a transition of the 1/2⟨111⟩ screw dislocation structure from a symmetric core to an asymmetric core, and to a reduction in Peierls stress-resulting in a "direct" improvement in the mobility of 1/2⟨111⟩ screw dislocations.

The properties of W-transition metal alloys (W-TM), were modeled using the virtual crystal approximation. The electronic structure of the system within density functional theory was calculated using the QUANTUM ESPRESSO package.

In comparison with a standard supercell method, we demonstrated that the virtual crystal approximation gives a fairly good description of such alloying, especially in the case of 4*d* and 5*d* transition metals. For the case of alloying with transition metals from group VIIIA, the modification of elastic constants can be understood within the rigid band approximation. This means that alloys with TM concentrations leading to the same number of electrons per atoms (*e*/*a*) exhibit a similar reduction of *C*' modulus and elastic anisotropy *A*.

We use a periodic quadrupolar arrangement for a 1/2⟨111⟩ screw dislocation in a reduced cell with 135 atoms. In bcc structures 1/2⟨111⟩ screw dislocations have three nonequivalent core configurations, that are referred to as "easy", "hard" and "split" – one stable and two metastable, respectively. We determined that the symmetric "hard" core configuration decays into the "split" core. Thus we assume that the dislocation migrates between the "easy" and the "split" core configurations. It was shown that the dislocation core structure is asymmetric in W-TM alloys where the concentration of transition metal were chosen to give the same (*e*/*a*) value, similar to W-Re.

The Peierls stress is defined as the minimum stress needed to move a dislocation core from one stable position to the next. Following a widely used technique, we apply pure shear strain in the ⟨111⟩ direction which results in a stress that has σ_{zx} as its main component.

Figure 37 shows the dependence of total energy (see inset) per dislocation per Burgers vector and shear stress as a function of strain, ε. At larger ε the energy dependence deviates from square dependence and abruptly drops. This drop in energy is caused by a jump of the dislocation core to the next stable "easy" core neighboring position. The corresponding stress and strain are the Peierls stress σ_p and strain ε_p. Alloying with either Re or Fe reduces values of ε_p and σ_p. For Fe this reduction is even larger than for Re (Table 6) although the solute concentrations corresponds to the same (*e*/*a*) value in both cases. The relative reduction of σ_p is 20 % for Re and 36 % for Fe. It should be mentioned that the solubility limit of Fe in W is near 2%, so if the concentration of Fe in limited to this value the reduction of Peierls barrier is about one half of that calculated for an alloy with 5% Fe. For the W-Ru alloy with a solubility limit of 3

%, σ_p is reduced by 6 %. This result is consistent with the experimentally observed reduction of ductile-brittle transition temperature in W-Ru alloy.

The second method used to estimate Peierls stress was originally proposed by Nabarro. Following Nabarro, we measure the system energy as a function of the dislocation location as it moves from “easy”- to “split” core positions. The energy dependence obtained is associated with the Peierls barrier and the Peierls stress is given by the maximum gradient of the function, $\sigma_p = 1/b\,(dV/dR_c)_{max}$, where b is the Burgers vector, V is energy per unit length of a straight dislocation and R_c is the distance along the dislocation core path. We use the drag method, also called the reaction coordinate method, to move the dislocation from "easy" to "split" core configuration. The result is that the shape of Peierls barrier is insensitive to type of solute, thus the difference between the “easy” and “split” core configurations energy provides an estimate of the Peierls barrier. The reduction of the Peierls barrier observed in these calculations correlates well with the reduction in Peierls stress estimated in the deformation simulation described above (Figure 38,). Alloying with Re or any group VIIIA transition metal at a concentration which corresponds to (*e*/*a*) = 6.10 reduces the barrier by 25 %. Fe reduces the Peierls barrier even more significantly, whereas Zr increases the barrier. The Peierls stress calculated using the direct deformation method, σ_p, and from the Peierls barrier, $\tilde{\sigma}_p$are presented in Table 6. For all alloys the Peierls stress values obtained from the Peierls barrier are lower than those from the direct method. The difference is largest, 14 %, for W alloys with 10 % Re, or 2 % Fe. Thus the $\tilde{\sigma}_p$ results; introduction of 2 % Fe to tungsten reduces the Peierls stress by 12 %.

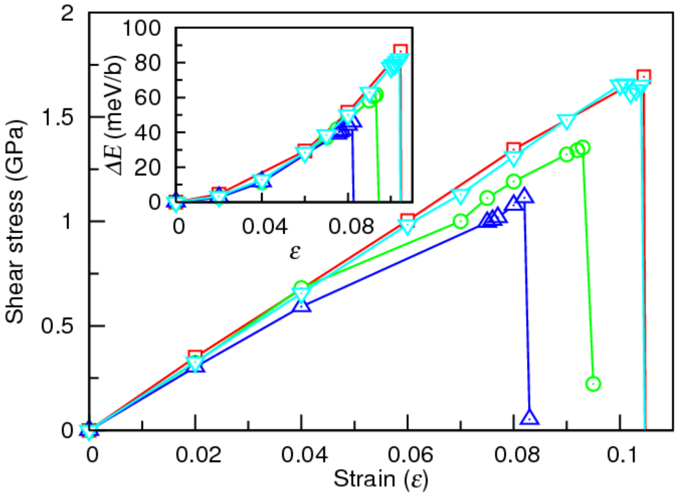

Figure 37. Shear stress and total energy, ΔE, per dislocation per Burgers vector $\vec{b}$ *(shown in the inset) as a function of strain, ε, for pure W (shown by squares),* $W_{0.90}Re_{0.10}$ *(shown by circles),* $W_{0.95}Re_{0.05}$ *(shown by up pointing triangles) and* $W_{0.98}Fe_{0.02}$ *(shown by down pointing triangles*

Thus the Peierls stress and barrier are reduced by alloying with transition metals from group VIIIA. In addition to the Peierls barrier reduction, alloying with any metal from this group changes the "easy" core dislocation structure from the symmetric to asymmetric configuration. This similarity allows us to conclude that the search for an alternative to Re could be reduced to transition metals from the group VIIIA.

FUTURE WORK

The initial scope of work on this subject has been completed, with no further effort now planned.

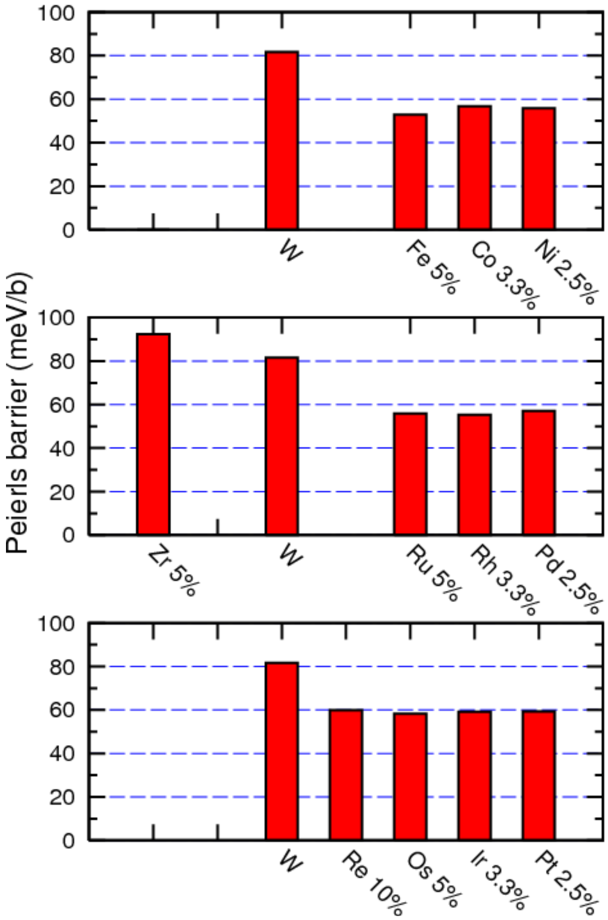

Figure 38. The height of Peierls barrier for the set of W alloys.

Table 6. The reduction of Peierls stress calculated using the direct deformation method, σ_P *in GPa, and from the Peierls barrier,* $\tilde{\sigma}_P$ *in several tungsten alloys.*

	σ_p	$\tilde{\sigma}_p$
W	1.71	1.64
$W_{0.95}Zr_{0.05}$	2.18	1.82
$W_{0.90}Re_{0.10}$	1.37	1.15
$W_{0.95}Fe_{0.05}$	1.09	1.05
$W_{0.98}Fe_{0.02}$	1.65	1.40
$W_{0.97}Ru_{0.03}$	1.60	1.35

7.0 SPECIAL PURPOSE MATERIALS

7.1 HIGH NEUTRON DOSE IRRADIATIONS OF DIELECTRIC MIRRORS

Keith J. Leonard (leonardk@ornl.gov), Lance L. Snead, and Gerald E. Jellison, Jr.

OBJECTIVE

Diagnostic mirrors are critical to understanding the performance and providing feedback to the plasma. ITER will use highly polished metal mirrors for this purpose. The objective of this work is to extend the recent, very positive results demonstrating that radiation-hardened dielectric mirrors can provide superior performance in such an application.

SUMMARY OF PROJECT

Multilayered thin-film dielectric mirrors can significantly improve transmission of reflected UV range electromagnetic energy (>99%) compared to metallic mirrors (40-80%). This can be important for their use as focusing mirrors for inertial confinement fusion systems and in plasma diagnostic systems for magnetic confinement systems. Our experimental work to date on commercially produced HfO_2/SiO_2 and Al_2O_3/SiO_2 multilayer films on sapphire substrates irradiated to 0.1 dpa at 448 K finds no change in absolute reflectivity of either mirror type and only minor shifts in the range of wavelength in which peak reflectivity occurs. These results indicate an impressive (more than an order of magnitude higher) irradiation resistance compared to literature data and suggested a wider applicability of dielectric mirrors in fusion systems. However, chemical intermixing between the Al_2O_3/SiO_2 layers and crystallinity changes in HfO_2 are evident in these mirrors with increasing irradiation dose, and suggest that these changes could lead to severe degradation in optical properties at higher irradiation doses or temperatures (Figure 39).

To identify the upper limits of radiation and thermal stability, HfO_2/SiO_2 and Al_2O_3/SiO_2 mirrors are currently being irradiated to $1x10^{21}$ and $4x10^{21}$ n/cm^2 (E>0.1 MeV) at 448 K, corresponding to 1 and 4 displacements per atom (dpa). A schematic diagram of the sample holders designed for the HFIR neutron irradiation is shown in Figure 40 . The irradiated samples are due out of reactor at the end of cycle 444 in November 2012, with post irradiation examination (PIE) of the mirrors expected to begin in early 2013. PIE will include measurement of changes in relative spectral reflectance versus wavelength and absolute reflectivity at 248 nm, the wavelength the mirrors are tuned for. The mirrors will be examined in the irradiated condition and following 1 hour thermal anneals starting at 573 K. Samples consisting of monolayer films of SiO_2, HfO_2 and Al_2O_3 on sapphire substrates were also included in the irradiation for more detailed ellipsometry examination of the film/substrate interactions. The changes in optical properties will be correlated to microstructural changes in the films determined through transmission electron microscopy examination.

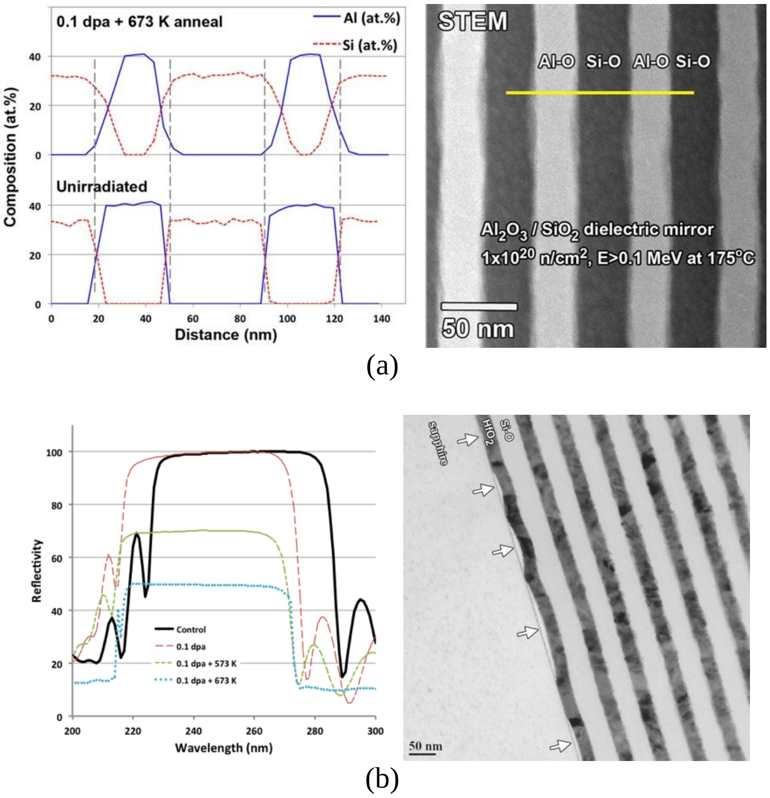

(a)

(b)

Figure 39. Summary of earlier results of neutron irradiation tests on dielectric mirrors up to 0.1 dpa. (a) Al_2O_3/SiO_2 mirror showing energy dispersive spectroscopy results through scanning transmission electron microscopy (STEM), indicating diffusion of Si into the aluminum oxide layers (both layers are amorphous) with increasing neutron dose and annealing temperature. (b) Reflectance versus wavelength of the HfO_2/SiO_2 mirror showing degradation of the mirror following annealing after 0.1 dpa irradiation. The changes are the result of delamination at the HfO_2/sapphire interface.

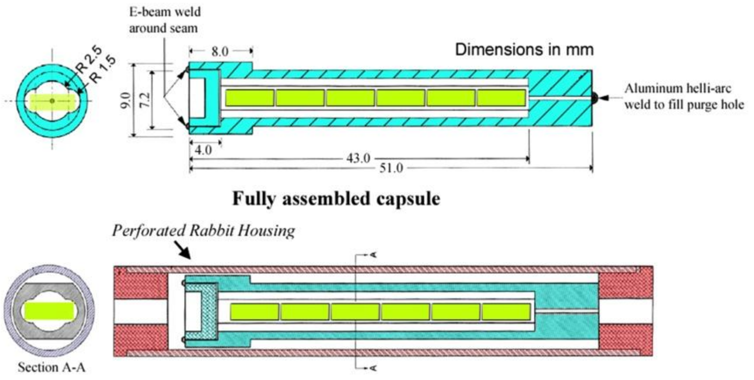

Figure 40. Schematic of holders for the neutron irradiation experiments of dielectric mirrors. Mirror samples, 6 mm diameter by 2 mm thick and shown in yellow, are loaded into aluminum holders that hold the samples in place by contact only at the sample edges. SiC temperature monitors are loaded under the samples, with no contact with the mirror surfaces. Samples are sealed in a He atmosphere then inserted into a perforated rabbit housing for irradiation in the peripheral hydraulic tube.

7.2 IRRADIATION RESPONSE OF NEXT GENERATION HIGH TEMPERATURE SUPERCONDUCTING RARE-EARTH AND NANOPARTICLE-DOPED $YBa_2Cu_3O_{7-x}$ COATED CONDUCTORS FOR FUSION ENERGY APPLICATIONS

Keith J. Leonard (leonardk@ornl.gov),Tolga Aytug, William J. Weber Albert Gapud (U South Alabama), Alejandro Perez-Bergquist, Marty Rupich (American Superconductor Corporation)

OBJECTIVE

The superconducting magnets, supporting cryoplant, and magnet shielding constitute a significant fraction of the projected cost of fusion power plants. However with the recent commercialization of “high temperature” superconductors with high critical current capacity, both magnet size and the cryoplant costs can possibly be reduced. This assumes irradiation tolerance of the conductor. The objective of this work is to evaluate the irradiation response of the newest generation of high temperature superconducting (HTS) materials based on $YBa_2Cu_3O_{7-x}$ (YBCO) for possible use in future magnetic confinement reactors.

PROGRESS

This effort is directed at reducing reactor costs and complexity associated with the low temperatures required for the Nb_3Sn conductors. In addition to the higher critical temperature of YBCO over Nb_3Sn (T_c = 92 K versus 18 K), YBCO conductors offer higher critical current density (J_c), increases in J_c with neutron irradiation up to $1x10^{22}$ n/m^2 (E>0.1 MeV) due to their smaller flux pinning coherency length and a smaller effective neutron capture cross section. However, earlier HTS materials have been limited to self-field applications such as power transmission due to their inability to maintain magnetic flux pinning under externally applied fields. The newest generation of YBCO conductors incorporate engineered textured substrates and nanoparticle additions to the conductor to produce correlated defect structures in the YBCO lattice that increase J_c values with reduced dependence on magnetic field.

The materials under examination are based on the best performing coated conductor technologies as summarized in Table 7. The coated conductors consist of biaxial textured films of $YBa_2Cu_3O_{7-x}$, $GdBa_2Cu_3O_{7-x}$ and $DyBa_2Cu_3O_{7-x}$ (1.0-1.5 µm thick) deposited by metalorganic chemical vapor deposition onto buffered Ni-alloy tapes. The biaxial texturing of the HTS films needed for the flow of current along the length of the tape is generated from either the rolling assisted bi-axial textured metallic substrate or developed within the buffer layer. The addition of different dopants to the MOCVD films result in the development of nanoparticles, or nanodots, produced by reaction with constituent elements of the HTS material. Improved angular and field dependent J_c values of the HTS conductor are derived from the flux pinning effects these nanodots provide, and the defect structures they generate within the film. Figure 41 shows the tape architecture and examples of the pinning structures.

Characterization of the pre-irradiated electrical properties is near complete, with ion irradiations to be performed at the UT/ORNL Ion Materials Laboratory early in FY2013. Ion irradiations at lower energy levels (electronic energy loss values < 20 keV/nm) will simulate neutron cascade damage and avoid columnar defect formation from high-energy ion damage. Ions and energies considered are 10 MeV O, 25 MeV Cu, and 25 MeV Au at fluences between 10^{11} and 10^{14} ions/cm^2. These will provide a range of test data encompassing the start of measureable responses to irradiation up to, and possibly exceeding, the dose limits for these materials. Ion penetration depths will be well into the Ni-alloy substrate to avoid introduction of impurities and unintended variables.

FUTURE WORK

Work in FY2013 will provide a first investigation into the radiation effects on the most advanced HTS materials. The effects on superconducting properties through the changes to pre-existing flux pinning centers and the development of radiation-induced defects will be examined. This work will expand later into low temperature irradiation testing of specific materials that will include *in situ* measurement of self-field superconducting properties as a function of dose, with a further analysis of defect annihilation and the effects of temperature excursions on conductor properties.

Table 7. High temperature superconductors, substrate architecture (by company which fabricated tapes) and type of flux pinning created for improved use in magnetic field applications.

Material	Substrate	Features
$DyBa_2Cu_3O_{7-x}$	American Superconductor	50% substitution of Y in $YBa_2Cu_3O_{7-x}$ chemistry. Development of $(Dy,Y)_2O_3$ nanoparticles, enhanced H//ab pinning. Increased stacking faults ($YBa_2Cu_4O_8$ intergrowths) in the film.
$GdBa_2Cu_3O_{7-x}$	SuperPower	Substitution of Gd for Y in the $YBa_2Cu_3O_{7-x}$ chemistry. High density stacking fault generation from mismatch in growth domains from buffer and Gd_2O_3 particles, yielding improvements in H//ab pinning.
Zr-doped $YBa_2Cu_3O_{7-x}$	SuperPower	Creation of $BaZrO_3$ nanodots aligned along the c-axis direction, producing enhanced H//c pinning.
Nb-doped $YBa_2Cu_3O_{7-x}$	SuperPower	YBa_2NbO_6 nanoparticle alignment in c-axis direction, for enhanced H//c pinning, in addition to increased H//ab pinning from stacking faults generated.

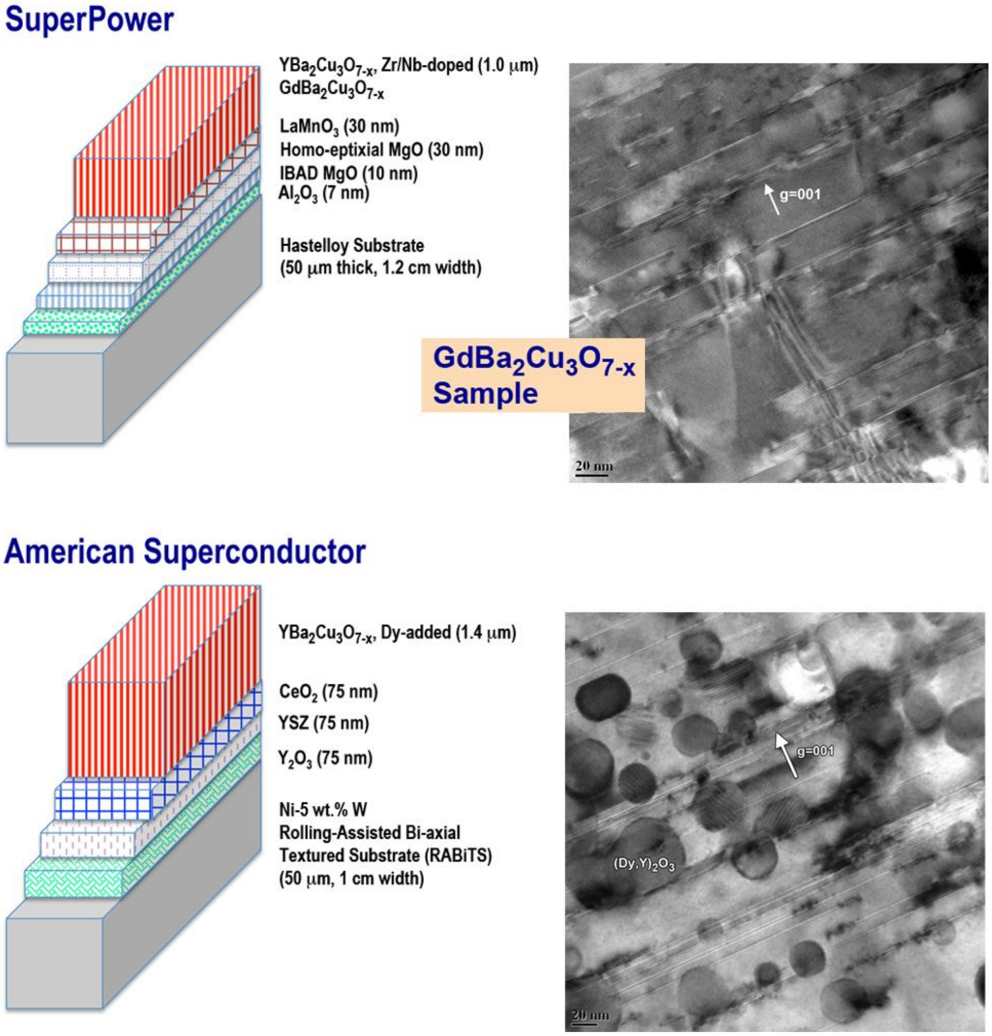

Figure 41. SuperPower and American Superconductor tape architectures along with TEM of two test materials prior to irradiation showing the different mechanisms (stacking fault generation and nanoparticles) for magnetic flux pinning.

7.3 DUAL LAYER MHD COATING COMPATIBILITY WITH FLOWING Li

K. A. Unocic <unocicka@ornl.gov> and B. A. Pint

OBJECTIVE

The MHD (magneto-hydrodynamic) induced pressure drop is a critical problem for any liquid metal blanket system. It is considered especially significant in the V-Li system because Li dissolves many electrically insulating oxides. The current experiment was designed to demonstrate the compatibility of an MHD coating with an outer vanadium layer and an inner insulating oxide layer in flowing Li at temperatures up to 700°C.

SUMMARY

Characterization was performed on two-layer V/Y_2O_3 coatings deposited on V-4Cr-4Ti and exposed to liquid Li in a thermal convection loop at 400-700°C for 2,355h. The figure of merit for these coatings is the high temperature electrical resistivity after exposure, which was measured in a vacuum rig to prevent oxidation of the vanadium coating and substrate. Significant degradation of the resistivity was observed after exposure, especially for exposure temperatures above 500°C. At the highest temperatures, an apparent second phase formed at the Y_2O_3-substrate interface suggesting that the coating fabrication was not optimized. There was no evidence of Li penetration through the vanadium outer layer. Characterization has included TEM to identify the second phase. However, no Li has been detected in this phase by EELS or XPS. Another possibility is that recrystallization of the oxide occurred at this interface, but that does not explain the drop in resistivity after exposure and no layer formed during a thermal anneal at 700°C without Li.

PROGRESS AND STATUS

Coupons were coated by electron-beam-physical vapor deposition (EB-PVD) and exposed for 2,355h at temperatures from 400 to 700°C in a monometallic thermal convection loop run in 2007. The Y_2O_3 and V layers were ~15µm thick each. The exposure temperature was estimated based on location in the loop. After exposure, specimens were cut from the coated coupons to electrically isolate the Y_2O_3 layer. The electrical resistance was measured in vacuum at 100°C increments to 700°C. Figure 42 shows the high temperature electrical resistivity measurements and the horizontal dashed line shows the literature value of the minimum resistivity (10^5 Ohm-cm) needed to reduce the MHD pressure drop to acceptable levels based on the insulating layer thickness. Typically, resistivity drops with temperature as is shown for literature values of bulk Y_2O_3. However, the resistivity drops below the critical minimum value for many of the exposed coatings, especially those exposed at high temperature in the loop. While there was considerable scatter in these difficult measurements, the observation of high resistivity for many of the specimens exposed at low temperatures suggests a Li-induced degradation.

Characterization indicated that a “second phase” had formed in the coatings exposed at the highest temperature, but not in a specimen annealed for 2,355h at 700°C or in the lower temperature Li exposures. The layer appeared darker gray in a backscattered electron image indicating a lower average atomic number than Y_2O_3, perhaps $YLiO_2$. EPMA indicated a higher O content and lower Y content. An example of the layer formed at 573°C is shown in a TEM cross-section in Figure 43a. However, further characterization by XPS and EELS (Figure 43b) conducted on the 437 and 563°C specimens showed no Li 1s peak in the oxide or metal spectra.

FUTURE PLANS

The V/Li system is no longer the focus of the U.S. Fusion Materials program and no future work is planned in this area. After completing TEM characterization of the 627°C specimen, these results will be published and this subtask completed.

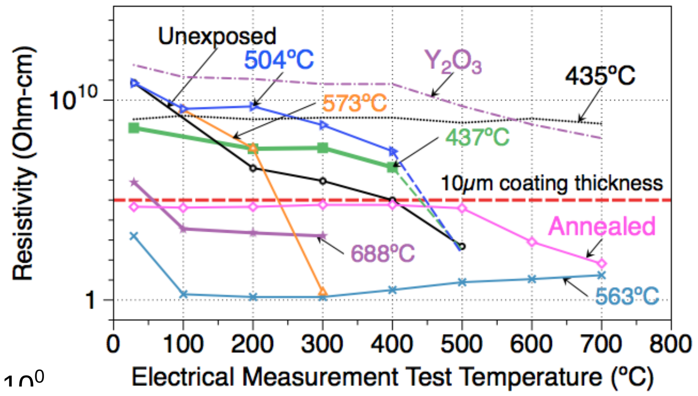

Figure 42. Resistivity as a function of temperature measured in a vacuum rig for V/Y_2O_3 specimens exposed at different temperatures to flowing Li.

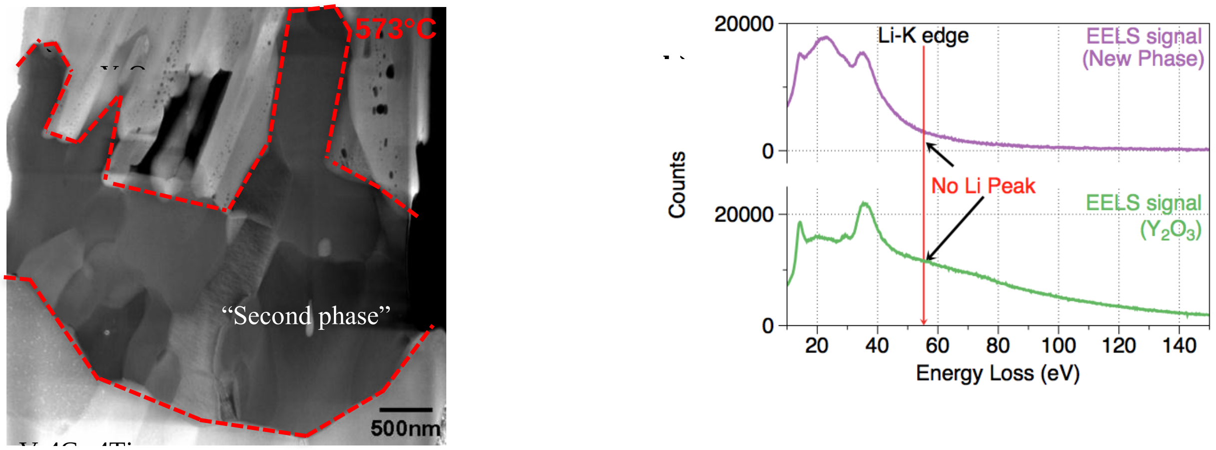

Figure 43. a) HAADF image of the Y_2O_3/second phase/V-4Cr-4Ti interface exposed to 573°C. b) EELS spectrums indicating no Li present.

8.0 IRRADIATION FACILITIES

8.1 ION IRRADIATION FACILITY AVAILABLE FOR FUSION MATERIALS RESEARCH

Yanwen Zhang, <zhangy1@ornl.gov>, W.J. Weber

OBJECTIVE

The objective of this project, funded outside of the fusion program, was to provide a multipurpose accelerator-based facility for ion irradiation and ion beam analysis. It is anticipated that this facility will be routinely used in the screening of candidate fusion materials and for fundamental studies such as helium effects for which no fusion-relevant source is available.

FACILITY DESCRIPTION

The UT-ORNL Ion Beam Materials Laboratory is or will be equipped with two ion sources, a 3 MV NEC tandem accelerator (9SDH-2), three beamlines and four target chambers that provide the following capabilities:

- **Ions:** most elements from H up to Au, including ^{3}He, ^{4}He, C ^{16}O, Al, ^{18}O, Si, Fe, Ni, Br, Sr, Pt, I, etc
- **Energy:** may be controlled from a few keV to ~ 25 MeV (depending on ions and current needed)
- **Penetration depth** or the modification depth may be varied from a few tens nm to 30 µm.
- **Dose rate:** can be as high as 0.02 dpa/s, or 500 dpa in one day at temperature up to 1475 K.

Ion Accelerator Facility

The ion acceleratory facility at the University of Tennessee, shown in Figure 44 , can be used for ion irradiation. The acceleratory facility is equipped with two ion sources, a 3 MV tandem accelerator, three beamlines, and three endstations. Most ions from H to Au can be produced with energies from a few tens of keV to a few tens of MeV, which provide the energy range needed for fusion research. One beamline and endstation is devoted to rapid routine ion beam analysis and can be used to probe composition, H/He redistribution, and obtain elemental depth profiles. Two other beamlines with temperature-controlled endstations are equipped with beam raster scanners to produce uniform irradiations over large areas for controlled irradiation. An intermediate-temperature endstation (-120 to 500°C) is equipped with a manipulator with 3 axes of rotations and 3 axes of translation; it is equipped with various ion beam analysis techniques. An NEUP infrastructure grant has been received for a new high-temperature irradiation capability (25 to 1200°C), as part of a third endstation. This high-temperature irradiation target chamber, which will be available soon, will consist of a custom-designed target chamber and a temperature-controlled manipulator (room temperature to 1200°C) with ±180° of polar rotation around the vertical axis and 20 cm of vertical motion.

Ion irradiation to simulate fusion conditions

The ion irradiation facility will be used for focused experiments on fusion program materials. Ion irradiation has advantages as it can be carried out under a range of well-controlled conditions (dose, dose rate, ion energy, ion mass, and temperature) that allow for separate effects evaluation and testing, as well as combined or simultaneous effects of several conditions. Ion irradiation can be used to simulate conventional knock-on damage across a wide temperature range (high does rate events at high temperatures) and, therefore, provides an effective approach to evaluate materials performance in neutron irradiation environments (low dose rate events at a lower temperature). Ion irradiation also has the advantage of well-controlled irradiation conditions and easy sample handling (not producing highly radioactive samples as compared to neutron irradiation). Irradiation effects in advanced structural materials to various doses can be carried out through low damage rate proton and high damage rate self-ion or heavy ion irradiation. Proton irradiations over a range of temperatures can be used to evaluate the radiation response by producing uniform damage region over several tens of microns in depth that is readily characterized by a variety of bulk property tests. Heavy ion irradiation can be used to simulate damage created by primary recoils generated by fast neutron irradiation. Since irradiation with ions is an accelerated approach resulting from much higher dose rate than in-reactor neutron irradiation environments, the dose rate study will be investigated in a wide temperature range. The range of irradiation temperatures can provide some guidance about the kinetics of radiation effects, in particular those associated with cascade-induced precipitate dissolution and radiation-enhanced precipitate coarsening processes, which can serve as a basis to extrapolate the higher-dose rate ion irradiations to lower dose rate neutron irradiation environments.

FUTURE PLANS

This facility will be used by the ORNL Fusion Materials program for single variable and mechanistic studies on materials of interest for fusion. These studies will assist in the understanding of the basic physics of the processes controlling the response of materials to irradiation components of the fusion environment.

Figure 44. Overview of the newly commissioned accelerator facility at the University of Tennessee.

8.2 DESIGN AND CONSTRUCTION OF HFIR IRRADIATION EXPERIMENTS

J. McDuffee (mcduffeej@ornl.gov), N. Cetiner, R. Howard

OBJECTIVE

This program element is tasked with the design, fabrication and assembly of experiments for the irradiation of fusion program materials in HFIR.

SUMMARY

A total of 73 experiments were built for the ORNL Fusion Materials Program in FY 2012. These were all rabbit capsule type experiments, with a wide range of materials, specimen geometries and irradiation conditions. While the majority of the capsules were modifications of previously used experiment concepts, 6 new capsule designs were developed during the year. No full length HFIR irradiation capsules were built in FY 2012.

EXPERIMENT DESIGNS

Torsion Joint Experiment

Three capsules were designed and built to irradiate a new type of torsion joint specimen. Each contains 16 specimens of SiC wafers joined at a circular face. The combined specimens are stacked inside a standard rabbit holder fabricated from either V-4Cr4Ti or molybdenum, selected depending on the desired irradiation temperature. Figure 45 shows the basic dimensions and assembly layout for these capsules.

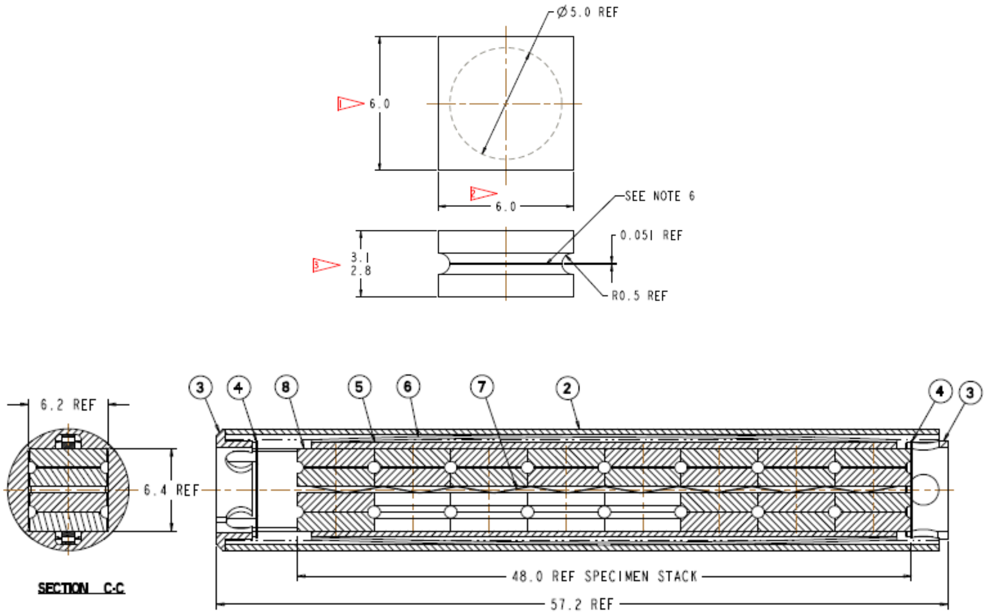

Figure 45. Specimen Details and Capsule Layout for the Torsion Joint Capsules. Dimensions are in mm.

Fiber BSR Experiment

The Fiber Bend-Stress Relaxation (BSR) experiment is shown in Figure 46. The specimen fiber is wound through a block designed to keep the specimen at a specific stress-state throughout the irradiation. Four of these experiments were designed for irradiation in FY2012. Irradiation temperatures are 500°C and 1200°C. The lower temperature capsules used a V-4Cr4Ti holder, while the high temperature capsule used a molybdenum holder.

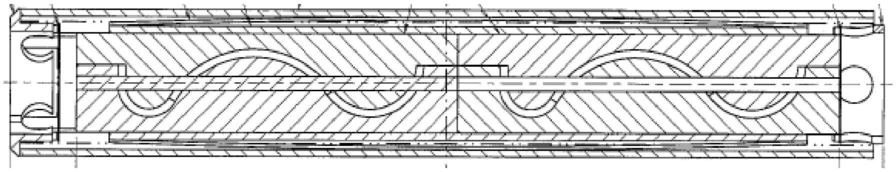

Figure 46. Fiber BSR Capsule Assembly

High Temperature Specimen Holders

Because of concerns of chromium movement out of the V-4Cr4Ti matrix at very high temperatures, a molybdenum holder was designed to provide the same experiment space as the previously used holders. A previous attempt at using molybdenum with the standard holder design was unsuccessful, as most of the fabricated holders cracked along the corners of the specimen cutout where the web thickness is thin. The revised molybdenum holder is shown in Figure 47. The centering thimble has been replaced by extension tabs from the holder itself. These tabs center the holder inside the outer aluminum housing as well as lift the experiment stack axially away from the housing bottom. The tabs are strategically placed at the cutout corners to provide additional support at the ends where cracking typically originates.

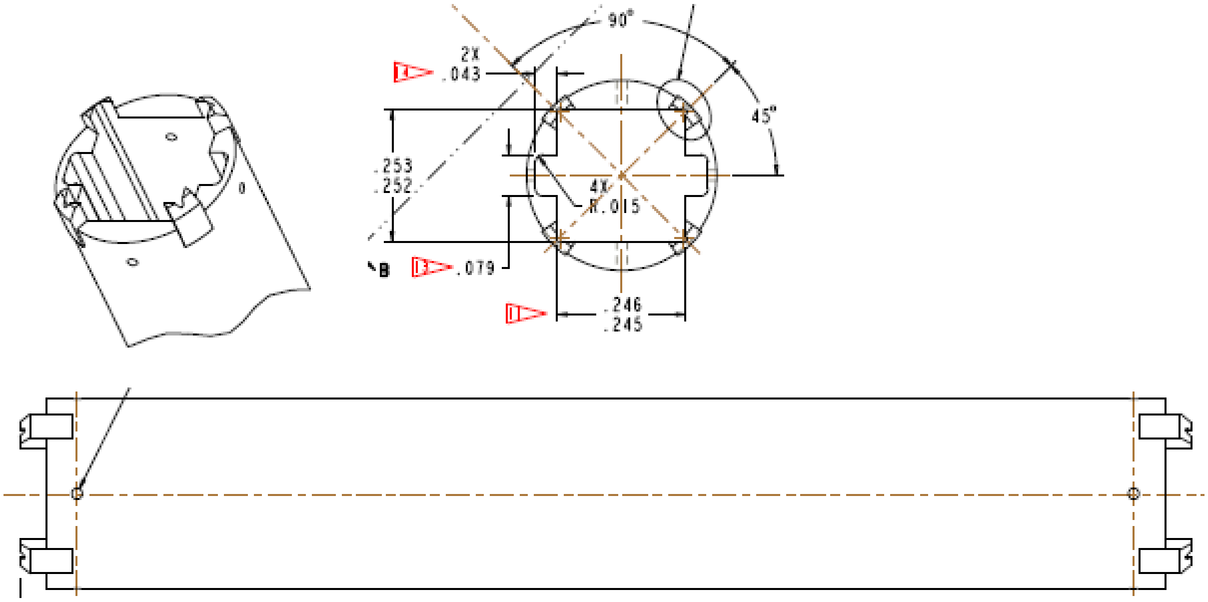

Figure 47. New Molybdenum Holder for High Temperature Capsules. Dimensions in inches.

Multiple Specimen Type Metals Assembly Experiments

A total of 36 metals assembly rabbit capsules were designed and fabricated in FY2012. These capsules contained a variety of tensile, coupon, TEM, and other types of specimens, many selected to meet the needs of the TITAN US-Japan collaboration. Figure 48 shows a typical design assembly, while Figure 49 shows a typical specimen loading. Design temperatures for these capsules ranged from 300 to 650°C and irradiation doses ranged from a few hours in the hydraulic tube to 9 full HFIR cycles.

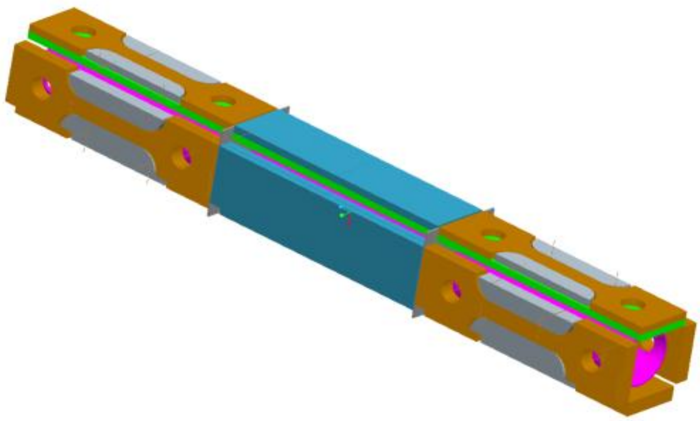

Figure 48. Typical Design for the TITAN Metals Rabbit Capsules

Figure 49. Typical Specimen Load for a TITAN Metals Rabbit Capsule

Dielectric Mirror Experiments

Two new dielectric mirror experiments were built in FY2012. The capsule design was developed in 2006-2007, and a number of rabbits were fabricated at that time. This was a follow-up experiment, and the design is discussed and depicted in section 7.1.

Silicon Carbide Composite Experiments

The SiC/SiC composite experiment design is shown in Figure 50. A total of 8 rabbits were fabricated in FY2012, and each rabbit contained 20 composite specimens, along with thermometry and SiC liners to prevent specimen/metal interactions. All 8 rabbits were designed for 950°C irradiation for a range of 6 to 47 cycles.

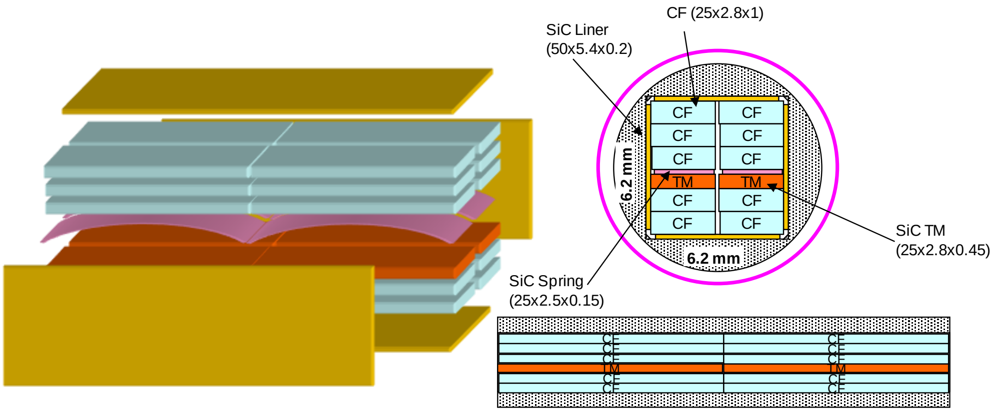

Figure 50. SiC/SiC Composite Design

Tensile Creep Rabbit Capsules

A set of 20 new rabbit capsules have been designed to exert a tensile stress on specimens of V-4Cr4Ti, SiC, Graphite, and F82H steel during irradiation. A stainless steel bellows is pressurized after capsule assembly, which imparts a known force on the tensile specimen located at the bottom of the stack. The specimen is accompanied by two unstressed reference specimens of the same material. The capsules are currently in fabrication and are scheduled to begin irradiation in November 2012. Figure 51 shows a cutaway view of the creep capsule. This is the most difficult and complicated rabbit ever designed at ORNL.

A description of the use and testing of this capsule type is given in section 8.3.

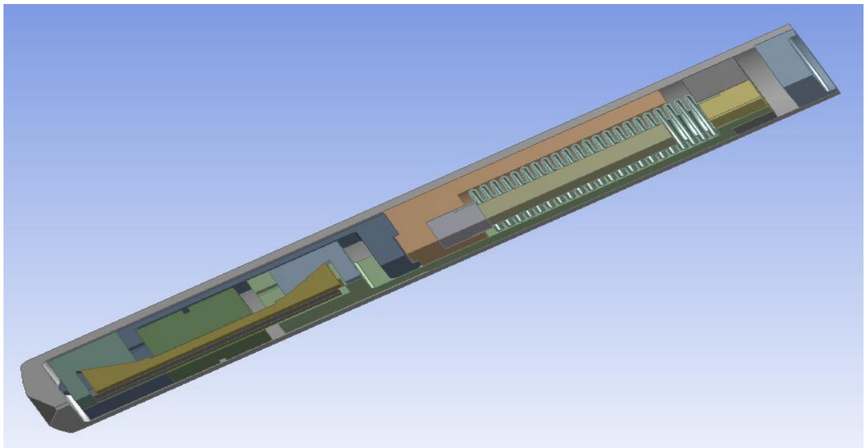

Figure 51. A 90° Cutaway View of the Tensile Creep Rabbit Design

CONCLUSIONS

Six new rabbit designs and 73 total rabbit irradiation experiments for HFIR were designed and built to support the fusion materials program in FY2012. While there are similarities between all of these experiments, almost none are truly identical. Each one requires some measure of analysis and design to accommodate the specimen load and provide the irradiation temperature specified. New challenges come with each experiment! The experiments irradiated in FY 2012 occupied a large fraction of the available space in the HFIR flux trap region.

8.3 DEVELOPMENT OF IN-SITU IRRADIATION CREEP TECHNOLOGY

T.S. Byun (byunts@ornl.gov), M. Li (ANL), Y. Katoh, J.L. McDuffee, L.L. Snead

OBJECTIVE

This work is directed at developing irradiation creep testing technology using gas-pressurized mini-bellows. The system will be used to examine the in-reactor creep of metallic and ceramic fusion materials in HFIR.

SUMMARY

Irradiation creep testing technology using gas-pressurized mini-bellows has been established to apply to the in-reactor creep tests of metallic and ceramic materials in HFIR. Both the theoretical model and the experimental result confirmed that a gas-pressurized bellows can produce high enough stress to induce irradiation creep in subsize specimens. Experimental and calculational procedures to obtain in-situ applied stress values from post irradiation in-furnace force measurements were developed.

PROGRESS AND FUTURE PLAN

Principle of Bellows Loading

The gas-filled bellows used as the load generator in the frame is a miniature elastic vessel that can be compressed or extended depending on the pressure difference between the inside and outside of the bellows. To calculate the net force exerted on the specimen, all contributing components including the force generated by gas pressure (p), spring force from the elastic deformation (δ) of bellows wall ($E\delta$), and friction force in the system (F_f) must be taken into account. In practical applications any elastic spring force will be diminished by irradiation induced relaxation and a negligible friction force is preferred for application of consistent loading. The net force exerted by a compressed bellows can be calculated by including the three force components. Since the bellows effective cross-sectional area (A_{eff}) and internal pressure determine the load that can be applied to a specimen, having large enough A_{eff} is important in selection of bellows. Depending on its design, the stress applied to the specimen can be tensile or compressive. The magnitude of the stress applied to a specimen (σ) can be obtained by dividing the bellows-generated force (F) by the cross-sectional area of the specimen gage section (A_{sp}):

$$\sigma = F / A_{sp} = (A_{eff} \cdot p(T) \cdot f(\delta) - E(T)\delta - F_f) / A_{sp} \qquad (1)$$

Conceptual Design and Applied Stress in a Specimen

Irradiation creep testing using gas-pressurized bellows can be performed in either tensile or compressive mode depending on how the internal frame and specimen are designed and assembled. Two likely applications considered during this design development were irradiation creep experiments with graphite in the compression mode and experiments with metallic materials under tensile loading. The conceptual design proposed for the tensile mode in-situ creep capsule is illustrated in Figure 52. Schematics like this were used as the basis for engineering design and thermal calculation for particular experiments. To assemble an experiment the specimen-bellows pair is set in a rigid internal frame before the bellows is pressurized. Pressure is set in a chamber, communicating through a very thin hole in the top endcap (or endplug). When the pressure is at the desired level, the end cap hole is sealed by electron or laser beam welding. A rabbit irradiation capsule housing holds the load frame-specimen assembly but does not confine deformation of the specimen. The empty volumes and gas gaps within the capsule are carefully controlled based on thermal calculations, to achieve the specimen target temperature during irradiation. Figure 53gives the stress values in an SS-3 tensile specimen with bellows internal gas pressures of 2 to 12 MPa, calculated for the irradiation capsule in Figure 52.

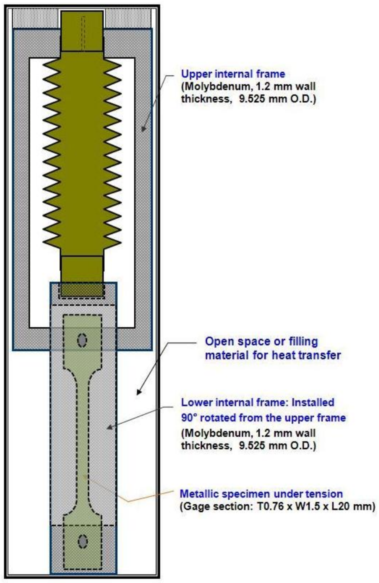

Figure 52. (left). Conceptual design of a bellows-loaded creep capsule for testing an SS-3 tensile specimen.

Figure 53. (right). Temperature dependence of stress in SS-3 tensile specimen applied by 316 SS mini-bellows pressurized to 2 – 12 MPa.

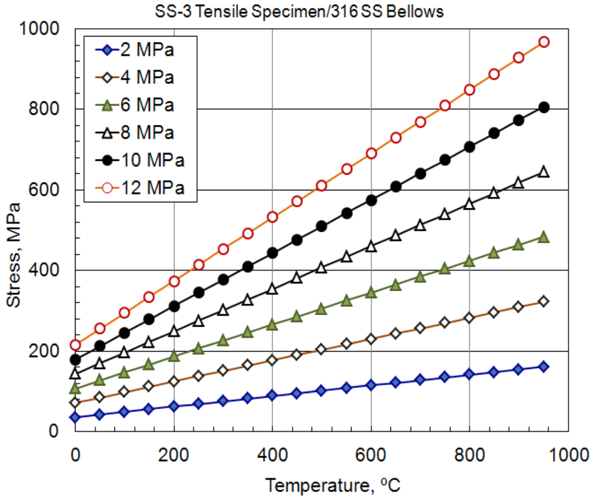

Post-irradiation In-furnace Force Measurement

The post-irradiation in-furnace tests have been carried out for two purposes: to evaluate the actual applied stress in the specimens and to confirm that the bellows and welds are intact after irradiation. Any leak developed during irradiation would lead to nil pressure in the in-furnace testing after irradiation; otherwise the load applied to the specimen at the irradiation temperature can be evaluated from the loads measured at the same temperatures after irradiation. As an example, the load-displacement responses of bellows were obtained for irradiated graphite test capsules by vertically compressing the bellows through the top endcap in a mechanical testing machine, Figure 54. The load increases at a much lower rate after the knee point, and the increase is due to the compression of the gas-filled bellows. The load measured at the knee is the total force exerted on the specimen at the temperature (=*F*). Comparison of the curves for room temperature and with those for elevated temperatures, i.e., 300 and 400°C shows the strong test temperature dependence because the gas expansion law dominates other contributions such as spring force and friction.

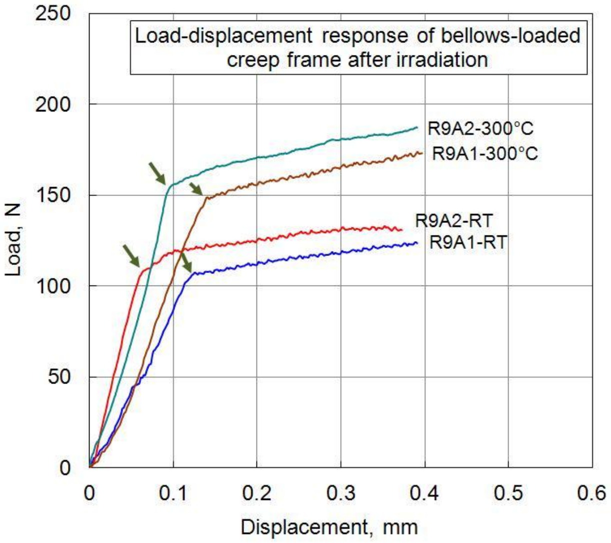

Figure 54. Load-displacement (compressive) responses of the graphite creep capsules R9A1 & A2 after irradiation. The arrows at the knee indicate the load where the top shoulder of the bellows detaches from the frame. The knee load is equivalent to the load applied to the graphite specimen.

8.4 HFIR IRRADIATIONS COMPLETED IN FY 2012

Y. Katoh (katohy@ornl.gov), M.A. Fechter, J.L. McDuffee, C. Bryan

SUMMARY

Neutron irradiation experiments were performed in support of the research and development of fusion reactor materials using various materials irradiation facilities in the High Flux Isotope Reactor (HFIR).

During FY-2012, 31 target zone rabbit capsules completed HFIR irradiation, achieving the target neutron fluences. Those capsules are listed in Table 8along with supplemental information regarding material, specimen type, and temperature, fluence, and period of irradiation. All the capsules in Table 8are associated with TITAN US-Japan collaboration, with most capsules containing materials of interest to the US program.

Table 8. Fusion materials program capsules that completed HFIR irradiation in FY-2012.

Experiment Designation	Primary Materials	Specimen Types*	Irradiation Temperature (°C)	Max Exposure (dpa)	Number of Reactor Cycles	Irradiation Period From – To (month/year)
300-LD-1	Steels	SSJ, MC	300	2	1	5/12 – 6/12
500-LD-1	Steels	SSJ, MC	500	2	1	5/12 – 6/12
650-LD-1	Steels	SSJ, MC	650	2	1	5/12 – 6/12
650-LD-2	Steels	SSJ, MC	650	2	1	5/12 – 6/12
300-LD-2	Steels, W	SSJ, MC	300	2	2	7/12 – 8/12
500-LD-3	Steels, W	SSJ, MC	500	2	1	7/12 – 8/12
PC1	Various	SSJ, MC	80/100	0.02	HT**	6/12 – 6/12
PC1A	Various	SSJ, MC	80/100	0.02	HT	6/12 – 6/12
PC2	Various	SSJ, MC	80/100	0.1	HT	6/12 – 6/12
PC2A	Various	SSJ, MC	80/100	0.1	HT	6/12 – 6/12
PC3	Various	SSJ, MC	80/100	0.5	HT	6/12 – 6/12
PC3A	Various	SSJ, MC	80/100	0.5	HT	6/12 – 6/12
PC4	Various	SSJ, MC	80/100	2	1	6/12 – 7/12
PC4A	Various	SSJ, MC	80/100	2	1	6/12 – 7/12
TB-300-1	Steels, W	SSJ, MC	300	0.02	HT	8/12 – 8/12
TB-300-2	Steels, W	SSJ, MC	300	0.1	HT	8/12 – 8/12
TB-300-3	Steels, W	SSJ, MC	300	0.5	HT	8/12 – 8/12
TB-500-1	Steels, W	SSJ, MC	500	0.1	HT	8/12 – 8/12
TB-500-2	Steels, W	SSJ, MC	500	0.5	HT	8/12 – 8/12
TB-650-1	Steels, W	SSJ, MC	650	0.1	HT	8/12 – 8/12
TB-650-2	Steels, W	SSJ, MC	650	0.5	HT	8/12 – 8/12
TTN09	SiC	Joint	500	3.4	2	8/11 – 11/11
TTN10	SiC	Joint	500	4.1	2	8/11 – 11/11
TTN11	SiC	Joint	800	4	2	3/12 – 5/12
TTN02	SiC	BSR	300	10	6	2/11 – 12/11
TTN04	SiC	BSR	500	10	6	5/11 – 4/12
TTN06	SiC	BSR	800	10	6	5/11 – 4/12
TTN08	SiC	BSR	1200	10	6	5/11 – 8/12
TTN16	SiC	Fiber BSR	500	1	1	11/11 – 12/11
TTN17	SiC	Fiber BSR	500	10	6	8/11 – 6/12
TTN19	SiC	Fiber BSR	1200	1	1	3/12 – 4/12

*SSJ = Tensile, MC = Multipurpose Coupon, Joint = Torsional specimen containing a Joint, BSR = Bend Stress Relaxation Creep. Some experiments also contain TEM disks, other special purpose specimens, and monitors occupying small spaces.
**Hydraulic tube – fractional cycle exposures.

8.5 HFIR IRRADIATIONS CONTINUING BEYOND FY 2012

Y. Katoh (katohy@ornl.gov), M.A. Fechter, J.L. McDuffee, C. Bryan

SUMMARY

Neutron irradiation experiments are being performed in support of the research and development of fusion reactor materials using various materials irradiation facilities in the Oak Ridge National Laboratory High Flux Isotope Reactor (HFIR). At the end of FY-2012, 4 full length target zone capsules and 32 target zone rabbit capsules are continuing irradiation in HFIR toward their target neutron fluences. Those capsules are listed in Table 9 along with the supplemental information regarding materials, specimen types, and temperatures, fluences, and periods of irradiation.

Table 9 HFIR fusion materials program capsules that are continuing irradiation beyond FY-2012

Experiment Designation	Primary Materials	Specimen Types*	Irradiation Temperature (°C)	Max Exposure (dpa)	Number of Reactor Cycles	Irradiation Period From – To (month/year)		
Target zone full-length capsules (DOE-JAEA)								
JP-28	F82H	T, FT	300,400,500	80	~50	4/05	–	
JP-29	F82H	T, FT	300,400,500	80	~50	1/05	–	
JP-30	F82H	T, FT	300,400,650	20	~10	11/11	–	
JP-31	F82H	T, FT	300,400,650	20	~10	11/11	–	
Target zone rabbit capsules (DOE-JAEA)								
F8A1	F82H	T, FT	300	50	28	2/09	–	
F8A2	“	“	“	“	“	“	–	
F8B1	“	“	“	“	“	“	–	
F8B2	“	“	“	“	“	“	–	
JCR-8	SiC/SiC	BB	800	>50	>25	10/04	–	
F11A3	F82H	T, FT	300	20	12	5/11	–	
F11A4	“	“	“	“	“	“	–	
F11B3	“	“	“	“	“	“	–	

*T/SSJ = Tensile, FT = Fracture Toughness, MC = Multipurpose Coupon, BB = Bend Bar, BSR = Bend Stress Relaxation Creep. Most experiments also contain TEM disks, other special purpose specimens, and monitors occupying small spaces.

(Table 9 continues next page)

Table 9 (Continued): HFIR fusion materials program capsules that are continuing irradiation beyond FY-2012.

Experiment Designation	Primary Materials	Specimen Types*	Irradiation Temperature (°C)	Max Exposure (dpa)	Number of Reactor Cycles	Irradiation Period From – To (month/year)		
Target zone rabbit capsules (TITAN)								
MTTN01	Steels	T, MC	300	4.8	4	1/12	–	
300-HD-1	Steels	SSJ, MC	300	12	6	5/12	–	
500-HD-1	Steels	SSJ, MC	500	12	6	5/12	–	
500-HD-2	Steels	SSJ, MC	500	12	6	5/12	–	
500-HD-3	Steels	SSJ, MC	500	12	6	5/12	–	
650-HD-1	Steels	SSJ, MC	650	12	6	5/12	–	
650-HD-2	Steels	SSJ, MC	650	12	6	5/12	–	
300-MD-1	Steels, W	SSJ, MC	300	7	4	7/12	–	
500-LD-2	Steels, W	SSJ, MC	500	2	2	10/12	–	
300-LD-3	Steels, W	SSJ, MC	300	2	2	7/12	–	
300-HD-2	Steels, W	SSJ, MC	300	12	8	7/12	–	
500-HD-4	Steels, W	SSJ, MC	500	12	6	7/12	–	
650-LD-3	Steels, W	SSJ, MC	650	2	2	10/12	–	
650-HD-3	Steels, W	SSJ, MC	650	12	8	7/12	–	
PC5	Various	SSJ, MC	80/100	20	9	6/12	–	
TB-300-4	Steels, W	SSJ, MC	300	7	5	7/12	–	
TB-500-3	Steels, W	SSJ, MC	500	7	4	7/12	–	
TB-650-3	Steels, W	SSJ, MC	650	7	5	7/12	–	
TB-650-4	Steels, W	SSJ, MC	650	20	11	7/12	–	
TTN03	SiC	BSR	300	20	11	2/11	–	
TTN05	SiC	BSR	500	20	11	5/11	–	
TTN07	SiC	BSR	800	20	11	5/11	–	
TTN18	SiC	Fiber BSR	500	20	11	8/11	–	
TTN20	SiC	Fiber BSR	1200	10	6	3/12	–	

*T/SSJ = Tensile, FT = Fracture Toughness, MC = Multipurpose Coupon, BB = Bend Bar, BSR = Bend Stress Relaxation Creep. Most experiments also contain TEM disks, other special purpose specimens, and monitors occupying small spaces.

9.0 INTERNATIONAL COLLABORATION PROGRAMS

Y. Katoh (katohy@ornl.gov), L.L. Snead, R.E. Stoller

SUMMARY

ORNL participates in two major, long-running collaborations with Japan and several less formal collaborations. The TITAN Project with the National Institute of Fusion Science and the participating universities in Japan and the JAEA-DOE HFIR Collaboration continued to be the primary international collaboration programs involving the ORNL fusion materials program. Activities and achievements related with these collaborations are briefly summarized below. Coordination meetings, workshops, and irradiation capsules associated with these collaboration programs are summarized in other sections of this report. Additional collaborations that were not explicitly budgeted in the ORNL program but were maintained or initiated in FY-2012 include the one with Karlsruhe Institute of Technology (Germany) on tungsten materials R&D for plasma facing components and spallation neutron irradiation at the Paul Scherrer Institute SINQ Target Irradiation Program (STIP).

PROGRESS AND STATUS

TITAN PROJECT

The objective of the TITAN Project is to obtain the fundamental understanding needed for establishing tritium and thermofluid control in fusion systems, based on experiments under simulated fusion. The results will be applied through the integrated modeling to advancement of design for tritium and heat control of magnetic and inertial fusion energy systems. The project consists of three tasks: Transport Phenomena, Irradiation Synergism, and System Integration Modeling. ORNL is involved in research for subtasks on Joining and Coating Integrity, on Dynamic Deformation of Fusion Materials, and to a limited extent on Irradiation-Tritium Synergism.

The objective of Task 2-2 is to develop and examine irradiation performance of joints and coatings of fusion materials. The major activities in FY 2012 included development of vacuum plasma spray (VPS) tungsten coatings on steels, friction stir welding (FSW) of ODS steels by both parties, development of electron beam (EB)-welding for reduced activation ferritic/martensitic steels, irradiation of these steel joint specimens and tungsten-coated steel specimens in HFIR, and post-irradiation examination. A large number of irradiation capsules were prepared and irradiated in support of this Task in FY 2012 as listed elsewhere. Silicon carbide ceramic joints were also developed and evaluated in this task, as reported in the Composite Materials section.

The objective of Task 2-3 on Dynamic Deformation is to acquire fundamental understanding of the dynamic behavior of blanket materials under stress in fusion-relevant conditions. This includes determination of tritium interactions of structural ceramics during neutron irradiation. The Phase-I (low dose stress-relaxation) experimental program of stress effects on dimensional stability of fusion materials was completed. New and essential information on transient irradiation creep for SiC was obtained. Phase-II (higher dose stress-relaxation creep) irradiation is in progress with all capsules started irradiation in HFIR and some completed irradiation. A Phase-III (bellows-loaded tensile creep) experiment is in progress.

JAEA-DOE COLLABORATION

The Japan Atomic Energy Agency – DOE Collaboration on Irradiation and Examination of Fusion Reactor First Wall and Blanket Structure Materials is currently in its Phase VI Program. The program objective is to advance understanding on the effects of neutron irradiation on materials for magnetic fusion reactor blanket first wall and structures with the main focus on mechanical properties of reduced-activation ferritic/martensitic steels.

During FY 2012, two new HFIR target position experiments JP-30 and -31 began irradiation and are currently at about half of the ~20 dpa goal. . These experiments will provide data on F82H steel specimens with weld joints and will augment the experimental matrices of previous HFIR target capsules. The US side also included ODS steels and nitride-strengthened steels in the high temperature part of these experiments.

A vigorous program of testing and characterizing irradiated materials and associated control materials continued through the past year. Ferritic steels and SiC composites from several experiments were included in this work.

Ferritic Steel Testing - The spectrally tailored, Li-bonded RB 15J experiment contained variants of F82H irradiated at 300 and 400°C and was designed to provide data for use in the design of ITER-TBMs. Specimen types include tensile, fracture toughness, creep and fatigue – including F82H base and joint material. Hardness, tensile, fracture toughness and some physical property testing has been accomplished, with fatigue testing, fractography and microstructural characterization remaining. The early results are generally comparable to results from earlier experiments. Some size effects have been seen in the data, pointing to underestimates of the total elongation.

SiC Composite Evaluation – High dose (70 dpa) material from HFIR rabbit capsules were examined to determine stability under irradiation. Measurements of swelling, dynamic Young’s modulus, thermal conductivity and tensile bend properties showed significant changes in properties, compared to the results following 40 dpa irradiation in earlier experiments. Changes are tentatively attributed to effects in the pyrolytic carbon interphase layers, and possibly to some degradation in the fibers themselves. Additional evaluation is planned to pin down the reasons for the irradiation effects.

Discussion has begun on possible activities to be included in the anticipated extension of this collaboration into a Phase VII, starting in April, 2014. R&D on ferritic steels and SiC composites will be included, with new HFIR irradiation experiments planned to provide needed data on these materials.

FUTURE PLANS

It is anticipated that both of the collaborations with Japan will continue into new phases at the completion of current terms. Active discussions are underway to lay the basis for continuation of the work of interest to both parties.

10.0 PUBLICATIONS BY ORNL FUSION MATERIALS PROGRAM PARTICIPANTS

These publications are arranged alphabetically by the first-listed ORNL author.

T.D. Burchell and A.A. Ogale, “Neutron Irradiation Induced Changes in the Microstructure of Carbon and Graphite Fibers” submitted to the Journal of Nuclear Materials (ICFRM 15)

J.P. Wharry, Z. Jiao, V. Shankar, J.T. Busby and G.S. Was “Radiation-induced segregation and phase stability in ferritic-martensitic alloy T91”, Journal of Nuclear Materials 417 (2011) 140-144

J.T. Busby , P.J. Maziasz, A.F. Rowclie, M.Santella and M. Sokolov “Development of high performance cast stainless steels for ITER shield module applicationsl” Journal of Nuclear Materials 417 (2011) 866-869

S. I. Golubov, A. V. Barashev, and R. E. Stoller, "Radiation Damage Theory," Chapter in Comprehensive Nuclear Materials, R. J. M. Konings, T. R. Allen, R. E. Stoller, and S. Yamanaka, Editors, Elsevier Ltd., Amsterdam, 2012, pp. 357-391.

T. Suzudo, S.I. Golubov, R.E. Stoller, M. Yamaguchia, T. Tsurua, and H. Kaburaki, "Annealing Simulation of Cascade Damage in a-Fe - Damage Energy and Temperature Dependence Analyses," Journal of Nuclear Materials 423 (2012) 40-46.

T. Suzudo, S. I. Golubov, R. E. Stoller, M. Yamaguchi, T. Tsuru, and H. Kaburaki, "Kinetic Monte Carlo Annealing Simulation of Cascade Damage in a-Fe," Progress in Nuclear Science and Technology 2 (2011) 56-63.

D.T. Hoelzer, M.A. Sokolov and Z. Feng, “Joining of 14YWT and F82H by Friction Stir Welding,” submitted to Journal of Nuclear Materials, ICFRM-15 Conference, 2011.

Y. Katoh, L. L. Snead, I Szlufarska, W. J. Weber “Radiation Effects in SiC for Nuclear Structural Application.” Current Opinion in Solid State and Materials Science, 16 (2012) 143-152.

K. Ozawa, Y. Katoh, T. Nozawa, T. Hinoki, L. L. Snead. “Evaluation of Damage Tolerance of Advanced SiC/SiC Composites after Neutron Irradiation.” IOP Conference Series: Materials Science and Engineering 18, 162005. 2011.

Y. Katoh, L.L. Snead, C.M. Parish, T. Hinoki, Observation and Possible Mechanism of Irradiation Induced Creep in Ceramics, J. Nucl. Mater., (submitted).

M. Ferraris, M. Salvo, S. Rizzo, V. Casalegno, S. Han, A. Ventrella, T. Hinoki, Y. Katoh, Torsional shear strength of silicon carbide components pressurelessly joined by a glass-ceramic, International Journal of Applied Ceramic Technology, 9 (2012) 786-794.

Y. Katoh, L.L. Snead, I. Szlufarska, W.J. Weber, Radiation Effects in SiC for Nuclear Structural Applications, Current Opinion in Solid State & Materials Science, 16 (2012) 143-152.

H.C. Jung, T. Hinoki, Y. Katoh, A. Kohyama, Development of a shear strength test method for NITE-SiC joining material, J. Nucl. Mater., 417 (2011) 383-386.

S. Kondo, Y. Katoh, L.L. Snead, Concentric ring on ring test for unirradiated and irradiated miniature SiC specimens J. Nucl. Mater., 417 (2011) 406-410.

K. Ozawa, Y. Katoh, T. Nozawa, L.L. Snead, Effect of Neutron Irradiation on Fracture Resistance of Advanced SiC/SiC Composites, J. Nucl. Mater., 417 (2011) 411-415.

Y. Katoh, T. Nozawa, L.L. Snead, K. Ozawa, H. Tanigawa, Stability of SiC and its Composites at High Neutron Fluence, J. Nucl. Mater., 417 (2011) 400-405.

Y. Katoh, K. Ozawa, T. Hinoki, Y.B. Choi, L.L. Snead, A. Hasegawa, Mechanical Properties of Advanced SiC Fiber Composites Irradiated at Very High Temperatures, J. Nucl. Mater., 417 (2011) 416-420.

M. Ferraris, M. Salvo, V. Casalegno, S. Han, Y. Katoh, H.C. Jung, T. Hinoki, A. Kohyama, Joining of SiC-based materials for nuclear energy applications, J. Nucl. Mater., 417 (2011) 379-382.

C.P.C. Wong, M. Abdou, N. Morley, B. Merrill, S. Smolentsev, E. Marriott, M.E. Sawan, M. Youssef, Y. Katoh, R.J. Kurtz, B.A. Pint, A. Lumsdaine, S. Willms and B. Williams, “Progress on DCLL Blanket Concept” submitted to Fusion Science and Technology (TOFE Proceedings)

Y.K.M, Peng (with Y.Katoh and others) “Fusion Nuclear Science Facility (FNSF) Before Upgrade to Component Test Facility (CTF)”, Fusion Science and Technology 60 (2011) 441-448.

**M. C. Brandes, L. Kovarik, M. K. Miller, M. J. Mills, Morphology, Structure, and Chemistry of Nanoclusters in a Mechanically-Alloyed Nanostructured Ferritic Steel, J. Mater. Sci., 47 (2012) 3913–3923.

**M. C. Brandes, L. Kovarik, M. K. Miller, G. S. Daehn, and M. J Mills, Creep Behavior and Deformation Mechanisms in a Nanocluster Strengthened Ferritic Steel, Acta Mater., 60 (2011) 1827–1839.

**X.-L. Wang, C. T. Liu, U. Keiderling, A. D. Stoica, L. Yang, M. K. Miller, C. L. Fu, D. Ma, and K. An, Unusual Thermal Stability of Nano-structured Ferritic alloys, Journal of Alloys and Compounds, 529 (2012) 96– 101.

**C. Capdevila, M. K. Miller, G. Pimentel and J. Chao, Influence of recrystallization on phase separation kinetics of oxide dispersion strengthened Fe–Cr–Al alloy, Scripta Mater., 66 (2012) 254–257.

J. Yang, Yu. N. Osetskiy, and R. E. Stoller, "The Effect of Twist Angle on Anisotropic Mobility of {110} Hexagonal Dislocation Networks in alpha-Iron," Scripta Materialia 66 (2012) 761-764.

D. M. Stewart, Yu. N. Osetskiy, and R. E. Stoller, "Atomistic Studies of Properties of Helium in BCC iron," Journal of Nuclear Materials 417 (2011) 1110-1114.

B. A. Pint, “The Effect of Coatings on the Compatibility of Fe-Cr Steels in Pb-Li,” J. Nuc. Mater. 417 (2011) 1195-1199.

A. Rouaix-Vande Put and B. A. Pint, (2012) “Inhibited Aluminization of an ODS FeCr Alloy,” Surf. Coat. Technol. 206 (2012) 5036.

B. A. Pint, L. R. Walker and K. A. Unocic, (2012) “Material Compatibility with Isothermal Pb-Li,” Mater. High Temp. 29 (2012) 129.

B. A. Pint and K. A. Unocic, “Pb-Li Compatibility Issues for DEMO” submitted to Journal of Nuclear Materials (ICFRM-15).

G. D. Samolyuk, S. I. Golubov, Yu. N. Osetsky, and R. E. Stoller, "Molecular Dynamics Study of Influence of Vacancy Types Defects on Thermal Conductivity of ß-SiC," Journal of Nuclear Materials 418 (2011) 174-181.

GD Samolyuk, YN Osetsky RE Stoller "The influence of transition metal solutes on dislocation core structure and values of Peierls stress and barrier in tungsten." submitted to Journal of Physics: Condensed Matter 08/06/2012.

L. L. Snead and M. Ferraris. “Graphite as a Fusion Plasma-Facing Material”. Chapter in Comprehensive Nuclear Materials, R.J.M. Konings, T.R. Allen, R.E. Stoller, and S. Yamanaka editors, volume 4, pp. 583-620. Amsterdam, Elsevier. 2012

L.L. Snead, T. Nozawa, M. Ferraris, Y. Katoh, R. Shinavski, M. Sawan, Silicon carbide composites as fusion power reactor structural materials J. Nucl. Mater., 417 (2011) 330-339.

L.L. Snead, Y. Katoh, K. Ozawa, Stability of 3-D Carbon Fiber Composite to High Neutron Fluence, J. Nucl. Mater., 417 (2011) 629-632.

M. Sawan, N. Ghoniem, L.L. Snead, Y. Katoh, Damage Production and Accumulation for SiC in Inertial and Magnetic Fusion Systems, J. Nucl. Mater., 417 (2011) 445-450.

L. L. Snead, Y. Katoh, T. Nozawa, “Radiation Effects in SiC and SiC-SiC” chapter in Comprehensive Nuclear Materials R.J.M. Konings, T.R. Allen, R.E. Stoller, and S. Yamanaka editors, volume 4, pp215-240. Amsterdam, Elsevier. 2012

R.E. Nygren, R. Raray, D. Whyte, M.A. Urickson, M. Baldwin and L.L. Snead “Making tungsten work”. Journal of Nuclear Materials 417 (2011) 451-456

Y. Hatano, M. Shimada, Y. Oya, G. Cao, M. Kobayashi, M. Hara, B.J. Merrill, K. Okuno, M.A. Sokolov, Y. Katoh, Retention of Hydrogen Isotopes in Neutron Irradiated Tungsten (Review), Materials Transactions, (submitted).

T. Hirose, N. Okubo, H. Tanigawa, M. Ando, M. A. Sokolov, R. E. Stoller, and G..R. Odette, "Irradiation Hardening in F82H Irradiated at 573 K in the HFIR," Journal of Nuclear Materials 417 (2011) 108-111.

N. Okubo, M.A. Sokolov, H. Tanigawa, T. Hirose, S. Jitsukawa, T. Sawai, G.R. Odette, and R.E. Stoller, "Heat Treatment Effect on Fracture Toughness of F82H Irradiated in HFIR," Journal of Nuclear Materials 417 (2011) 112-114.

T. Yamamoto, G.R. Odette and M.A. Sokolov “On the Fracture Toughness of Irradiated F82H: Effects of loss of constraint and strain hardening capacity”, Journal of Nuclear Materials 417 (2011) 115-119

R. J. M. Konings, T. R. Allen, R. E. Stoller, and S. Yamanaka, Editors, Comprehensive Nuclear Materials, Elsevier Ltd., Amsterdam, 2012.

R. E. Stoller, "Primary Radiation Damage Formation," chapter in Comprehensive Nuclear Materials, R. J. M. Konings, T. R. Allen, R. E. Stoller, and S. Yamanaka, Editors, Elsevier Ltd., Amsterdam, 2012, pp. 293-332..

R. E. Stoller, “The Potential Impact of Ballistic Helium Resolutioning on Bubble Evolution,” accepted for Journal of Nuclear Materials (2012).

R. E. Stoller and D. M. Stewart, "An Atomistic Study of Helium Resolution in bcc Iron," Journal of Nuclear Materials 417 (2011) 1106-1109.

H. Tanigawa, K. Shiba, A. Moeslang, R.E. Stoller, R. Lindau, M.A. Sokolov, G.R. Odette, R.J. Kurtz, and S. Jitsukawa, "Status and Key Issues of Reduced Activation Ferritic/Martensitic Steels as the Structural Material for a DEMO Blanket," Journal of Nuclear Materials 417 (2011) 9-15.

M. Wendel, M. Dayton, W. Lu, T. McManamy, P. Rosenblad, and R. Stoller, “Fusion Material Irradiation Test Facility at SNS,” Proc. 24th IAEA Fusion Energy Conference, San Diego, USA, October 8–13, 2012.

L. Tan, Y. Yang, J.T. Busby, Effects of alloying elements and thermomechanical treatment on 9Cr reduced activation ferritic-martensitic (RAFM) steels, submitted to Journal of Nuclear Materials (ICFRM15).

K. A. Unocic, D. N. Leonard, H. M. Meyer, M. J. Lance and B. A. Pint, "Compatibility of V/Y2O3/V-4Cr-4Ti Coatings with Liquid Flowing Li," in Proceedings of the 8th International Symposium on High Temperature Corrosion and Protection of Materials, Les Embiez, France, May 2012, Paper#176.

K. A. Unocic, M. Lance and B. A. Pint, “Characterization of Specimens Exposed in a Li Loop,” submitted to Journal of Nuclear Materials (ICFRM-15).

K. A. Unocic, D. T. Hoelzer and B. A. Pint, “Effect of Liquid Flowing Li on Mechanical and Structure Properties of V-4Cr-4Ti Alloy,” draft for submission to Journal of Nuclear Materials.

H Y Xiao, Y Zhang, L L Snead, Y Shutthanandan, H Z Xue, W J Weber. “Near-Surface and Bulk Behavior of Ag in SiC.” Journal of Nuclear Materials. 420 (2012) 123-130.

Y. Zhang, M. Ishimaru, T. Varga, T. Oda, C. Hardiman, H.Z. Xue, Y. Katoh, S. Shannon, W.J. Weber, Nanoscale Engineering of Radiation Tolerant Silicon Carbide, Physical Chemistry Chemical Physics, 14 (2012) 13429-13436.

S.J. Zinkle, “Radiation-Induced Effects on Microstructure”, Chapter 1.03 in Comprehensive Nuclear Materials, Eds. R. Konings, T.R. Allen, R.E. Stoller and S. Yamanaka, vol. 1 (Elsevier, 2012) pp. 65-98, ISBN: 978-0-08-056027-4.

M. Li and S.J. Zinkle, “Physical and Mechanical Properties of Copper and Copper Alloys”, Chapter 4.20 in Comprehensive Nuclear Materials, Eds. R. Konings, T.R. Allen, R.E. Stoller and S. Yamanaka, vol. 4 (Elsevier, 2012) pp. 667-690, ISBN: 978-0-08-056027-4.

S.J. Zinkle, "Effects of H and He Irradiation on Cavity Formation and Blistering in Ceramics", 16th International Conference on Radiation Effects in Insulators, Beijing, China, Aug. 14-19, 2011, Nucl. Instr. Meth. Phys. Res. B 286, (2012) 4-19. doi: 10.1016/j.nimb.2012.03.030

S.J. Zinkle and N.M. Ghoniem “Prospects for acceleratd development of high performance structural materials”, Journal of Nuclear Materials 417 (2011) 2-8

V.R. Barabash, G.M. Kalinin, S.A. Fabritsiev and S.J. Zinkle “Specification of CuCrZr alloy properties after various thermo-mechanical treatments and design allowables including neutron irradiation effects” Journal of Nuclear Materials, 417 (2011) 904-907

[1]

** paper on ORNL Fusion Program material, but the work not sponsored by DOE-OFES